Telomere length sensitive regulation of Interleukin Receptor 1 type 1 (IL1R1) by the shelterin protein TRF2 modulates immune signalling in the tumour microenvironment

Ananda Kishore Mukherjee[1,2,#,], Subhajit Dutta[1,2,$], Ankita Singh[1,$], Shalu Sharma[1,2], Shuvra Shekhar Roy[1,2], Antara Sengupta[1,2], Megha Chatterjee[1], Soujanya Vinayagamurthy[1,2], Sulochana Bagri[1,2], Divya Khanna[1], Meenakshi Verma[1], Dristhi Soni[1,2], Anshul Budharaja[3], Sagar Kailasrao Bhisade[4], Vivekanand[,2,6], Ahmad Perwez[1],Nija George[7], Mohammed Faruq[,2,5,6], Ishaan Gupta[3,4], Radhakrishnan Sabarinathan[7], and Shantanu Chowdhury[1,2,5,8,9*]

$ Equal contribution

[1]Integrative and Functional Biology Unit, CSIR-Institute of Genomics and Integrative Biology, New Delhi 110025, India

[2]Academy of Scientific and Innovative Research (AcSIR), Ghaziabad 201002, India

[3]IIT Delhi, Hauz Khas, Delhi

[4]IISER Bhopal, Bhauri, Bhopal

[5]GNR Knowledge Centre for Genome and Informatics, CSIR-Institute of Genomics and Integrative Biology, New Delhi 110025, India

[6] Genomics and molecular medicine, CSIR-Institute of Genomics and Integrative Biology, New Delhi 110007, India

[7]National Centre for Biological Sciences, Tata Institute of Fundamental Research, Bellary Road, Bangalore 560065, Karnataka,India

current affiliation: Kennedy Institute of Rheumatology, NDORMS, University of Oxford, Oxford, UK.

[8]Distinguished Professor, Trivedi School of Biosciences, Ashoka University, Sonepat, Haryana-131029

[9]Lead contact *Correspondence: shantanuc@igib.in

Abstract

Telomeres are crucial for cancer progression. Immune signalling in the tumour microenvironment has been shown to be very important in cancer prognosis. However, the mechanisms by which telomeres might affect tumour immune response remain poorly understood. Here, we observed that interleukin-1 signalling is telomere-length dependent in cancer cells. Mechanistically, non-telomeric TRF2 (Telomeric Repeat binding Factor 2) binding at the IL-1-receptor type-1 (IL1R1) promoter was found to be affected by telomere length. Enhanced TRF2 binding at the *IL1R1* promoter in cells with short telomeres directly recruited the histone-acetyl-transferase (HAT) p300, and consequent H3K27 acetylation activated IL1R1. This altered NF-kappa B signalling and affected downstream cytokines like *IL6, IL8* and *TNF*. Further, *IL1R1* expression was telomere-sensitive in triple-negative breast cancer (TNBC) clinical samples. Infiltration of tumour-associated macrophages (TAM) was also sensitive to the length of tumour cell telomeres and highly correlated with *IL1R1* expression. The use of both IL1 Receptor antagonist (IL1RA) and *IL1R1* targeting ligands could abrogate M2 macrophage infiltration in TNBC tumour organoids. In summary, using TNBC cancer tissue (>90 patients), tumour-derived organoids, cancer cells and xenograft tumours with either long or short telomeres, we uncovered a heretofore undeciphered function of telomeres in modulating IL1 signalling and tumour immunity.

Introduction

Telomeres are composed of DNA repeats (TTAGGG) and associated ‘shelterin’ proteins present at the end of each eukaryotic chromosome. Gradual shortening of telomeres and change in the telomeric structure with cell division leads to cellular senescence/death, which is crucial for tissue homeostasis (Jacobs, 2013; Karlseder, 2002; Shay and Wright, 2000). During oncogenic transformation, the telomere shortening mediated cellular senescence is bypassed-resulting in uncontrolled cell proliferation and cancer progression; underlining the impact of telomeres in cancer (Blackburn, 2000; Hanahan and Weinberg, 2000; Maciejowski and Lange, 2017; Paeschke et al., 2010; Shay, 2016).

Shortening of telomeres with ageing contributes to compromised immune response (Goronzy et al., 2006; Hodes et al., 2002; Pawelec et al., 2014; Sansoni et al., 2008; Weng, 2012). However, despite its relevance in cancer prognosis and intervention (Artandi and DePinho, 2009; Aviv et al., 2017; Chew et al., 2012; F Balkwill et al., 2001; Greider, 1998; Hanahan and Weinberg, 2011; Wang et al., 2017), how telomeres influence tumour immune response is poorly understood.

Major advances show how immune cells including tumour-infiltrating-lymphocytes (TIL), tumour-associated-macrophages (TAM), natural-killer and dendritic cells impact cancer progression (Binnewies et al., 2018; Gonzalez et al., 2018; Jochems and Schlom, 2011; Salgado and Gevaert, 2021). TAMs - typically M2 macrophage-like – predominantly promote immunosuppressive tumour microenvironment (TME) through secretion of anti-inflammatory cytokines (Burkholder et al., 2014; Cassetta et al., 2016; DeNardo and Ruffell, 2019; Gonzalez et al., 2018; Pittet et al., 2022; SD et al., 2020), implicating the role of TAMs in aggressive tumour growth (Hu et al., 2015; Pittet et al., 2022).

Poor prognosis in triple-negative breast cancers (TNBC) [negative for estrogen receptor (ER-), progesterone receptor (PR-), and HER2 receptor(HER2-)] has been frequently associated with TAMs(Wang et al., 2022; Z. Y. Yuan et al., 2014). Multiple reports show M2-like TAMs to be the most abundant monocytic immune cells in TNBC and implicate their role in invasiveness and aggressive tumour growth (Burkholder et al., 2014; Jeong et al., 2019; Mantovani and Locati, 2013; Medrek et al., 2012; Oner et al., 2020; Shun et al., 2005; Z.-Y. Yuan et al., 2014).

How the telomere length (TL) of cancer cells affects macrophage infiltration has not been studied. Seimiya. H and colleagues noted that telomere elongation led to differential expression of genes associated with innate immunity(Hirashima et al., 2013). A published work on colorectal cancer showed the association of telomere length of cancer cells to immunity-related genes(Lopez-Doriga et al., 2018). Another recent article showed that telomere maintenance by Telomerase (the key enzyme responsible for telomere maintenance) and ATL (alternative telomere lengthening) related mechanisms led to alteration of markers of TAM like CD163 in glioblastomas(Hung et al., 2016). Taken together, these suggest the possibility of molecular links between TAM infiltration and telomeres.

TRF2 (Telomeric Repeat binding Factor 2) is a canonical member of the telomere capping complex called ‘shelterin’ with reported extra-telomeric functions(Martínez and Blasco, 2011; Vinayagamurthy et al., 2020). We have reported earlier that the telomeric protein TRF2 alters gene expression in a telomere length-dependent fashion (Mukherjee et al., 2018). TRF2, although

91 primarily a telomere-binding protein, was found to associate with gene promoters throughout the
92 genome independent of its telomere-specific functions (Mukherjee et al., 2019a; Simonet et al.,
93 2011; Yang et al., 2011). Interestingly, TRF2 was sequestered at the telomeres and away from
94 gene promoters in cells with relatively longer telomeres, and vice-versa in the case of cells with
95 shorter telomeres. This led to TRF2-mediated transcriptional regulation that was dependent on
96 telomere length (a scheme of this model shown in **Additional Supplementary Figure 1**)
97 (Mukherjee et al., 2018; Vinayagamurthy et al., 2023, 2020).

98 We found that non-telomeric TRF2 transcriptionally activated Interleukin-1-receptor type-1
99 (IL1R1) in a telomere-dependent fashion: resulting NF-kappaB (p65)-phosphorylation led to the
100 upregulation of downstream cytokines. Telomere-sensitive IL1 signalling in TNBC was found to
101 be correlated with enhanced TAM infiltration within the TME in tumours with relatively short
102 telomeres. Together, these implicate telomere-sensitive immune-microenvironment in tumours.
103

104 ## Results

105

106 ## Non-telomeric TRF2 binding at the IL1 receptor type 1 (*IL1R1*) promoter is telomere
107 length dependent

108 ### Cytokine and their receptor related genes are telomere-sensitive in cancer cells

109 We performed an RNA-seq experiment using our previously reported fibrosarcoma model of
110 telomere elongation(Mukherjee et al., 2018). The transcriptomic profile of HT1080 cells (short
111 telomere cells) was compared with HT1080-LT (long telomere cells). The difference in telomere
112 length between the cells was confirmed using flow cytometry (**Supplementary Figure 1A**). The
113 HT1080-LT cells had constitutively higher expression of *TERT* and *TERC* as previously described
114 (**Supplementary Figure 1B**). The telomere length of the cells was further confirmed using *in-situ*
115 hybridization of telomeric probes (**Supplementary Figure 1C**). Upon analyzing the RNA-seq
116 data, we observed that several cytokine-related genes like *IL1B*, *IL1R1*, *TNF*, *IL15* and *IL37* had
117 higher expression in HT1080 (short telomere) cells (**Supplementary Figure 1D**). We looked at
118 the enriched pathways (KEGG) in genes that were upregulated (2 fold or higher expression) and
119 down-regulated (0.5 fold or lower expression) in HT1080 cells (short telomere) compared to
120 HT1080-LT (long telomere) cells (**Supplementary Figure 1E-F; Supplementary File 1**). It was
121 observed that 'Cytokine- cytokine receptor interaction' was one of the top 5 most enriched
122 pathways for the upregulated genes (**Supplementary Figure 1E**). While telomere elongation

123 affected multiple pathways, we were most interested in cytokine-related genes that were
124 differentially expressed due to the now well-established focus on the telomere-immunity
125 axis(Barthel et al., 2017; Goronzy et al., 2006; Hirashima et al., 2013; Weng, 2012; Ye et al.,
126 2014). We revisited our published ChIP-seq data in HT1080 fibrosarcoma cells(Mukherjee et al.,
127 2019a) and found multiple cytokine-related gene promoters where TRF2 had peaks within 1000
128 bp from the transcriptional start site (TSS) (**Supplementary File 2**). We validated these sites by
129 ChIP-qPCR in HT1080 fibrosarcoma cells and found that the *IL1R1* promoter had the most
130 prominent TRF2 enrichment among the sites (**Supplementary Figure 1G**). We further performed
131 ChIP-qPCR spanning +200 to -1000 bp of the *IL1R1* TSS to confirm promoter TRF2 binding
132 across multiple cell lines- HT1080 fibrosarcoma, MDAMB231 breast cancer, HEK293T
133 immortalized kidney and MRC5 fibroblast cells (**Supplementary Figure 1H**).

134 **Telomere-dependent IL1R1 regulation in ex-vivo fibrosarcoma cells**

135 Next, we tested the telomere dependence of TRF2 binding based on TL-sensitive non-telomeric
136 TRF2 binding observed earlier (Mukherjee et al., 2018). TRF2-ChIP in ex-vivo cultured HT1080-
137 LT/HT1080 cells showed that TRF2 occupancy at the *IL1R1* promoter was significantly reduced
138 in cells with long telomeres relative to short telomere cells (**Figure 1A**). *IL1R1* mRNA expression
139 was significantly lower in HT1080-LT relative to HT1080 cells (**Figure 1B**) conforming to the RNA-
140 seq data described earlier (**Supplementary Figure 1D**). We found that the IL1R1 protein was
141 also lower in HT1080-LT cells (flow cytometry; **Figure 1C**; Western Blot in **Supplementary**
142 **Figure 1I**). Consistent with this, expression of IL1R1 at the cell surface was significantly lower in
143 HT1080-LT compared to HT1080 cells (**Figure 1D**).

144 **Telomere-dependent IL1R1 regulation in xenograft tumors**

145 We generated xenograft tumours using HT1080 and HT1080-LT cells in NOD-SCID mice (see
146 methods for details). We confirmed that there was higher expression of *TERT* and *TERC* in the
147 HT1080-LT xenograft tumours (**Supplementary Figure 1J**). We found that the xenograft tumours
148 from HT1080-LT cells had higher mean telomere length than those from HT1080 cells and had
149 lower IL1R1 expression at the protein level (**Figure 1E**). It was observed that TRF2 occupancy
150 (**Figure 1F**), as well as *IL1R1* mRNA (**Figure 1G**) expression, was lower in HT1080-LT-derived
151 xenograft tumours.

152

153 **TERT-inducible model of telomere elongation in fibrosarcoma cells**

154 Telomere-dependent TRF2 binding at the *IL1R1* promoter was further checked using *hTERT*-
155 inducible HT1080 cells that gradually increased telomeres by ~50% over 12 days following hTERT
156 induction (**Figure 1H**, **Supplementary Figure 1K**): gradual reduction of *IL1R1* promoter TRF2
157 binding (**Figure 1I**) and *IL1R1* expression (**Figure 1J**) with telomere elongation over the 12 days
158 was notably consistent with observations made using HT1080/HT1080-LT cells (**Figure 1A-B**).

159 **Telomere elongation model in MDAMB231 breast cancer cell line**

160 An alternative telomere elongation model was made from TNBC (triple negative breast cancer)
161 MDAMB-231 cells using G-rich-telomere-repeat (GTR) oligonucleotides as reported earlier
162 (Mukherjee et al., 2018; Wright et al., 1996). In the resulting MDAMB-231-LT cells with ~1.8-2-
163 fold increase in TL (**Supplementary Figure 1L**), *IL1R1* promoter TRF2 occupancy and *IL1R1*
164 expression were significantly lower (**Figure 1K-L**). The results collectively suggest that TRF2
165 occupancy at the *IL1R1* promoter and the expression of the gene is telomere length dependent.

166

167 TRF2 transcriptionally activates *IL1R1*

168 We, next, investigated the role of TRF2 in the regulation of *IL1R1*.TRF2 over-expression (Flag-
169 TRF2) showed an increase in *IL1R1* mRNA expression and protein, and TRF2 silencing reduced
170 *IL1R1* in HT1080 cells (**Figure 2A**, and **Supplementary Figure 2A**) indicating that TRF2
171 activated *IL1R1* expression. Flag-tagged TRF2-full-length, or a truncated version of flag-tagged
172 TRF2 protein without the necessary domains for DNA binding [N-terminal Basic-domain (TRF2-
173 delB) or C terminal MYB-domain (TRF2-delM)], showed that both TRF2 occupancy and *IL1R1*
174 promoter activity was compromised in case of the mutants; indicating TRF2 DNA binding as
175 necessary for *IL1R1* activation (**Figure 2B-C**). We developed a doxycycline-inducible TRF2
176 model using HT1080 cells. Upon induction of TRF2, IL1R1 expression was also enhanced
177 (**Figure 2D-E**). We checked and found that IL1R1 expression of the cell surface was also
178 significantly higher in cells with higher TRF2 (**Figure 2F**). Further, TRF2-dependent activation
179 of *IL1R1* was clear in MDAMB-231 cells (**Supplementary Figure 2B**), normal MRC5 fibroblasts
180 and HEK293T cells (**Supplementary Figure 2C**). HT1080 cells with doxycycline-inducible-TRF2
181 were used to make tumour xenografts in NOD-SCID mice. TRF2-induced tumours had enhanced
182 IL1R1 relative to the xenograft tumours where TRF2 was not induced (**Figure 2G**).

183

184

185 **G-quadruplex DNA secondary structure necessary for TRF2 binding to the *IL1R1***
186 **promoter**

187 We reported TRF2 binding to G-quadruplex (G4) DNA secondary structures within promoters
188 throughout the genome (Mukherjee et al., 2019a); further, the role of G4s in epigenetic regulation
189 was noted (Mukherjee et al., 2019b). Here, we found two G4s within the *IL1R1* promoter TRF2-
190 binding site (**Figure 3A, Supplementary Figure 3A**). We confirmed that the DNA sequences
191 formed G4 structures in solution and specific base substitutions disrupted the structure formation
192 (**Figure 3B**); both G4 forming motif sequences showed the characteristic Circular Dichroism
193 signatures for 'parallel' G-quadruplex structures which were largely abrogated when the
194 sequences were mutated (**Figure 3B**). BG4 antibody (against G4s (Biffi et al., 2013)) ChIP was
195 enriched ~200 bp upstream on the *IL1R1* promoter in HT1080 cells(**Figure 3C**); TRF2-dependent
196 *IL1R1* promoter activity was significantly compromised on introducing G4-deforming G>T
197 substitutions on both the G4 motifs (**Figure 3D**), while the effect of the mutation was more for G4
198 motif B. In the presence of the intracellular G4-binding ligand 360A (Granotier et al., 2005), the
199 TRF2 occupancy in HT1080 cells was found to be significantly reduced at the *IL1R1* promoter
200 consistent with results from other TRF2 binding sites (Mukherjee et al., 2019a) (**Supplementary**
201 **Figure 3B**). Upon treatment of HT1080 cells with 360A, TRF2-induced IL1R1 promoter activity,
202 and expression/protein were significantly reduced (**Figure 3E**). Using CRISPR, we artificially
203 inserted an *IL1R1* luciferase-reporter-cassette (-1500 bp) at the CCR5 safe-harbour locus in
204 HEK293T cells; TRF2-dependent promoter activity from the inserted *IL1R1* promoter-reporter and
205 TRF2 binding was reduced when the G4 motif B was mutated supporting earlier results (**Figure**
206 **3F-G**). Furthermore, CRISPR-mediated G>T editing in the G4 motif (motif B) within the
207 endogenous *IL1R1* promoter resulted in a reduction of TRF2 binding and *IL1R1* expression
208 (**Supplementary Figure 3C-D**).

209 **TRF2-dependent recruitment of histone acetyltransferase p300 induces H3K27ac**
210 **modification at the *IL1R1* promoter**

211 We had previously reported that TRF2 occupancy alters the local epigenetics at gene
212 promoters(Mukherjee et al., 2018). Here we sought to understand if TRF2 occupancy brought
213 about any epigenetic alteration at the *IL1R1* promoter. Screening of activation (H3K4me3 and

214 H3K27ac) and repressive (H3K27me3, H3K9me3) histone marks at the *IL1R1* promoter following
215 TRF2 induction, showed enhanced H3K27acetylation (**Supplementary Figure 4A**). In both
216 HT1080 and MDAMB-231 cells, *IL1R1* promoter H3K27 acetylation increased/reduced on TRF2
217 induction/silencing respectively (**Figure 4A**). We sought to find a potential histone
218 acetyltransferase (HAT) and noted canonical HATs p300/CBP(Roth et al., 2003) at the *IL1R1*
219 promoter in multiple cell lines in ENCODE (**Supplementary Figure 4B**). ChIP-qPCR confirmed
220 p300 occupancy within upstream 200-400 bp promoter of *IL1R1* in TRF2-up conditions, which
221 reduced significantly on TRF2 downregulation, in HT1080 and MDAMB-231 cells (**Figure 4B**).
222 Furthermore, occupancy of acetylated-p300/CBP (activated HAT) was enriched at the *IL1R1*
223 promoter on TRF2-induction in HT1080 cells (**Figure 4C**). Together these showed TRF2-
224 mediated recruitment and acetylation of p300/CBP, resulting in H3K27 acetylation at the *IL1R1*
225 promoter. *IL1R1* promoter occupancy of p300, CBP, ac-p300/CBP and H3K27ac was relatively
226 low in HT1080-LT compared to HT1080 cells with shorter telomeres (**Figure 4D**) consistent with
227 lower TRF2 occupancy at the *IL1R1* promoter in LT cells (**Figure 1A**).

228 A recent work showed that TRF2 can physically interact with p300 and p300 acetylates TRF2 at
229 specific lysine residues(YR and IK, 2013). We found that TRF2 directly interacted with p300,
230 evident from co-immunoprecipitation using lysate from HT1080 cells (**Supplementary Figure**
231 **4C**). To ascertain direct TRF2-p300 interaction and consequent H3K27 acetylation, we did
232 histone-acetyl-transfer assays using purified p300, histone H3, and acetyl-CoA (substrate for the
233 acetyl group) with or without recombinant TRF2. Transfer of the acetyl group to histone H3 was
234 significantly enhanced in the presence of both TRF2 and p300, relative to p300 only; and TRF2
235 co-incubated with p300 without H3 gave marginal HAT activity (**Supplementary Figure 4D**).
236 These together demonstrate a direct function of TRF2 in recruitment and HAT activity of p300 in
237 H3K27 acetylation at the *IL1R1* promoter.

238 Acetylation of TRF2 at Lysine residue 293 is necessary for p300 recruitment on the 239 *IL1R1* promoter

240 We sought to understand if the acetylation of TRF2 was important for p300-TRF2 complex
241 recruitment to the *IL1R1* promoter. We found that several residues on TRF2 have been reported
242 to be acetylated /deacetylated (Rizzo et al., 2017; YR and IK, 2013) (**Figure 5A**). To test the
243 direct function of TRF2 acetylation in p300 recruitment, Flag-TRF2 mutants (K176R, K179R,
244 K190R and K293R (Rizzo et al., 2017; YR and IK, 2013)) were screened (**Figure 5B**) for effect
245 on *IL1R1* expression. TRF2-K293R gave notably compromised activation of *IL1R1* at mRNA and

246 protein levels (**Figure 5B-D**). The binding of flag-TRF2-293R at the *IL1R1* promoter was similar
247 to TRF2-WT (**Figure 5E**) suggesting that the loss in *IL1R1* activation was not due to lower
248 promoter binding by TRF2-293R. However, TRF2-293R significantly reduced p300 and ac-
249 p300/CBP recruitment on the *IL1R1* promoter relative to TRF2-wildtype (WT) induction (**Figure**
250 **5E**). TRF2 293R also showed lower physical interaction with p300 in an immunoprecipitation
251 experiment in comparison to TRF2 WT (**Supplementary Figure 5A**). The TRF2 mutant K293R,
252 devoid of H3K27 acetylation activity, gave a loss of function (**Figure 5B-D**). Therefore, TRF2-
253 K293R was fused to dead-Cas9 (dCas9-TRF2-K293R), and dCas9-TRF2 was used as control.
254 On using sgRNA against the *IL1R1* promoter, we found significant activation or downregulation
255 of *IL1R1* in the case of dCas9-TRF2 or dCas9-TRF2-K293R, respectively, in HT1080 and
256 MDAMB231 cells. In contrast, other TRF2-target genes (Mukherjee et al., 2018) remained
257 unaffected indicating single-gene specificity (**Figure 5F**). We further checked the role of the TRF2
258 mutant K293R on other targets of TRF2 that we had previously validated(Mukherjee et al., 2019a)
259 (**Supplementary Figure 5B**). While the TRF2 mutant K293R did not show much effect on genes
260 wherein TRF2 acted as a transcriptional repressor, the effect on the candidate 'activation' targets
261 of TRF2 was not uniform as well. The Lysine 293 in TRF2 seems to be important for activation
262 but not repression. However, while the mutant K293R diminished TRF2-mediated activation of
263 *IL1R1* and *PDGFR-B*, it did not affect *WRNIP1*. This suggests that the TRF2 PTMs might have
264 context-dependence at specific loci in the genome.

265

266 Cancer cells with higher TRF2 are sensitive to IL1-mediated NF-kappaB (p65) 267 activation

268 Primarily ligands IL1A/B via receptors IL1R1/R2 activate IL1 signaling through NF-KappaB
269 (p65/RELA)-Ser536 phosphorylation (A et al., 2010). This induces *IL1B* and other inflammatory
270 genes including *IL6, IL8* and *TNF.* Here we checked NF-kappaB-Ser536 phosphorylation
271 following stimulation with IL1B in the presence/absence of TRF2 in HT1080 and MDAMB-231
272 cells. TRF2-induction gave relatively enhanced NF-kappaB-Ser536 phosphorylation that
273 sustained for a longer duration compared to uninduced controls in both cell types; total NF-
274 kappaB levels remained unaltered (**Figure 6A-B**). Accordingly, on stimulation with either IL1A or
275 IL1B in a TRF2-silenced condition, expression of the NF-kappaB targets *IL6, IL8* and *TNF* were
276 reduced (**Figure 6C**). Further, the ligand TNFα was reported to induce NF-kappaB in an IL1-
277 independent fashion (Liu et al., 2017) suggesting this pathway would be unaffected by the

278 presence/absence of TRF2. Indeed, the expression of NF-kappaB targets (*IL6, IL8* and *TNF*)
279 remained unaffected upon stimulation by TNFα in the absence of TRF2, supporting the role of
280 TRF2 in IL1 signalling specifically (**Figure 6C**). Additionally, TRF2 induction enhanced the
281 expression of *IL6*, *IL8* and *TNF*, which was rescued in the presence of the receptor antagonist
282 IL1RA, further confirming the specific role of TRF2-IL1R1 in NF-kappaB activation (**Figure 6D**).
283 When tested in NOD SCID mouse xenograft tumour samples, we observed that the ratio of
284 phosphor-NF-kappaB to total NF-kappaB B was significantly higher in TRF2-induced tumours
285 (**Figure 6E**).

286 As shown in **Figure 5F** (mRNA expression of *IL1R1*), dCas9-TRF2-K293R diminished IL1R1
287 levels (**Supplementary Figure 6A**).This resulted in reduced NF-kappaB-Ser536 phosphorylation
288 indicating attenuated NF-kappaB activation in HT1080 and MDAMB 231 cells; dCas9-TRF2 as
289 expected showed activation of IL1R1 and NF-kappaB (**Supplementary Figure 6A**).

290 To directly test the function of IL1R1 in TRF2-mediated NF-kappaB activation, *IL1R1*-knockout
291 (KO; CRISPR-mediated) was made in HT1080 cells having doxycline-inducible-TRF2: NF-
292 kappaB activation (Ser536-phosphorylation), including upregulation of the NF-kappaB-target
293 genes *IL2, IL6* and *TNF*, was significantly reduced following TRF2 induction in the KO cells
294 compared to HT1080 cells (**Supplementary Figure 6B**). Together, these demonstrate the direct
295 role of TRF2 in the induction of IL1 signalling through upregulation of *IL1R1*.

296 We reasoned that in cells with longer telomeres IL1 signaling would be affected due to reduced
297 TRF2 binding at the *IL1R1* promoter resulting in attenuated activation of *IL1R1*. In the case of
298 HT1080-LT cells, notable increase in NF-kappaB-Ser536 phosphorylation, following IL1B
299 stimulation, was notably delayed (3 hr in HT10180-LT vs 30 min in HT1080 respectively;
300 **Supplementary Figure 6C**).

301

302 **IL1R1 expression in Triple Negative Breast cancer (TNBC) is sensitive to variation**
303 **in telomere length**

304 To check if our findings were clinically relevant, we used TNBC tumour samples to characterize
305 telomere length and *IL1R1* expression. The IL1(interleukin 1) pathway is relevant in TNBC
306 prognosis as indicated by past studies(Lappano et al., 2020; M et al., 2016), and therefore it was
307 relevant for us to use TNBC samples. We checked 94 TNBC samples and variation in telomeres
308 across tumours was evident (**Figure 7A-C**).

309 We measured TL (telomere length) in tissues from 94 breast cancer [triple-negative breast cancer
310 (TNBC)] patients: Median TL was ~3.6 kb (quantitative-telomeric-RTPCR (O'Callaghan et al.)
311 (Telo-qPCR-see methods); **Figure 7A, Supplementary file 3**). Tumours with TL <50% of median
312 were designated TNBC-short-telomeres (TNBC-ST) and >50% of median length TNBC-long-
313 telomeres (TNBC-LT) (**Figure 1D**). TLs were confirmed by flow cytometry and in-situ hybridization
314 (**Figure 7B**).

315 Further, reads from the whole genome sequence of the TNBC samples were analyzed for
316 estimation of TL using the reported pipline- TelSeq (Ding et al., 2014): TL difference between
317 TNBC-ST and LT was clear, and cancer tissue had lower TL than adjacent normal tissue
318 consistent with earlier reports(Aviv et al., 2017). We found that, while there were inter-tumour
319 telomere length variations, about ~ 70% or more (45 out of 66 TNBC samples and 11 out of 14 in
320 tel-seq analysis) samples for which data was available for adjacent normal tissue – showed lower
321 telomere length in tumour samples (**Figure 7D**).

322 EpCAM^{+ve} (tumour-cell marker) (Went et al., 2004) cells within the TME had significant
323 heterogeneity in TL (lower in TNBC-ST vis-a-vis LT), whereas the difference in TL of EpCAM^{-ve}
324 cells was insignificant indicating TL variation in TME was primarily from cancer cells (**Figure 7E**
325 and **Supplementary Figure 7A**). Details for the Tel-seq data have been tabulated with details of
326 TL estimation for individual samples (**Supplementary Figure 7B**). We surprisingly found that
327 telomerase activity negatively correlated with telomere length in TNBC (**Supplementary Figure**
328 **7C**), and while *TERT* was not found to be significantly higher, *TERC* was found to be significantly
329 enhances in TNBC-LT samples (**Supplementary Figure 7D**). This indicates that *TERC* is
330 possibly a more important determinant for telomere length in TNBC.

331 Next, along with *IL1R1*, a curated set of pro- and anti-inflammatory cytokines commonly studied
332 concerning tumour immunity (B Homey, 2002; Briukhovetska et al., 2021) was screened in TNBC
333 tissue (12 patients- 6 long telomere, 6-short telomere). We found that *IL1R1, IL1B, TNF and IL3*
334 were lower in long telomere samples (**Figure 7F**). Patient-derived organoids (TNBC-organoids
335 from short (TNBO-ST) or long (TNBO-LT) telomeres) (**Supplementary Figure 7E**) were made
336 and tested for telomere length. We found that the expected difference in telomere length was
337 observable between the TNBO-ST and TNBO-LT samples (**Figure 7G**). When the same set of
338 genes as in **Figure 7F** was tested in the TNBO samples, the same trend was observed for *IL1R1*,
339 *IL1B* and *TNF*. In this case, *IL10* was also lower in TNBO-LT samples (**Figure 7H**). Secreted IL1B
340 into the organoid media was also found to be lower in TNBO-LT samples (**Figure 7I**). For

341 comparison, the same genes were looked at in HT1080 tumour xenograft and ex-vivo cells with
342 long/short telomeres (**Figure 7J**).

343 *IL1B* and *IL1R1* expression was significantly low in the case of tumours/cells with relatively long
344 telomeres and notably consistent across clinical tissue, organoids, xenografts and cells, in
345 contrast to the other cytokines which showed model-specific variation (**Figure 7K**). Additionally,
346 mRNA expression correlation from 34 TNBC samples further confirmed the inverse (negative)
347 correlation of *IL1R1* with RTL (relative telomere length) and the consistent positive correlation
348 between *IL1R1* and *IL1B* (**Supplementary Figure 7F**); showed key IL1 signalling genes largely
349 upregulated in the short-telomere cells. Interestingly, *TRF2* showed a strong positive correlation
350 with *IL1R1* and *IL8* but not with other pro-inflammatory cytokines.

351 We, next, used publicly available TCGA gene expression data of breast cancer samples (BRCA)
352 (**Supplementary file 4**) to assess the effect of *IL1R1* expression on cancer prognosis. We
353 categorized samples based on *IL1R1* expression: *IL1R1* high (N=254) and *IL1R1* low samples
354 (N= 709). Notably, overall patient survival was significantly lower in *IL1R1* high samples (Log-
355 rank p value: 0.0149) (**Supplementary Figure 7G**). We also checked the frequency of occurrence
356 of various breast cancer sub-types in *IL1R1* high and low samples (**Supplementary Figure 7H**).
357 While invasive mixed mucinous carcinoma (the most abundant sub-type) was predominantly seen
358 in *IL1R1* low samples, metaplastic breast cancer was only found within the *IL1R1* high samples.
359 Interestingly, metaplastic breast cancer has been frequently found to be 'triple negative', i.e., ER-
360 , PR- and HER2-. (Reddy et al., 2020).

361

362 Telomere length sensitive IL1R1 expression modulates Tumour-associated 363 macrophage (TAM) infiltration in TNBC

364 Previous studies have implicated many telomere-sensitive genes to be related to immune
365 regulation (Barthel et al., 2017; Hirashima et al., 2013). A recent study analyzed transcriptomic
366 data across 31 cancer types to identify genes that are altered with telomere length(Barthel et al.,
367 2017). The authors found that while sub-telomeric genes (up to 10 MB from the nearest telomeres)
368 were altered with changes in telomere length as previously ascribed to the Telomere position
369 effect (TPE) (Baur et al., 2001; Kim et al., 2016; Pedram et al., 2006; Robin et al., 2015), many
370 'telomere-sensitive' genes were distributed far from telomeres throughout the genome. This is
371 consistent with a previous report that telomeres can affect transcription in regions far beyond sub-

372 telomeres independent of TPE(Mukherjee et al., 2018). An intriguing observation made by this
373 study was that when the top 500 genes to be altered with telomere elongation were functionally
374 segregated, the highest number of genes fell under the category of 'Immune response'. When a
375 Gene Ontology analysis was done by us using these genes, 'macrophage inhibitory factor
376 signalling' was the top biological process (**Supplementary Figure 8A**). Recent studies have
377 implicated IL1R1-related signalling in M2 tumour-associated macrophage (TAM) infiltration in
378 tumours(Chen et al., 2023; Zhang et al., 2022). In our data, we had observed consistent change
379 in *IL1R1* and *IL1B* in long versus short telomere tumours and also noted that IL1 signalling has
380 been widely implicated with TAM infiltration in multiple cancers (Carmi et al., 2009; Chittezhath et
381 al., 2014; Lappano et al., 2020; Mantovani et al., 2019).

382 When breast cancer transcriptomic data from TCGA was segregated into high and low *IL1R1*
383 groups (**Supplementary file 4**). Within the differentially expressed genes between high and low
384 *IL1R1* groups, we looked at key immune markers such as reported TAM markers (*CD163,*
385 *MRC1,D86,CD80*), TAM chemo-attractants (*CCL2, CCL3,CCL5, CCL8,CXCL12*) (Unver, 2019)
386 as well as reported tumor infiltrating lymphocyte markers (*CD3G, CD4,CD8A, FOXP3 ,ENTPD1,*
387 *PDCD1*) (**Figure 8A ,Supplementary file 5**). We found that *MRC1* (gene coding for CD206-M2
388 macrophage marker) was the most significantly upregulated marker in *IL1R1* high samples.
389 Interestingly, *TERT* (often correlated/associated with high telomere length) (Greider, 1998;
390 McNally et al., 2019) was found to be significantly downregulated in *IL1R1* high samples. This
391 observation aligns with our finding that *IL1R1* was higher in short telomere samples in TNBC and
392 TNBO.

393 With these in mind, we checked TAM infiltration in TNBC-ST vis-à-vis TNBC-LT. Nine TNBC-ST
394 and nine TNBC-LT tumours were analyzed for M2-type TAMs by double-positive CD11b
395 (monocyte-derived cells) (Cassetta et al., 2016) and CD206 (M2-specific) (Jaynes et al., 2020)
396 labelling: TNBC-LT had relatively low TAM infiltration (mean 1.78%, range: 0.18 – 5.41%) than
397 TNBC-ST (mean 7.34%, range: 3.76-16.80%; **Figure 8B**,**Supplementary Figure 8B**).
398 Accordingly, CD206 expression was found to be lower in tissue sections from TNBC-LT relative
399 to TNBC-ST tumours (**Figure 8C**). We further found that the total proportion of immune cells (%
400 of CD45 +ve) did not vary significantly between short and long telomere TNBC samples
401 (**Supplementary Figure 8C**). However, TNBC-ST samples had a higher percentage of myeloid
402 cells (CD11B +ve) within the CD 45 +ve immune cell population. We checked in three TNBC-ST
403 and TNBC-LT samples and found that the percentage of M1 macrophages (CD86 ^{high} CD 206 ^{low})
404 in the myeloid population was lower than that of the M2 macrophages (CD 206 ^{high} CD 86 ^{low}) and

405 unlike the latter, did not vary significantly between TNBC-ST and TNBC-LT samples
406 (**Supplementary Figure 8C**).

407 We used the available data for *TERT/TERC* expression for a subset of the samples and plotted
408 the telomerase activity for these TNBC samples (**Supplementary Figure 8D**). Upon checking we
409 found that while *TERT* did not significantly correlate with either telomere length or telomerase
410 activity, the correlation with *TERC* was significant with telomere length. *TERC* was earlier shown
411 to vary significantly between short and long-telomere TNBC samples (**Supplementary Figure**
412 **7D**). Therefore, in TNBC, *TERC* seems to be critical for telomere length. Individually, neither
413 *TERT* nor *TERC* correlated significantly with % TAM in TNBC tissue. As expected from our other
414 results, % TAM correlated significantly with RTL. This indicates that in TNBC tissue, telomere
415 length is possibly a more important determinant for TAM infiltration than either *TERT*, *TERC* or
416 telomerase activity.

417 TAM infiltration was further tested using patient tumour-derived organoids from five long and five
418 short telomere cases. M2-type macrophage derived from THP1 cells (**Supplementary Figure**
419 **8E**) were labelled (red-tracker dye) before co-incubating with each of the five TNBO-ST or five
420 TNBO-LT: Following 12 hr incubation TNBO-ST had on average 8.56% infiltration of M2-type
421 macrophages (range: 6.54-10.9%) compared to 3.14% (range: 0.99-4.88%) for TNBO-LT (**Figure**
422 **8D**).

423 Further, we used the IL1R1-receptor antagonist IL1RA to directly test IL1R1 dependence. The
424 minimum dosage of IL1RA where expression of inflammatory markers was found to be altered in
425 TNBO was used in the assays (**Supplementary Figure 8F**). Organoids treated with IL1RA before
426 co-incubating with dye-labelled M2-type macrophages showed >50% reduction in macrophage
427 infiltration (**Figure 8E**).

428 Finally, we screened several G4 binding ligands in MDAMB231 cells and found that a few ligands
429 (JD83, 12459 and NMM) could reduce *IL1R1* expression (**Supplementary Figure 8G**). These
430 ligands were tested in TNBO and we found JD83 to be effective in reducing *IL1R1* expression at
431 5 μM concentration (**Figure 8F**). We found that JD83 is also effective in reducing M2 migration in
432 TNBO, showing promise for future therapeutic interventions.

433

434

435 **Discussion**

436 Recently we described the TL-sensitive expression of genes distant from telomeres (Mukherjee
437 et al., 2018). Cells with relatively long telomeres sequestered more TRF2 at the telomeres
438 affecting non-telomeric binding, and vice-versa. Proposed as the telomere-sequestration-partition
439 (TSP) model (Vinayagamurthy et al., 2020), this is independent of telomere-positioning-effect
440 (TPE) on expression of sub-telomeric genes (up to 10 Mb from telomeres) (Robin et al., 2014).
441 TL-dependent *IL1R1* activation by non-telomeric TRF2 is in tune with the TSP model. It needs to
442 be noted that the *IL1R1* gene is located above 100 MB away from the nearest telomere in humans,
443 and hence far out of the proposed 10MB range of the TPE model. Altered transcription when
444 telomere maintenance is affected in varied contexts (Hirashima et al., 2013; Mukherjee et al.,
445 2018), particularly across 31 cancer types(Barthel et al., 2017), appears consistent with TSP and
446 support our observations related to TL-dependent IL1 signalling. A model of telomere length and
447 TRF2-dependent *IL1R1* expression and the potential modulation of TAM infiltration is presented
448 as a graphical summary (**Figure 9**).

449 Besides TRF2, the non-telomeric function of the shelterin protein RAP1 has been reported as part
450 of complex with NF-kappaB (Teo et al., 2010). Although TRF2 has been implicated in influencing
451 Natural Killer (NK) cells and infiltration of Myeloid Derived immuno-Suppressive Cells (MDSC)
452 (Biroccio et al., 2013; Cherfils-Vicini et al., 2019) underlying mechanisms were unclear. However,
453 the function of non-telomeric TRF2 in either IL1 signaling or in a telomere-sensitive role in immune
454 signalling, has not been previously studied.

455 Mechanistically, we found that DNA secondary structure G4s present on the *IL1R1* promoter are
456 necessary for TRF2 binding. Perturbation of the G4s genetically by destabilizing base
457 substitutions, or upon using small molecules that bind to G4 inside cells resulted in reduced
458 promoter TRF2 binding and *IL1R1* expression. This is in line with our earlier results showing G4-
459 dependent non-telomeric TRF2 binding throughout the genome, and how TRF2 recruitment to
460 specific promoters leads to epigenetic histone modifications (Mukherjee et al., 2019a, 2019b,
461 2018; Shalu Sharma et al., 2021). We recently noted the transcription repression of telomerase
462 (*hTERT*) to be TRF2-mediated in a PRC2-repressor-dependent fashion(Shalu Sharma et al.,
463 2021).This, interestingly, suggests the emerging role of TRF2 as a transcriptional modulator with
464 repressor/activator (as shown here) functions depends on cofactor engagement that is possibly
465 contextual.

466 The histone-modifying enzyme complex-p300/CBP have been keenly studied in cancer
467 epigenetics specifically breast cancers (Iyer et al., 2004; Ramadan et al., 2021; Ring et al., 2020).
468 Recent findings also show acetylated H3K27 enrichment at the telomeres through p300-
469 dependent HAT activity (Cubiles et al., 2018); however role of TRF2 in p300 engagement or
470 H3K27 acetylation at the telomeres was not investigated. Here, notably, we found TRF2-
471 dependent p300 recruitment, and HAT activity resulting in H3K27 acetylation at the *IL1R1*
472 promoter. Together, these support the role of non-telomeric TRF2 as an activating transcription
473 factor through p300 implicating a broader role of TRF2-p300-dependent histone modifications in
474 cancer. Further, these suggest the possibility of similar functions of telomeric TRF2 in H3K27
475 acetylation at the telomeres (Cubiles et al., 2018). The lysine residue K293 acetylation on TRF2
476 seems to be crucial for p300-TRF2 interaction.

477 It has been noted previously that TERT can have effects on NF-kappa B signalling independent
478 of telomere length alterations(Ghosh et al., 2012). We observed that in long telomere HT1080-LT
479 cells, while NF-kappa B signalling was retarded- a late surge of NFKappa-B activation occurred.
480 We are inclined to think this could be a potential effect of TERT over-expression. Understanding
481 the extent to which TERT influences the inflammatory signalling in TNBC independent of telomere
482 length would require further work.
483
484 IL1 signalling in relation to inflammation in cancer has been extensively studied and consequently,
485 IL1B blockers and the receptor antagonist IL1RA are of clinical interest (B Homey, 2002;
486 Chittezhath et al., 2014; F Balkwill et al., 2001; Kaplanov et al., 2019; Lappano et al., 2020).
487 Further, the effect of altered IL1 signalling on M2-type TAM infiltration was reported in multiple
488 cancer types (Chanmee et al., 2014; Hu et al., 2015). TAM infiltration has been consistently linked
489 to tumour aggressiveness (Oner et al., 2020) and recent work on targeting (Lee et al., 2019; TL
490 and I, 2011) and modifying TAMs from M2-like states to a more anti-tumourigenic M1-like states
491 (Jaynes et al., 2020) have shown promise as strategies for intervention in cancer. The clinical
492 significance of blocking IL1 signalling in cancers has been widely reported (Briukhovetska et al.,
493 2021; Kaplanov et al., 2019; Mantovani et al., 2018). Based on our findings, we attempted TRF2-
494 mediated single-gene-targeted epigenetic silencing of *IL1R1* in cell lines and ligand-based
495 approaches in TNBC organoids. A combination of single gene editing and small molecule/ ligand-
496 based intervention might be useful in therapy.

497 For the functional significance of TL in TME, we focused on IL1-signalling and TAM. Results from
498 TNBC organoids here show that blocking IL1R1 using IL1RA was sufficient for restricting M2

499 infiltration (**Figure 8E**) suggesting that the IL1 signaling within the tumour cell is important.
500 However, particularly because macrophages are known to be a rich source of IL1B (Carmi et al.,
501 2009; Duque and Descoteaux, 2014; Mantovani et al., 2018), and given the model-specific
502 changes in inflammatory cytokines noted by us, further experiments will be required to understand
503 how telomeres influence paracrine/ juxtracrine IL1 signalling between cancer cells and TAM.

504 It is quite possible that TL affects tumour-immune signalling through other immune cell types as
505 well (implied by altered immune-response genes in TL-dependent gene-expression analysis
506 (Barthel et al., 2017; Hirashima et al., 2013)) and/or influences the nature of TAM (Hung et al.,
507 2016), which is known to vary contextually (Mantovani and Locati, 2013). These possibilities,
508 together with the well-established effect of IL1-targeting in improving cancer prognosis
509 (Briukhovetska et al., 2021; Cristofari and Lingner, 2006; Mantovani et al., 2019, 2018) underline
510 the need for further work to attain a deeper understanding of telomere-sensitive IL1 signalling in
511 the TME.
512
513 Although we observed a range of telomere lengths across cancers in TNBC patients (**Figure 7A-**
514 **C**), as also noted by other groups (Londoño-Vallejo, 2004; Pellatt et al., 2013; Shen et al., 2007;
515 Wentzensen et al., 2011; Willeit et al., 2010), tumours largely have been reported to maintain
516 shorter telomeres than normal tissue (Aviv et al., 2017). Here we found that tumour cells with
517 shorter TL-activated IL1 signalling increase M2-type TAM infiltration, which is known to aid
518 immunosuppression (Allavena et al., 2008). Based on our results, and other reports suggesting
519 immunomodulation in cancers with relatively short telomeres (Barthel et al., 2017; Hirashima et
520 al., 2013), it is therefore tempting to speculate that short-telomere cancer cells might be
521 'selectively' better equipped to evade host immune cells. To sum up- our work reveals new
522 molecular connections between telomeres and tumour immunosuppression, presenting a
523 conceptual framework for a better understanding of patient-specific responses to cancer
524 immunotherapy.

525

526

527

528

529

530 ## Materials and Methods:

531 ### Cell lines, media and culture conditions

532 HT1080 fibrosarcoma cell line was purchased from ATCC. HT1080-LT cells(Cristofari and
533 Lingner, 2006) were a kind gift from Dr. J. Ligner. HT1080 and MRC5 (purchased from ATCC)
534 cells and corresponding telomere elongated cells were maintained in Modified Eagle's medium
535 (MEM) (Sigma-Aldrich) supplemented with 10% Fetal Bovine Serum (FBS) (Gibco). MDAMB231
536 (gift from Mayo Clinic, Minnesota, USA) and HEK293T (purchased from NCCS, Pune) cells were
537 maintained in DMEM-HG (Dulbecco's Modified Eagle's medium - High Glucose) (Sigma-Aldrich)
538 with a supplement of 10% FBS. All THP1 cell lines (gift from Dr Vivek Rao, IGIB, Delhi and
539 subsequently purchased from NCCS, Pune) and derivative cell types were maintained in RPMI
540 with 10% FBS and 1X Anti-Anti (anti-biotic and anti-mycotic from Thermo Fisher Scientific). All
541 cultures were grown in incubators maintained at 37ºC with 5% CO_2. All stable lines generated
542 from these cell types were maintained in the same media with 1X Anti-Anti.

543 ### Processing of tumour/xenograft tissue:

544

545 Tissues collected for this study were stored in RNA later (Sigma-Aldrich) at -80 °C. Approximately
546 10 milligrams of tumour tissue were weighed and washed thrice with ice-cold 1X PBS- 1 ml
547 (filtered). About 300 microlitres of PBS was left to submerge the tissue after the final wash. Using
548 a sanitized razor blade, the tumour was cut into small pieces (the efficiency of the digestion is
549 dependent on how well the tumour is minced; large pieces will not digest properly and may need
550 extra digestion time). The tumour soup was transferred into a 15 ml tube using a P1000 pipette
551 (cut the top of the tip to be able to take all the tissue) and the volume was adjusted to 4 ml of 1X
552 pre-chilled PBS. 80 µl of Liberase TL stock solution (Roche) was mixed using a vortex and
553 incubated for 45 min at 37 °C under continuous rotation. The sample was checked visually; the
554 cell suspension should look smooth (if the cell suspension still contains tissue fragments digest
555 for an additional 15 min). To end the enzymatic digestion,10 ml PBS with 1 % w/v BSA (Sigma-
556 Aldrich) was added. The cells were filtered using a 100 µm cell strainer in a 50 ml tube and the
557 volume adjusted to 20 ml with 1X PBS (pre-chilled). Cells were centrifuged for 7 min at 500 g and
558 4 °C. The supernatant was discarded and the cells were re-suspended in 1 ml Serum-free
559 media. Subsequently, cells were counted and volume was made up to get a cell density of 1
560 million cells/ ml. Following this, the cell suspension was used for ChIP, DNA/RNA isolation and
561 flow cytometry.

562

563 **Organoid generation and culture:**

564

565 TNBC tissue was used to make tumour organoids using the following protocol-

566 1. The fresh tissue was stored in 5 ml of Media 1 (Advanced DMEM F12 + 1X Glutamax + 10mM
567 HEPES + 1X AA).

568 2. 1-3 mm^3 tissue piece was cut, washed and minced in 10ml (Media 1).

569 3. The minced tissue was digested overnight on a shaker in Media 1 with 1-2mg/ml of collagenase.

570 4. After overnight incubation the digested tissue was sequentially sheared using a 1 ml pipette.

571 5. After each shearing step, the suspension was strained using a 100µm filter to retain tissue
572 pieces. Thus entering in subsequent shearing step with approximately 10 ml Advanced DMEM
573 F12.

574 6. To this, 2% FCS was added and centrifuged at 400 g.

575 7. The pellet was resuspended in 10mg/ml cold cultures growth factor reduced BME Type 2 and
576 40µl drops of BME suspension was allowed to solidify on pre-warmed 24 well culture plates at
577 37°C 5% CO_2 for 30 min.

578 8. Upon complete gelation 400 µl of BC organoid medium was added to each well and plates
579 transferred to 37°C 5% CO_2.

Medium component	Supplier	Catalogue number	Final concentration
R-Spondin 3	R&D	3500-RS/CF	250 $ng \cdot ml^{-1}$
Neuregulin 1	Peprotech	100-03	5 nM
FGF 7	Peprotech	100-19	5 $ng \cdot ml^{-1}$
FGF 10	Peprotech	100-26	20 $ng \cdot ml^{-1}$
EGF	Peprotech	AF-100-15	5 $ng \cdot ml^{-1}$ [a]
Noggin	Peprotech	120-10C	100 $ng \cdot ml^{-1}$
A83-01	Tocris	2939	500 nM
Y-27632	Abmole	Y-27632	5 mM

SB202190	Sigma	S7067	500 nM [b]
B27 supplement	Gibco	17504-44	1x
N-Acetylcysteine	Sigma	A9165-5g	1.25 mM
Nicotinamide	Sigma	N0636	5 mM
GlutaMax 100x	Invitrogen	12634-034	1x
Hepes	Invitrogen	15630-056	10 mM
Penicillin/Streptomycin	Invitrogen	15140-122	100 $U \cdot ml^{-1}$ / 100 $mg \cdot ml^{-1}$
Primocin	Invivogen	Ant-pm-1	50 $mg \cdot ml^{-1}$
Advanced DMEM/F12	Invitrogen	12634-034	1x

9. The media was changed every fourth day.

10. The culture was grown for 10 days before passaging.

II. Passaging Organoid Cultures

1. Cultrex growth factor reduced BME Type 2 geltrex was thawed overnight on ice at 4 °C.

2. Media was removed from the organoid wells and washed twice with PBS-EDTA.

3. For each well of 24 well plate 300 µl of TrypLE was added and incubated at 37°C 5% CO_2 for 5 min.

4. 600 µl of washing media (DMEM F12) was added and organoids were dissociated vigorously by pipetting.

5.. Organoid solution was transferred to 15 ml falcon with 5 ml washing media and centrifuged at 1000rpm for 5 min to pellet organoids.

6. Supernatant was carefully aspirated leaving behind 200ul media and 500ul of fresh media, mixed well gently and transferred to 1.5ml tube for centrifugation at 650*g for 5min at 4 °C .

7. Supernatant was gently aspirated and resuspended in cold cultrex and 40ul drop/well was seed in a pre-warmed 24 well plate.

8. Incubated for 30 min and add 400 µl of BC organoid medium.

598 **M2 macrophage generation from THP1 cells:**

599 THP1 cells (0.5 million cells in 1ml) were seeded in a 35 mm dish and treated with PMA (10 ng/ml)
600 (Sigma-Aldrich) for 24 hrs in RPMI complete media (+ 10% FBS) (Gibco). PMA was removed and
601 cells were cultured for 48 hrs in RPMI to get semi-adherent M0 cells. Following this, cells were
602 treated with IL4 (10 ng/ml) (Gibco) and IL13 (20 ng/ml) (Gibco) for 24 hrs in RPMI complete media.
603 Cells were checked for expected morphological changes and trypsinized for use as M2
604 macrophages.

605 **M2 macrophage infiltration assay in TNBC tumour organoids:**

606 M2 macrophages were labelled with Cell Tracker red dye (Thermo Fisher Scientific) for 30 mins
607 and the excess dye was washed off. 10000 labelled M2 macrophages in 20 ul 1X PBS were
608 introduced in a 96 well with TNBC organoids in a dome with supplement enriched media (200 µl).
609 12 hrs. later, the media was washed off with 3 1X PBS washes and the organoid dome was
610 extracted with 100 µl TrypLE (Gibco) and resuspended with 100 ul chilled 1X PBS. This cocktail
611 was kept on ice for 5 mins and centrifuged at 1000g for 10 mins. The supernatant was removed
612 and the process was repeated.

613 The cells were resuspended in 500 ul chilled 1X PBS and subjected to Flow-cytometric analysis
614 for scoring percentage of labelled (red) M2 macrophages infiltrating the organoids.

615 **Xenograft tumour generation in NOD-SCID mice:**

616 The xenograft tumour generation in NOD SCID tumours was outsourced to a service provider (
617 Vivo Bio TechLtd – Telangana, India). 2.5 million cells (HT1080, HT1080-LT or HT1080-TRF2
618 inducible) were subcutaneously injected in healthy male mice (4-6 weeks old) and tumour growth
619 was allowed. In case of TRF2 inducible HT1080 cells, tumours were allowed to grow to 100 mm^3
620 before oral dosage of doxycycline (or placebo control) was started at 2 mg/kg of body weight of
621 mice. Mice were sacrificed to obtain tumours when tumours reached an average volume of 600
622 mm^3(± 100).

623 **Telomeric Fluorescent *in-situ* hybridization (FISH)**

624 Telomere-specific PNA probe [TelC-FITC-F1009-(CCCTAA)n from PNABio] was used following
625 the manufacturer protocol with minor modifications. Briefly, the cells grown in chamber slides up
626 to ~70% confluency and were treated with RNase solution for 5-10 mins in 1X PBS at room
627 temperature. For tissue section, rehydrated tissue sections on slides were used prior to RNase

628 treatment. Slides were washed in chilled PBS twice followed by dehydration with an increasing
629 concentration of ethanol gradient. Slides were briefly warmed at 80ºC and then 250 nM PNA was
630 added with hybridization buffer (20 mM Tris, pH 7.4, 60% formamide (Sigma-Aldich), 0.5% of 10%
631 Goat Serum). Slides were heated and covered with the buffer at 85ºC for 10 mins, kept at room
632 temperature in a dark humid chamber for 4 hrs to overnight to facilitate slow cooling and
633 hybridization. The unbound PNA was washed with wash buffer (2X SSC, 0.1% Tween-20(Thermo
634 Fisher Scientific)) followed by PBS wash twice. DAPI solution (Sigma-Aldrich) was added for 5
635 mins and then the slides were washed in PBS. ProLong Gold Antifade Mountant (Thermo Fisher
636 Scientific) was added and the section was covered with a cover glass. Imaging was done with a
637 Leica SP8 confocal microscopy system. Images were analyzed using open source image analysis
638 software Fiji (Image J, imagej.net/software/fiji/).
639

640 **DNA and RNA extraction from TNBC/xenograft tissue:**

641 Allprep DNA/RNA Universal kit (Qiagen) was used as per manufacturer's suggested protocol for
642 extraction of DNA and RNA from single cell suspension prepared from tissues as described
643 before.

644 **Telo-qPCR:**

645 For telomere length assessment by qRT PCR, telomere specific primers and single copy number
646 gene 36B4 for normalization was used in PCR reactions with sample DNA using reported
647 protocol(O'Callaghan et al.).

648 The primers used are as follows:

649 Tel F CGGTTTGTTTGGGTTTGGGTTTGGGTTTGGGTTTGGGTT

650 Tel R GGCTTGCCTTACCCTTACCCTTACCCTTACCCTTACCCT

651 36B4F CAGCAAGTGGGAAGGTGTAATCC

652 36B4R CCCATTCTATCATCAACGGGTACAA

653 The relative telomere length of TNBC patient tissue samples were estimated by normalizing to
654 telomere signal of HT1080 fibrosarcoma cells (reference cell type) as follows:

655 Telomere signal= $2^{-(Ct\ Tel - Ct\ 36B4)}$

656 Relative telomere length (RTL) = Telomere signal (sample) / Telomere signal (reference)

657 **Flow-cytometry:**

658 The procedure for Flow-cytometry was adapted from basic flow cytometry guidelines from CST
659 and has been previously reported in Sharma *et al*,2021(Shalu Sharma et al., 2021). The cell
660 suspension was fixed with 4% formaldehyde and permeabilized with 0.1% triton X (in 1XPBS) for
661 nuclear proteins. Incubation of primary antibody (1:500 v/v in 1% BSA in 1X PBS) for 1 µg/ml
662 antibody concentration for 2 hours at RT or at 4ºCovernight, was followed by PBS wash (3 times)
663 and fluorescently labelled secondary antibody (1:1000 v/v) for 2 hours at RT. Following this, cells
664 were washed with 1X PBS (3 times) and re-suspended in 1XPBS for flow-cytometric analysis
665 using BD Accuri C6 or BD FACSAria III. Equal number of events (10000 for most of the analysis)
666 were recorded for calculating percentage infiltration.

667 For single channel analysis, histogram prolife (log scale) was generated in ungated sample-SSC-
668 FSC plots. For quadrant gating for double positive cells (two channels), biex- scale plots or log
669 scale were used. All statistics like mean fluorescence intensity and standard deviation were
670 estimated using built-in tools for analysis in the software FlowJo.

671 **Relative Telomeres length (RTL) by Flow-cytometry:**

672 The RTL value is calculated as the ratio between the telomere signal of each sample and the
673 control cell. The Telomere PNA Kit/FITC kit from Dako (Agilent) was used to estimate Telomere
674 length signal in samples. The process has been previously standardized and reported (Mukherjee
675 et al., 2018).

676 **TelSeq- estimation of telomere length using sequencing data**

677

678 We used TelSeq(Ding et al., 2014) to estimate the average telomere length (TL) for each tumour
679 and normal sample in our dataset. TelSeq was run with default parameters using WGS(whole
680 genome Sequencing) samples with coverage ≥ 30X, except the read length parameter (-r) which
681 was set to 150 to match with our data. Briefly, the TL was calculated as the total number of reads
682 containing seven or more telomeric repeats (“TTAGGG”) divided by the total number of reads with
683 GC content 48-52%. Further, the resultant value was multiplied with a constant value to account
684 for genome size and the number of telomeric ends. This was done separately for each read group
685 within a sample, and then the weighted average was calculated for each sample by taking into
686 account the number of reads per group (as weights).

687

688 The estimated average TL [represented in Kilobase-pair (Kb) units] for tumour and normal
689 samples has been provided in **Supplementary Figure 7B**. Overall, we found that the tumour
690 samples have lower TL scores (Median: 3.20 Kb) as compared to the matched normal samples
691 (Median: 4.67 Kb). Also, the TL estimates from our tumour samples (Median: 3.20 Kb, range:2.3
692 to 21.10 Kb) were comparable to the TCGA breast cancer cohort (WGS) (Median: 3.5 Kb, range:
693 1.4 to 29.7 Kb) analyzed by Barthel et al, 2017(Barthel et al., 2017).

694

695 To check if the tumour samples with high TL estimates were confounded by the aneuploidy and
696 tumour purity (which was not taken into account in the TelSeq analysis), we computed the purity
697 and ploidy values for each tumour sample (where possible) using ASCAT(Raine et al., 2016)
698 through Sarek pipeline(Garcia et al., 2020). However, we found no significant difference in the
699 purity (Wilcoxon test two-sided P = 0.25) and ploidy (Wilcoxon test two-sided P = 0.52*)* values
700 between tumour samples with high versus low TL scores, suggesting that the tumours with high
701 TL estimates were not influenced by these parameters.

702

703 **IL1B and IL1RA treatment:**

704 Reconstituted IL1B (Sigma-Aldrich) was treated to appropriate cells at 10ng/ml concentration
705 followed by assays. Similarly, IL1RA (Abcam) was treated to appropriate cell/TNBO at 20ng/ml
706 concentration followed by assays at appropriate time points in specific experiments.

707

708 **IL1B ELISA:**

709 IL1B ELISA was performed using Human IL-1 beta/IL-1F2 DuoSet ELISA kit by R&D Biosystems.
710 As per manufacturer's protocol 96 well microplate was coated with100ul per well of freshly
711 prepared Capture Antibody diluted 100 times in PBS without carrier protein. Thereafter the plate
712 was sealed and incubated overnight at room temperature. The following day, the capture antibody
713 was aspirated after which each well was washed three times with 1X Wash Buffer (PBST). After
714 the last wash, the remaining wash buffer was removed carefully and completely by aspiration and
715 blotting it against clean paper towels. The prepped, empty wells were blocked at room
716 temperature for 1hr by adding 300 µL of Reagent Diluent (20% BSA in 1X PBST) to each well.
717 Wash the wells as in the step above. Next we added the samples and standard protein of known
718 increasing concentrations (100ul in volume) diluted in Reagent Diluent. The plates were then
719 covered with an adhesive strip and incubated for 2 hours at room temperature. Post incubation,

720 the wells were washed as above for plate preparation. Following the washes we added 100ul of
721 freshly prepared Detection Antibody diluted 100 times in PBS. The plate was covered and
722 incubated for 2hrs at room temperature. Post incubation the wells were washed thrice as in the
723 previous step. Finally for generating detectable signal we added 100 µL of Streptavidin-HRP to
724 each well, covered the plate and incubated it in dark at room temperature for 20mins. Next the
725 wells were washed thrice as in steps above. After aspirating the wells clean of any buffer we
726 added 100ul of Substrate Solution to each well and incubated the plates again in dark at room
727 temperature for 20minutes. Finally, 50ul of stop solution was added to each well and mixed well
728 by gentle tapping. The signal was measured using a microplate reader set to 450 nm, 570 and
729 540nm. Perform wavelength correction by subtracting readings at 540 nm or 570 nm from the
730 readings at 450 nm.

731

732 **Antibodies**

733 **Primary antibodies:**

734 TRF2 rabbit polyclonal (Novus NB110-57130)- ChIP, IP, WB

735 TRF2 mouse monoclonal (Millipore 4A794)- Flow cytometry

736 TRF1 mouse monoclonal (Novus NB110-68281)-WB

737 IL1R1 rabbit polyclonal (abcam ab106278)- IF, Flow-Cytometry, WB

738 DDK/FLAG mouse monoclonal (Sigma-F1804)- ChIP, WB

739 BG4 recombinant antibody (Sigma Aldrich MABE917)- ChIP

740 P300 (CST D2X6N) rabbit monoclonal- ChIP, IF,WB

741 Ac-p300/CBP (CST 4771) rabbit monoclonal-ChIP,WB

742 CBP (CST 7389) rabbit monoclonal- ChIP,WB

743 P65(NFKB) (CST 8242) rabbit monoclonal- WB

744 Ser536 P p65 NFKB (CST 3033) rabbit monoclonal- WB

745 IKB (CST 4814) mouse monoclonal- WB

746 p-IKB (CST 2589) rabbit monoclonal- WB

747 CD44 (CST 3570) mouse monoclonal-IF

748 Histone H3 rabbit polyclonal (Abcam ab1791)-ChIP

749 H3K27ac rabbit polyclonal (Abcam ab4729)-ChIP

750 H3K4me3 rabbit polyclonal (Abcam ab8580)- ChIP

751 H3K27me3 rabbit monoclonal (abcam ab192985)- ChIP

752 H3K9me3 rabbit polyclonal (abcam ab8898)- ChIP

753 Beta-actin mouse monoclonal (Santacruz C4)-WB

754 GAPDH mouse monoclonal (Santacruz 6C5)-WB

755 CD11b Monoclonal Antibody (ICRF44), eBioscience™- Flow cytometry

756 CD206 Monoclonal Antibody (MR5D3) Invitrogen- Flow cytometry

757 APC anti-human CD326 (EpCAM) (9C4) BioLegend- Flow cytometry

758 FITC anti-human CD11B (ICRF44) BioLegend- Flow cytometry

759 PE anti-human CD45 (HI30) BioLegend- Flow cytometry

760 PE-Cy7 anti-human CD45 (W17233E) BioLegend- Flow cytometry

761 Anti-Rabbit IgG/Anti-mouse IgG (Millipore) was used for isotype control.

762 **Secondary antibodies:**

763 anti-Rabbit-HRP(CST), anti-Mouse-HRP(CST),mouse-ALP (sigma),rabbit-ALP(sigma) anti-rabbit
764 Alexa Fluor 488, anti-mouse Alexa Fluor 594 (Molecular Probes, Life Technologies).

765 **Real time PCR**

766 Total RNA was isolated from cells using TRIzol Reagent (Invitrogen, Life Technologies) according
767 to manufacturer's instructions. For TNBC tissue and xenograft, Allprep DNA/RNA Universal kit
768 from Qiagen was used. The cDNA was prepared using High-Capacity cDNA Reverse
769 Transcription Kit (Applied Biosystems) using manufacturer provided protocol. A relative transcript

770 expression level for genes was measured by quantitative real-time PCR using a SYBR Green
771 (Takara) based method. Gene expression was calculated as 2^{-delCT} with delCT being the
772 difference in threshold cycles (Ct) between test and internal control. *GAPDH* / 18S gene was used
773 as internal control for normalizing the cDNA concentration of each sample. For fold change of
774 gene expression calculations, 2^{-delCT} for the first replicate of the control sample was used for
775 normalization for the samples. Normalized expression values (fold change) were plotted and
776 compared with appropriate statistical testing.

777

778 RT PCR primers used have been enlisted as follows:

mRNA expression primers:

IL1R1FP	GGCTGAAAAGCATAGAGGGAAC
IL1R1 RP	CTGGGCTCACAATCACAGG
TRF2 FP	CAGTGTCTGTCGCGGATTGAA
TRF2 RP	CATTGATAGCTGATTCCAGTGGT
IL1B FP	ATGATGGCTTATTACAGTGGCAA
IL1B RP	GTCGGAGATTCGTAGCTGGA
IL1A FP	AGATGCCTGAGATACCCAAAACC
IL1A RP	CCAAGCACACCCAGTAGTCT
IL2 FP	CATTTGTGGTTGGGTCAGG
IL2 RP	AGTGAGGAACAAGCCAGAGC
IL6 FP	AGCACTCCTTGGCAAAACTG
IL6 RP	CGGAAGGAACCATCTCACTG
TNF FP	GCCAGAGGGCTGATTAGAGA
TNF RP	TCAGCCTCTTCTCCTTCCTG
IL8 FP	GAATGGGTTTGCTAGAATGTGATA
IL8 RP	CAGACTAGGGTTGCCAGATTTAAC
IL10 FP	GACTTTAAGGGTTACCTGGGTTG
IL10 RP	TCACATGCGCCTTGATGTCTG
IL4 FP	CCAACTGCTTCCCCCTCTG
IL4 RP	TCTGTTACGGTCAACTCGGTG
IL13 FP	GAAGGCTCCGCTCTGCAAT
IL13 RP	TCCAGGGCTGCACAGTACA

GAPDH FP	TGCACCACCAACTGCTTAGC
GAPDH RP	GGCATGGACTGTGGTCATGAG
18S FP	TTCGGAACTGAGGCCATGAT
18S RP	TTTCGCTCTGGTCCGTCTTG

779

780 TRF2 target gene expression primers from Mukherjee *et al,* 2018(Mukherjee et al., 2018).

781 **RNA-seq analysis:**

782 RNA was extracted using TRIzol TruSeq RNA Library Prep Kit v2 was used from preparation of
783 libraries for sequencing. Raw Illumina sequencing reads were checked for quality using FastQC
784 (version 0.11.9) followed by adapter clipping and trimming using Trimmomatic (version 0.39)with
785 default parameters. Trimmed reads were then aligned to the human reference genome (GRCh38,
786 GENCODE v36) using STAR aligner (version 2.7.8a)(Dobin et al., 2013). FeatureCounts (subread
787 package version 2.0.1) was used to quantify gene expression(Quinlan and Hall, 2010). Quality
788 checks were performed at each step using the MultiQC tool (version 1.10.1). Differential gene
789 expression analysis was performed using the DESseq2 package (version 1.30.0)(Love et al.,
790 2016) in R (version 4.0.3). The analysis was performed by removing the effects of confounding
791 variables such as batch and replicate using the appropriate design formula. Gene expression was
792 normalized using variant stabilizing transformation (vst) for visualization purposes. Genes with
793 BH-adjusted p value < 0.05 and absolute Log2 fold change greater than 1 (at least 100% fold
794 change in either direction) were taken as significantly differentially expressed. Two replicates for
795 each sample were used for differential gene expression analysis.

796 **ChIP (Chromatin Immunoprecipitation)**

797 ChIP assays were performed as as previously reported by Mukherjee *et al.*,2018,2019(Mukherjee
798 et al., 2019a, 2018). Briefly, 3-5 million cells were fixed with ~1% formaldehyde (Sigma-Aldrich)
799 for 10 min and lysed. Chromatin was sheared to an average size of ~300-400 bp using Biorupter
800 (Diagenode). 10% of the sonicated fraction was processed as input using phenol–chloroform and
801 ethanol precipitation. ChIP was performed for endogenous/ectopically expressed protein using
802 1:100 dilution (v/v) of the respective ChIP grade antibody incubated overnight at 4°C. Immune
803 complexes were collected using Salmon sperm DNA-saturated Magnetic Dynabeads (-50 µg per

804 sample) and washed extensively. Phenol-chloroform-isoamylalcohol was used to extract DNA
805 from the immunoprecipitated fraction. ChIP DNA was quantified by Qubit HS ds DNA kit (Thermo
806 Fisher Scientific). Quantified ChIP samples were validated by qRT-PCR.

807 ChIP enrichment was calculated over 1% input as : $2^{-(\text{ CT ChIP-CT 1\% input})}$. Following this , the ChIP
808 enrichment was normalized to enrichment value for respective IgG (Mock) or total H3 ChIP.

809 The ChIP-qRT PCR primers are as follows:

ChIP- qRT PCR primers:

IL1R1-1000 FP	CCCCTTCCACAGAAGAAACCTGG
IL1R1-1000 RP	CGCAGAAGCCAGTGGGAGG
IL1R1-800 FP	AGCCCAGGTGGGTGCCA
IL1R1-800 RP	ATGACAGAATGATTCTTTGCTCTGTGG
IL1R1-600 FP	TATTTGTCAGGCGCCCCTGG
IL1R1-600 RP	CATACATCTGTGTGTGCCTGGG
IL1R1-400 FP	CAGGAAGCCATACATCTGTGTAGC
IL1R1-400 RP	GAATGTTATACACACACTCATACACACACACA
IL1R1-200 FP	GAGTGTGTGTATAACATTCATTACTGCAAAC
IL1R1-200 RP	ATGAAAAGATACAAGTGAAGAGCTGCC
IL1R1+200 FP	TGGGAGGTGACACCCAGTTTAAG
IL1R1+200 RP	CCAACTCTGGGCCTTCCCAC
IL1R1 3' UTR FP	TCCTTTGACTTATTGTCCCCACT
IL1R1 3' UTR RP	TCTTCAACACTTAGGGCATCTT
IL1R1 -20 KB FP	TTGTCCTGAATAGCCGCAGG
IL1R1 -20 KB RP	CCCTCGAGAAAACAGCCCAT

810

811 **Immunofluorescence microscopy:**

812 Adherent cells were seeded on coverslips and allowed to reach a confluency of ~ 70%. Cells were
813 fixed using freshly prepared 4% Paraformaldehyde by incubating for 10 min at RT. Cells were
814 permeabilized with 0.25% Triton™ X-100 (10 min at RT) and treated with blocking solution (5%
815 BSA in PBS) for 2 hrs at RT. All the above stated were followed by three washes with ice cold
816 PBS for 5 mins each. Post-blocking, cells treated with relevant antibodies (1:500 for TRF2, 1:500
817 for IL1R1 and 1:1000 for CD44/p300) and incubated overnight at 4ºC in a humid chamber. Post-
818 incubation, cells were washed alternately with PBS and PBST three times and probed with
819 secondary Ab (rabbit Alexa Fluor 488(1:1000) / mouse Alexa Fluor 594 (1:1000)) for 2 hrs at RT.

820 Cells were washed again alternately with PBS and PBST three times and mounted with Prolong
821 Gold anti-fade reagent with DAPI. Images were taken on Leica TCS-SP8 confocal microscope/
822 Cytiva Deltavision microscope. Lasers of emission wavelength 405nm, 488nm and 532 nm were
823 used imaging for DAPI, Alexa Fluor 488 secondary Ab and Alexa Fluor 594 Ab respectively. Laser
824 intensity was kept 20% for DAPI and 40-60% for Alexa Fluor secondary antibodies. ImageJ (FIJI)
825 software was used to calculate signal intensity (a.u.).

826 **Western blotting:**

827 For western blot analysis, protein lysates were prepared by suspending cell pellets in 1X RIPA
828 (with 1x mammalian protease inhibitor cocktail). Protein was separated using 10%/12% SDS-
829 PAGE and transferred to polyvinylidenedifluoride membranes (Immobilon FL, Millipore). After
830 blocking, the membrane was incubated with primary antibodies. Post incubation with primary
831 antibodies (1:1000 v/v), the membrane was washed with 1X PBS and then incubated with
832 appropriate secondary antibodies (1:2000 v/v). Following secondary antibody incubation, the
833 membrane was washed with 1XPBS. The blot was finally developed using HRP substrate/BCP
834 NBT and reagents from Millipore.

835

836 **HT1080 TRF2 and TERT inducible cells:**

837 TRF2 cDNA sequence was inserted into pENTR11 vector and the cassette was transferred into
838 lentiviral plasmid pCW57.1 by gateway cloning. Following this viral particles were generated from
839 HEK293T cells and the viral soup with polybrene (Sigma-Aldrich) was used for transduction. Cells
840 with insert were selected with 1µg/ml of puromycin and tested for TRF2 induction using varying
841 doxycycline concentrations.

842 Similarly TERT cDNA was amplified from a mammalian expression vector and inserted into
843 pENTR11 vector. Subsequently, the same strategy was used to generate and test TERT inducible
844 HT1080 cells.

845

846 **Vector constructs**

847 The pCMV6-myc-DDK(FLAG)-TRF2 vector (TRF2 WT) was procured from Origene (RC223601).
848 The mutants delB and delM constructs used in the study have been previously reported(Hussain

849 et al., 2017) and made through mutagenesis of the TRF2 WT construct. TRF2 shRNA was
850 procured from Origene (TL308880). Side-directed Mutagenesis was performed on the TRF2 WT
851 plasmid to generate the PTM mutants.

852 For customizing dCas9-TRF2 fusion plasmids, the backbone of dCAS9-VP64-GFP (Addgene
853 61422) was used. IL1R1 sgRNA was custom designed against IL1R1 promoter G-quadruplex
854 (G4-motif B) and cloned in pX333 (Addgene 64073) backbone after replacing Cas9 with mCherry.

855 **Transfections**

856 TRF2 wildtype (myc/DDK tag) or mutant mammalian expression vector pCMV6 was transfected
857 into HT1080 /MDAMB231 cells that were 60 % confluent using Lipofectamine 2000 transfection
858 reagent (following the manufacturers' protocol). 2-4µg of plasmid was used for transfection in a
859 35 mm well for each case.

860 In case of TRF2 shRNA (Origene)/TERC shRNA (Santa Cruz Biotechnology), 4µg of plasmid was
861 used for transfection in a 35 mm well for each case and Fugene HD transfection reagent was
862 used as per manufacturer's protocol. Cells were then maintained in 1µg/ml of puromycin for stable
863 shRNA maintenance. For dCAS9-TRF2 fusion constructs, co-transfected with IL1R1 sgRNA
864 plasmid, FugeneHD was used at recommended concentrations.

865 **TRF2 silencing by siRNA:**

866 HT1080 cells were transfected with TRF2 siRNA oligonucleotides (synthesized from Eurogenetics
867 Pvt. Limited)(Shalu Sharma et al., 2021) using lipofectamine 2000 (Invitrogen) transfection
868 reagent according to manufacturer's instructions. Silencing was checked after 48 hr of
869 transfection. Pooled scrambled siRNA was used as control.

870 **Luciferase assay:**

871 IL1R1 promoter (upto 1500 bp upstream of transcription start site) was cloned in PGL3 basic
872 vector upstream of firefly luciferase construct. G4 motif disrupting mutations were introduced in
873 the promoter construct by site directed mutagenesis.

874 Plasmid (pGL4.73) containing a CMV promoter driving Renilla luciferase was co-transfected as
875 transfection control for normalization. After 48h, cells were harvested and luciferase activities of
876 cell lysate were recorded by using a dual-luciferase reporter assay system (Promega).

877 **Circular Dichroism**

878 Circular Dichroism profiles (220 nm to 300 nm) were obtained for representative G4 motifs
879 identified within IL1R1 promoter and an overlap with TRF2 high confidence ChIP seqpeak.
880 Circular Dichroism showed the formation of G4-motif with the unaltered sequence while mutated
881 G4 sequence gave partial/complete disruption of the G4-motif under similar conditions (buffer
882 used for G- quadruplex formation -10mM Na cacodylate and 100 mM KCl). The circular dichroism
883 (CD) spectra were recorded on a Jasco-89spectropolarimeter equipped with a Peltier temperature
884 controller. Experiments were carried out using a 1mm path-length cuvette over a wavelength
885 range of 200-320 nm. Oligonucleotides were synthesized commercially from Sigma-Aldrich.
886 2.5uMoligonucleotides were diluted in sodium cacodylate buffer (10 mM sodium cacodylate and
887 100 mM KCl, pH 7.4) and denatured by heating to 95ºC for 5 min and slowly cooled to 15ºC for
888 several hours. The CD spectra reported here are representations of three averaged scans taken
889 at 20ºC and are baseline corrected for signal contributions due to the buffer.

890 **CCR5-IL1R1 promoter insert cells:**

891 IL1R1 promoter and downstream firefly luciferase (and G4 mutant variant) was inserted in
892 HEK293T cells by using strategy previously standardized and reported for TERT promoter-
893 gaussia insertion in the same locus(Shalu Sharma et al., 2021).

894 **IL1R1 promoter G4 mutant HEK cells:**

895 Custom designed gRNA pair was used to insert mutant G4 template sequence (G4 mutantB) into
896 the IL1R1 endogenous promoter by co-transfecting Cas9and gRNA pair with doner template
897 SSODN sequence. Following this, single cell screen was done for positive mutant colony. Once
898 identified an appropriate mutant colony was used for experiments.

899 sgRNA and SSODN details are as follows:

900 sgRNA1- 5'- GCTGCCAATGGGT**G**<u>GAGTC</u>TTG**G**G -3' (efficiency score (Doench et al)- 35)

901 -ve strand, ssODN: 91bp (PAM proximal)- 36bp (PAM distal)

902 Target strand is +ve strand. Non-target stand is –ve strand. ssODN shud be +ve strand.

903 **ssODN** (mutated): chr2:102070276-102070402

904 GGGACACTGCAGCCCTGGCCTGGCCTACTTTTCTCTTCTCCCATATCTGGAAAATGAAAGT
905 AGCCTGACGTATCCGGGGAC**A**CGGC**A**CAAGACTC**A**ACCCATTGGCAGCTCTTCACTTGTA
906 TCTTTT

907 sgRNA2- 5'- GCAATGGGT**G**GAGTCTTG**G**GCCG**G** -3' (efficiency score (Doench et al)- 40)

908 -ve strand, ssODN: 85bp (PAM proximal)- 42bp (PAM distal)

909

910 **Immunoprecipitation:**

911 Immunoprecipitation of proteins was performed using modified version of suggested IP protocol
912 from CST. Cells were lysed using cell lysis buffer ((1X) 20 mM Tris (pH 7.5), 150 mM NaCl (Sigma-
913 Aldrich), 1 mM EDTA (Sigma-Aldrich), 1 mM EGTA (Sigma-Aldrich), 1% Triton X-100 (Sigma-
914 Aldrich), 2X mPIC (Thermo Fisher Scientific)) and treated with relevant primary antibody (1: 100
915 v/v) overnight at 4ºC or mock IgG on rotor. 50 µg of Dyanbeads (blocked with BSA-5% for 60
916 mins at RT) was added to the lysis soup and kept for 2 hrs in mild agitation. Dynabeads were
917 magnetically separated and washed thrice (with 1X PBS with 0.1% Tween-20). The beads were
918 resuspended with 1X RIPA (50 µl) and 1X Laemmli buffer. This was followed by denaturation at
919 95ºCfor 10 mins and followed by western blot for specific proteins.

920 **HAT assay:**

921 Histone acetyl transferase (HAT) assay was performed as per manufacturers' protocol from Active
922 motif. Mammalian TRF2 and p300 full length were commercially procured from origene and
923 abcam respectively and used for the assay.

924 **IL1R1 knockout HT1080 cells:**

925 Two sets of gRNAs targeting either exon 3 or exon3-7 of *IL1R1* coding region were cloned in
926 PX459 (Addgene 62988) and co-transfected in HT1080 cells, followed by puromycin selection
927 and single cell screening for IL1R1 knockout cells. A knockout clone was selected (based on
928 IL1R1 depletion) and used for further experiments.

929 **Gene ontology and cBIO PORTAL ANALYSIS:**

930 Gene Ontology for KEGG pathway enrichment and associated figures were generated using
931 ShinyGO web portal(Ge et al., 2020). Gene ontology (Biological Process) analysis was done
932 using gene list (Barthel et al., 2017) using publicly available resource –The Gene Ontology
933 Resource database (http://geneontology.org/). Fold enrichment, FDR values and p-values were
934 calculated using PANTHER. Ontology plot was made using MS Excel multivariate plot. *IL1R1*
935 high/low samples were segregated, and differential gene expression gene list was generated

936 using cBioPortal (https://www.cbioportal.org/) using the TCGA Breast Invasive carcinoma dataset
937 (Firehose legacy). Sample IDs for the patient samples have been provided in **Supplementary**
938 **file 4**. For *IL1R1* high samples, the cut-off used was 1.5 times the standard deviation of the mean
939 expression value. Custom query commands were used to fetch the *IL1R1* high and low sample
940 IDs. DEG list and survival plots were generated using in-built functions of cBioPortal.

941 **TRAP (Telomere Repeat Amplification protocol) for telomerase activity:**

942 Protein lysate was prepared in 1X CHAPS Lysis Buffer and the assay was performed using
943 TRAPeze™ RT Telomerase Detection Kit (Merck) per manufacturer's instructions.

944 **Statistical Analysis:**

945 All statistical tests were performed using interface provided within GRAPHPAD PRISM software.
946 Median values and correlations were calculated using MS excel functions.

947

948 **Ethics statement:**

949 The authors declare that relevant ethical approvals were taken to procure and use human clinical
950 patient tissue and mouse xenograft tissue for experiments whose results have been shared in the
951 manuscript.

952 **Data availability:**

953 The authors declare that all data necessary to support the inferences are included in the
954 manuscript and supplementary information. Additionally, raw data for the RNA sequencing
955 (HT1080-HT1080-LT cells) has been made public (GSE267781).

956

957 ***Acknowledgements***

958 We acknowledge Manish Rai (confocal imaging), Debojyoti Chakraborty Lab (DeltaVision
959 Microscopy), Vivek Rao (THP1 cells) and Mohit Agarwal (ELISA experiments) from CSIR-IGIB.
960 Fellowships from CSIR (AKM, AS, SSR, SS, ASG, SVM, SB and DS); DBT-Wellcome Trust India
961 Alliance (AKM, AS, MC, MV and AP); UGC (SD) and DST (DK) are acknowledged. R.S and N.G
962 acknowledges intramural funding support from NCBS-TIFR. This work was supported by the
963 DBT/Wellcome Trust India Alliance Fellowship [grant number IA/S/18/2/504021] awarded to SC,

964 and research funding from the Council of Scientific and Industrial Research (CSIR), Ashoka
965 University and Department of Biotechnology (DBT).

966 ***Author Contributions***

967 Experimental design and execution: Tel-PNA FISH –SD; Tel-qRT PCR- MC,MV and AKM; Tel-
968 Flow- AKM;CD206 IHC-AS and AKM;CD206/CD11b Flow- AKM and MC;TNBO-M2 infiltration
969 flow-AKM; gene expression(TNBC)- AKM and MC, Telomerase activity-MC, gene
970 expression(TNBO, xenograft, ex-vivo)-AKM,SS. IF-AKM,SVM; ChIP-AKM,SS,ASG,AS;
971 Luciferase assays- AKM,SSR,ASG; WB- AKM,SVM,ASG,SSR,SD;IP-AKM;HAT Assay- AKM;
972 IL1B ELISA- SS,AKM; gene expression(dCAS9 related)-SD; Immuno-Flow for IL1R1- AKM,SD;
973 Immuno-Flow NFKB related- AKM,SD; Data Analysis and pipeline development-
974 AB,SKB,IG,NG,RS,SD,AKM;

975 Resources: TNBC tissue collection- AS; TNBO generation- DK, AKM,SVM,AS,AP; THP1-
976 Macrophage–AKM; NOD-SCID xenograft tumours-AKM,SD; Luciferase constructs-SSR, ASG;
977 CCR5-insert cells-SSR,AKM; HEK IL1R1 G4 mutant cells- SSR,AS; IL1R1 gRNA- SSR; HT1080-
978 TERT inducible- ASG,DS;HT1080-TRF2 inducible- ASG; HT1080 IL1R1 KO- SSR,AKM; HT1080
979 IL1R1 KO TRF2 inducible- AKM;MDAMB-231 LT cells-SS,AP; TRF2 PTM mutant plasmids- SB;
980 TRF2 protein extraction-SB and ASG; TNBC whole genome sequencing-AS;HT1080-HT1080-LT
981 RNA seq- SS,VA,MF;

982 Data collation-AKM, SD, AS, SSR, ASG, SVM, SC; Figure preparation-AKM, SD, AS, SC;
983 Manuscript writing and editing- AKM, SD, AS, SC; Conceptualization of idea and planning of
984 experiments- AKM and SC; Overall supervision and funding-SC.

985 ***Conflict of Interest***

986 The authors declare no conflict of interest.

987 ***Inclusion and diversity statement***

988 *We support inclusive, diverse, and equitable conduct of research.*

989 ***Materials & Correspondence***

990 *All correspondences should be addressed to SC* (e-mail: shantanuc@igib.in)

991

992 **References**

993 A W, P W, M K. 2010. Interleukin-1 (IL-1) pathway. *Sci Signal* **3**.
994 doi:10.1126/SCISIGNAL.3105CM1

995 Artandi SEE, DePinho RAA. 2009. Telomeres and telomerase in cancer. *Carcinogenesis* **31**:9–
996 18. doi:10.1093/carcin/bgp268

997 Aviv A, Anderson JJ, Shay JW. 2017. Mutations, Cancer and the Telomere Length Paradox.
998 *Trends in Cancer* **3**:253–258. doi:10.1016/J.TRECAN.2017.02.005

999 B Homey AMAZ. 2002. Chemokines: agents for the immunotherapy of cancer? *Nat Rev*
1000 *Immunol* **2**:175–184. doi:10.1038/nri748

1001 Barthel FPP, Wei W, Tang M, Martinez-Ledesma E, Hu X, Amin SBB, Akdemir KCC, Seth S,
1002 Song X, Wang Q, Lichtenberg T, Hu J, Zhang J, Zheng S, Verhaak RGWGWW. 2017.
1003 Systematic analysis of telomere length and somatic alterations in 31 cancer types. *Nat*
1004 *Genet 2017 493* **49**:349–357. doi:10.1038/ng.3781

1005 Baur J a J a, Zou Y, Shay JWJW, Wright WEWE. 2001. Telomere position effect in human cells.
1006 *Science* **292**:2075–2077. doi:10.1126/science.1062329

1007 Biffi G, Tannahill D, McCafferty J, Balasubramanian S. 2013. Quantitative visualization of DNA
1008 G-quadruplex structures in human cells. *Nat Chem* **5**:182–6. doi:10.1038/nchem.1548

1009 Binnewies M, Roberts EW, Kersten K, Chan V, Fearon DF, Merad M, Coussens LM, Gabrilovich
1010 DI, Ostrand-Rosenberg S, Hedrick CC, Vonderheide RH, Pittet MJ, Jain RK, Zou W,
1011 Howcroft TK, Woodhouse EC, Weinberg RA, Krummel MF. 2018. Understanding the tumor
1012 immune microenvironment (TIME) for effective therapy. *Nat Med* **24**:541–550.
1013 doi:10.1038/s41591-018-0014-x

1014 Biroccio A, Cherfils-Vicini J, Augereau A, Pinte S, Bauwens S, Ye J, Simonet T, Horard B,
1015 Jamet K, Cervera L, Mendez-Bermudez A, Poncet D, Grataroli R, de Rodenbeeke CT,
1016 Salvati E, Rizzo A, Zizza P, Ricoul M, Cognet C, Kuilman T, Duret H, Lépinasse F, Marvel
1017 J, Verhoeyen E, Cosset F-L, Peeper D, Smyth MJ, Londoño-Vallejo A, Sabatier L, Picco V,
1018 Pages G, Scoazec J-Y, Stoppacciaro A, Leonetti C, Vivier E, Gilson E. 2013. TRF2 inhibits
1019 a cell-extrinsic pathway through which natural killer cells eliminate cancer cells. *Nat Cell*
1020 *Biol* **15**:818–28. doi:10.1038/ncb2774

1021 Blackburn EH. 2000. Telomere states and cell fates. *Nature* **408**:53–56.

1022 Briukhovetska D, Dörr J, Endres S, Libby P, Dinarello CA, Kobold S. 2021. Interleukins in
1023 cancer: from biology to therapy **21**:481–499.

1024 Burkholder B, Huang RY, Burgess R, Luo S, Jones VS, Zhang W, Lv ZQ, Gao CY, Wang BL,
1025 Zhang YM, Huang RP. 2014. Tumor-induced perturbations of cytokines and immune cell
1026 networks. *Biochim Biophys Acta - Rev Cancer* **1845**:182–201.
1027 doi:10.1016/J.BBCAN.2014.01.004

1028 Carmi Y, Voronov E, Dotan S, Lahat N, Rahat MA, Fogel M, Huszar M, White MR, Dinarello CA,
1029 Apte RN. 2009. The Role of Macrophage-Derived IL-1 in Induction and Maintenance of
1030 Angiogenesis. *J Immunol* **183**:4705–4714. doi:10.4049/JIMMUNOL.0901511

1031 Cassetta L, Noy R, Swierczak A, Sugano G, Smith H, Wiechmann L, Pollard JW. 2016. Isolation
1032 of Mouse and Human Tumor-Associated Macrophages. *Adv Exp Med Biol* **899**:211.
1033 doi:10.1007/978-3-319-26666-4_12

1034 Chanmee T, Ontong P, Konno K, Itano N. 2014. Tumor-Associated Macrophages as Major
1035 Players in the Tumor Microenvironment. *Cancers 2014, Vol 6, Pages 1670-1690* **6**:1670–
1036 1690. doi:10.3390/CANCERS6031670

1037 Chen Z, Giotti B, Kaluzova M, Vallcorba MP, Rawat K, Price G, Herting CJ, Pinero G, Cristea S,
1038 Ross JL, Ackley J, Maximov V, Szulzewsky F, Thomason W, Marquez-Ropero M, Angione
1039 A, Nichols N, Tsankova NM, Michor F, Shayakhmetov DM, Gutmann DH, Tsankov AM,
1040 Hambardzumyan D. 2023. A paracrine circuit of IL-1β/IL-1R1 between myeloid and tumor
1041 cells drives genotype-dependent glioblastoma progression. *J Clin Invest* **133**.
1042 doi:10.1172/JCI163802

1043 Cherfils-Vicini J, Iltis C, Cervera L, Pisano S, Croce O, Sadouni N, Győrffy B, Collet R, Renault
1044 VM, Rey-Millet M, Leonetti C, Zizza P, Allain F, Ghiringhelli F, Soubeiran N, Shkreli M,
1045 Vivier E, Biroccio A, Gilson E. 2019. Cancer cells induce immune escape via glycocalyx
1046 changes controlled by the telomeric protein TRF2. *EMBO J* **38**:e100012.
1047 doi:10.15252/EMBJ.2018100012

1048 Chew V, Toh HC, Abastado JP. 2012. Immune microenvironment in tumor progression:
1049 Characteristics and challenges for therapy. *J Oncol* **2012**. doi:10.1155/2012/608406

1050 Chittezhath M, Dhillon MK, Lim JY, Laoui D, Shalova IN, Teo YL, Chen J, Kamaraj R, Raman L,
1051 Lum J, Thamboo TP, Chiong E, Zolezzi F, Yang H, VanGinderachter JA, Poidinger M,
1052 Wong ASC, Biswas SK. 2014. Molecular Profiling Reveals a Tumor-Promoting Phenotype
1053 of Monocytes and Macrophages in Human Cancer Progression. *Immunity* **41**:815–829.
1054 doi:10.1016/j.immuni.2014.09.014

1055 Cristofari G, Lingner J. 2006. Telomere length homeostasis requires that telomerase levels are
1056 limiting. *EMBO J* **25**:565–574. doi:10.1038/sj.emboj.7600952

1057 Cubiles MD, Barroso S, Vaquero-Sedas MI, Enguix A, Aguilera A, Vega-Palas MA. 2018.
1058 Epigenetic features of human telomeres. *Nucleic Acids Res* **46**:2347–2355.
1059 doi:10.1093/NAR/GKY006

1060 DeNardo DG, Ruffell B. 2019. Macrophages as regulators of tumour immunity and
1061 immunotherapy. *Nat Rev Immunol 2019 196* **19**:369–382. doi:10.1038/s41577-019-0127-6

1062 Ding Z, Mangino M, Aviv A, Spector T, Durbin R. 2014. Estimating telomere length from whole
1063 genome sequence data. *Nucleic Acids Res* **42**:e75. doi:10.1093/NAR/GKU181

1064 Dobin A, Davis CA, Schlesinger F, Drenkow J, Zaleski C, Jha S, Batut P, Chaisson M, Gingeras
1065 TR. 2013. STAR: ultrafast universal RNA-seq aligner. *Bioinformatics* **29**:15–21.
1066 doi:10.1093/BIOINFORMATICS/BTS635

1067 Duque GA, Descoteaux A. 2014. Macrophage Cytokines: Involvement in Immunity and
1068 Infectious Diseases. *Front Immunol* **5**. doi:10.3389/FIMMU.2014.00491

1069 F Balkwill AMM, Balkwill F, Mantovani A. 2001. Inflammation and cancer: back to Virchow?
1070 *Lancet* **357**:539–545. doi:10.1016/s0140-6736(00)04046-0

1071 Garcia M, Juhos S, Larsson M, Olason PI, Martin M, Eisfeldt J, DiLorenzo S, Sandgren J, Ståhl
1072 TD De, Ewels P, Wirta V, Nistér M, Käller M, Nystedt B. 2020. Sarek: A portable workflow
1073 for whole-genome sequencing analysis of germline and somatic variants. *F1000Research*
1074 **9**:63. doi:10.12688/F1000RESEARCH.16665.2

1075 Ge SX, Jung D, Jung D, Yao R. 2020. ShinyGO: a graphical gene-set enrichment tool for
1076 animals and plants. *Bioinformatics* **36**:2628–2629. doi:10.1093/BIOINFORMATICS/BTZ931

1077 Ghosh A, Saginc G, Leow SC, Khattar E, Shin EM, Yan TD, Wong M, Zhang Z, Li G, Sung W-K,
1078 Zhou J, Chng WJ, Li S, Liu E, Tergaonkar V. 2012. Telomerase directly regulates NF-κB-

1079 dependent transcription. *Nat Cell Biol* **14**:1270–1281. doi:10.1038/ncb2621

1080 Gonzalez H, Hagerling C, Werb Z, H G, C H, Z W. 2018. Roles of the immune system in cancer:
1081 from tumor initiation to metastatic progression. *Genes Dev* **32**:1267–1284.
1082 doi:10.1101/GAD.314617.118

1083 Goronzy JJ, Fujii H, Weyand CM. 2006. Telomeres, immune aging and autoimmunity. *Exp*
1084 *Gerontol* **41**:246–251.

1085 Granotier C, Pennarun GG, Riou L, Hoffschir FF, Gauthier LR, De Cian A, Gomez D, Mandine
1086 E, Riou J-FF, Mergny J-LL, Mailliet P, Dutrillaux B, Boussin FDFD, C G, G P, L R, F H, LR
1087 G, A DC, D G, E M, JF R, JL M, P M, B D, FD B. 2005. Preferential binding of a G-
1088 quadruplex ligand to human chromosome ends. *Nucleic Acids Res* **33**:4182–4190.
1089 doi:10.1093/nar/gki722

1090 Greider CW. 1998. Telomerase activity, cell proliferation, and cancer. *Proc Natl Acad Sci U S A*
1091 **95**:90–92. doi:10.1073/pnas.95.1.90

1092 Hanahan D, Weinberg R a. 2000. The hallmarks of cancer. *Cell* **100**:57–70. doi:10.1016/S0092-
1093 8674(00)81683-9

1094 Hanahan D, Weinberg RA. 2011. Hallmarks of cancer: the next generation. *Cell* **144**:646–674.
1095 doi:10.1016/j.cell.2011.02.013

1096 Hirashima K, Migita T, Sato S, Muramatsu Y, Ishikawa Y, Seimiya H. 2013. Telomere Length
1097 Influences Cancer Cell Differentiation In Vivo. *Mol Cell Biol* **33**:2988–2995.
1098 doi:10.1128/MCB.00136-13

1099 Hodes RJ, Hathcock KS, Weng NP. 2002. Telomeres in T and B cells. *Nat Rev Immunol* **2**:699–
1100 706. doi:10.1038/NRI890

1101 Hu W, Li X, Zhang C, Yang Y, Jiang J, Wu C. 2015. Tumor-associated macrophages in
1102 cancers. *Clin Transl Oncol 2015 183* **18**:251–258. doi:10.1007/S12094-015-1373-0

1103 Hung NA, Eiholzer RA, Kirs S, Zhou J, Ward-Hartstonge K, Wiles AK, Frampton CM, Taha A,
1104 Royds JA, Slatter TL. 2016. Telomere profiles and tumor-associated macrophages with
1105 different immune signatures affect prognosis in glioblastoma. *Mod Pathol 2016 293*
1106 **29**:212–226. doi:10.1038/modpathol.2015.156

1107 Hussain T, Saha D, Purohit G, Kar A, Kishore Mukherjee A, Sharma S, Sengupta S, Dhapola P,
1108 Maji B, Vedagopuram S, Horikoshi NTN, Horikoshi NTN, Pandita RK, Bhattacharya S,
1109 Bajaj A, Riou J-FF, Pandita TK, Chowdhury S. 2017. Transcription regulation of CDKN1A
1110 (p21/CIP1/WAF1) by TRF2 is epigenetically controlled through the REST repressor
1111 complex. *Sci Rep* **7**:11541. doi:10.1038/s41598-017-11177-1

1112 Iyer NG, Özdag H, Caldas C. 2004. p300/CBP and cancer. *Oncogene 2004 2324* **23**:4225–
1113 4231. doi:10.1038/sj.onc.1207118

1114 Jacobs JJL. 2013. Senescence: back to telomeres. *Nat Rev Mol Cell Biol* **14**:196–196.
1115 doi:10.1038/nrm3544

1116 Jaynes JM, Sable R, Ronzetti M, Bautista W, Knotts Z, Abisoye-Ogunniyan A, Li D, Calvo R,
1117 Dashnyam M, Singh A, Guerin T, White J, Ravichandran S, Kumar P, Talsania K, Chen V,
1118 Ghebremedhin A, Karanam B, Salam A Bin, Amin R, Odzorig T, Aiken T, Nguyen V, Bian
1119 Y, Zarif JC, Groot AE de, Mehta M, Fan L, Hu X, Simeonov A, Pate N, Abu-Asab M, Ferrer
1120 M, Southall N, Ock C-Y, Zhao Y, Lopez H, Kozlov S, Val N de, Yates CC, Baljinnyam B,
1121 Marugan J, Rudloff U. 2020. Mannose receptor (CD206) activation in tumor-associated
1122 macrophages enhances adaptive and innate antitumor immune responses. *Sci Transl Med*
1123 **12**:6337. doi:10.1126/SCITRANSLMED.AAX6337

1124 Jeong H, Hwang I, Kang SH, Shin HC, Kwon SY. 2019. Tumor-Associated Macrophages as
1125 Potential Prognostic Biomarkers of Invasive Breast Cancer. *J Breast Cancer* **22**:38–51.
1126 doi:10.4048/JBC.2019.22.E5

1127 Jochems C, Schlom J. 2011. Tumor-infiltrating immune cells and prognosis: the potential link
1128 between conventional cancer therapy and immunity. *Exp Biol Med (Maywood)* **236**:567.
1129 doi:10.1258/EBM.2011.011007

1130 Kaplanov I, Carmi Y, Kornetsky R, Shemesh A, Shurin G V., Shurin MR, Dinarello CA, Voronov
1131 E, Apte RN. 2019. Blocking IL-1β reverses the immunosuppression in mouse breast
1132 cancer and synergizes with anti–PD-1 for tumor abrogation. *Proc Natl Acad Sci* **116**:1361–
1133 1369. doi:10.1073/PNAS.1812266115

1134 Karlseder J. 2002. Senescence Induced by Altered Telomere State, Not Telomere Loss.
1135 *Science (80-)* **295**:2446–2449. doi:10.1126/science.1069523

1136 Kim W, Ludlow AT, Min J, Robin JD, Stadler G, Mender I, Lai T-P, Zhang N, Wright WE, Shay

1137 JW. 2016. Regulation of the Human Telomerase Gene TERT by Telomere Position
1138 Effect—Over Long Distances (TPE-OLD): Implications for Aging and Cancer. *PLOS Biol*
1139 **14**:e2000016. doi:10.1371/journal.pbio.2000016

1140 Lappano R, Talia M, Cirillo F, Rigiracciolo DC, Scordamaglia D, Guzzi R, Miglietta AM,
1141 Francesco EM De, Belfiore A, Sims AH, Maggiolini M. 2020. The IL1β-IL1R signaling is
1142 involved in the stimulatory effects triggered by hypoxia in breast cancer cells and cancer-
1143 associated fibroblasts (CAFs). *J Exp Clin Cancer Res 2020 391* **39**:1–22.
1144 doi:10.1186/S13046-020-01667-Y

1145 Lee C, Jeong H, Bae Y, Shin K, Kang S, Kim H, Oh J, Bae H. 2019. Targeting of M2-like tumor-
1146 associated macrophages with a melittin-based pro-apoptotic peptide. *J Immunother Cancer*
1147 *2019 71* **7**:1–14. doi:10.1186/S40425-019-0610-4

1148 Liu T, Zhang L, Joo D, Sun S-CC. 2017. NF-κB signaling in inflammation. *Signal Transduct*
1149 *Target Ther 2017 21* **2**:1–9. doi:10.1038/sigtrans.2017.23

1150 Londoño-Vallejo JA. 2004. Telomere length heterogeneity and chromosome instability, Cancer
1151 Letters.

1152 Lopez-Doriga A, Valle L, Alonso MH, Aussó S, Closa A, Sanjuan X, Barquero D, Rodríguez-
1153 Moranta F, Sanz-Pamplona R, Moreno V. 2018. Telomere length alterations in
1154 microsatellite stable colorectal cancer and association with the immune response. *Biochim*
1155 *Biophys Acta - Mol Basis Dis* **1864**:2992–3000. doi:10.1016/J.BBADIS.2018.06.010

1156 Love MI, Anders S, Huber W. 2016. Differential analysis of count data-the DESeq2 package.
1157 doi:10.1186/s13059-014-0550-8

1158 M J, J H, SJ N, JE L, S K. 2016. Elevated IL-1β expression induces invasiveness of triple
1159 negative breast cancer cells and is suppressed by zerumbone. *Chem Biol Interact*
1160 **258**:126–133. doi:10.1016/J.CBI.2016.08.021

1161 Maciejowski J, Lange T de. 2017. Telomeres in cancer: tumour suppression and genome
1162 instability. *Nat Rev Mol Cell Biol 2017 183* **18**:175–186. doi:10.1038/nrm.2016.171

1163 Mantovani A, Barajon I, Garlanda C. 2018. IL-1 and IL-1 Regulatory Pathways in Cancer
1164 Progression and Therapy. *Immunol Rev* **281**:57. doi:10.1111/IMR.12614

1165 Mantovani A, Dinarello CA, Molgora M, Garlanda C. 2019. Interleukin-1 and Related Cytokines

1166 in the Regulation of Inflammation and Immunity. *Immunity* **50**:778–795.
1167 doi:10.1016/J.IMMUNI.2019.03.012

1168 Mantovani A, Locati M. 2013. Tumor-associated macrophages as a paradigm of macrophage
1169 plasticity, diversity, and polarization lessons and open questions. *Arterioscler Thromb Vasc*
1170 *Biol* **33**:1478–1483. doi:10.1161/ATVBAHA.113.300168

1171 Martínez P, Blasco M a. 2011. Telomeric and extra-telomeric roles for telomerase and the
1172 telomere-binding proteins. *Nat Rev Cancer* **11**:161–176. doi:10.1038/nrc3025

1173 McNally EJ, Luncsford PJ, Armanios M. 2019. Long telomeres and cancer risk: the price of
1174 cellular immortality. *J Clin Invest* **129**:3474–3481. doi:10.1172/JCI120851

1175 Medrek C, Pontén F, Jirström K, Leandersson K. 2012. The presence of tumor associated
1176 macrophages in tumor stroma as a prognostic marker for breast cancer patients. *BMC*
1177 *Cancer 2012 121* **12**:1–9. doi:10.1186/1471-2407-12-306

1178 Mukherjee AK, Sharma S, Bagri S, Kutum R, Kumar P, Hussain A, Singh P, Saha D, Kar A,
1179 Dash D, Chowdhury S. 2019a. Telomere repeat-binding factor 2 binds extensively to extra-
1180 telomeric G-quadruplexes and regulates the epigenetic status of several gene promoters,
1181 Journal of Biological Chemistry. American Society for Biochemistry and Molecular Biology
1182 Inc.

1183 Mukherjee AK, Sharma S, Chowdhury S. 2019b. Non-duplex G-Quadruplex Structures Emerge
1184 as Mediators of Epigenetic Modifications. *Trends Genet* **35**:129–144.
1185 doi:10.1016/J.TIG.2018.11.001

1186 Mukherjee AK, Sharma S, Sengupta S, Saha D, Kumar P, Hussain T, Srivastava V, Roy SD,
1187 Shay JW, Chowdhury S. 2018. Telomere length-dependent transcription and epigenetic
1188 modifications in promoters remote from telomere ends. *PLOS Genet* **14**:e1007782.
1189 doi:10.1371/journal.pgen.1007782

1190 O'Callaghan NJ, Dhillon VS, Thomas P, Fenech M. A quantitative real-time PCR method for
1191 absolute telomere length **44**:807–809. doi:10.2144/000112761

1192 Oner G, Altintas S, Canturk Z, Tjalma W, Verhoeven Y, Berckelaer C Van, Berneman Z,
1193 Peeters M, Pauwels P, Dam PA van. 2020. Triple-negative breast cancer—Role of
1194 immunology: A systemic review. *Breast J* **26**:995–999. doi:10.1111/TBJ.13696

1195 Paeschke K, McDonald KRR, Zakian V a. a., Katrin Paeschke KRM and VAZ, Katrin P, R. MK,
1196 A. ZV, Paeschke K, McDonald KRR, Zakian V a. a. 2010. Telomeres: Structures in need of
1197 unwinding. *FEBS Lett* **584**:3760–3772. doi:10.1016/j.febslet.2010.07.007

1198 Pawelec G, Goldeck D, Derhovanessian E. 2014. Inflammation, ageing and chronic disease.
1199 *Curr Opin Immunol* **29**:23–28. doi:10.1016/J.COI.2014.03.007

1200 Pedram M, Sprung CN, Gao Q, Lo AWI, Reynolds GE, Murnane JP. 2006. Telomere position
1201 effect and silencing of transgenes near telomeres in the mouse. *Mol Cell Biol* **26**:1865–
1202 1878. doi:10.1128/MCB.26.5.1865-1878.2006

1203 Pellatt AJ, Wolff RK, Torres-Mejia G, John EM, Herrick JS, Lundgreen A, Baumgartner KB,
1204 Giuliano AR, Hines LM, Fejerman L, Cawthon R, Slattery ML. 2013. Telomere length,
1205 telomere-related genes, and breast cancer risk: The breast cancer health disparities study.
1206 *Genes, Chromosom Cancer* **52**:595–609. doi:10.1002/GCC.22056

1207 Pittet MJ, Michielin O, Migliorini D. 2022. Clinical relevance of tumour-associated macrophages.
1208 *Nat Rev Clin Oncol 2022 196* **19**:402–421. doi:10.1038/s41571-022-00620-6

1209 Quinlan AR, Hall IM. 2010. {BEDTools}: a flexible suite of utilities for comparing genomic
1210 features. *Bioinformatics* **26**:841–842. doi:10.1093/bioinformatics/btq033

1211 Raine KM, Van Loo P, Wedge DC, Jones D, Menzies A, Butler AP, Teague JW, Tarpey P, Nik-
1212 Zainal S, Campbell PJ. 2016. ascatNgs: Identifying Somatically Acquired Copy-Number
1213 Alterations from Whole-Genome Sequencing Data. *Curr Protoc Bioinforma* **56**:15.9.1-
1214 15.9.17. doi:10.1002/CPBI.17

1215 Ramadan WS, Talaat IM, Hachim MY, Lischka A, Gemoll T, El-Awady R. 2021. The impact of
1216 CBP expression in estrogen receptor-positive breast cancer. *Clin Epigenetics* **13**.
1217 doi:10.1186/S13148-021-01060-2

1218 Reddy TP, Rosato RR, Li X, Moulder S, Piwnica-Worms H, Chang JC. 2020. A comprehensive
1219 overview of metaplastic breast cancer: clinical features and molecular aberrations. *Breast*
1220 *Cancer Res* **22**:1–11. doi:10.1186/S13058-020-01353-Z/TABLES/2

1221 Ring A, Kaur P, Lang JE. 2020. EP300 knockdown reduces cancer stem cell phenotype, tumor
1222 growth and metastasis in triple negative breast cancer. *BMC Cancer* **20**.
1223 doi:10.1186/S12885-020-07573-Y

1224 Rizzo A, Iachettini S, Salvati E, Zizza P, Maresca C, D'Angelo C, Benarroch-Popivker D,
1225 Capolupo A, Del Gaudio F, Cosconati S, Di Maro S, Merlino F, Novellino E, Amoreo CA,
1226 Mottolese M, Sperduti I, Gilson E, Biroccio A. 2017. SIRT6 interacts with TRF2 and
1227 promotes its degradation in response to DNA damage. *Nucleic Acids Res* **45**:1820–1834.
1228 doi:10.1093/NAR/GKW1202

1229 Robin JD, Ludlow AT, Batten K, Gaillard M-C, Stadler G, Magdinier F, Wright W, Shay JW.
1230 2015. SORBS2 transcription is activated by telomere position effect-over long distance
1231 upon telomere shortening in muscle cells from patients with facioscapulohumeral
1232 dystrophy. *Genome Res* . doi:10.1101/gr.190660.115

1233 Robin JD, Ludlow AT, Batten K, Magdinier F, Stadler G, Wagner KR, Shay JW, Wright WE.
1234 2014. Telomere position effect: regulation of gene expression with progressive telomere
1235 shortening over long distances. *Genes Dev* **28**:2464–2476. doi:10.1101/gad.251041.114

1236 Roth SY, Denu JM, Allis CD. 2003. Histone Acetyltransferases.
1237 *http://dx.doi.org/101146/annurev.biochem70181* **70**:81–120.
1238 doi:10.1146/ANNUREV.BIOCHEM.70.1.81

1239 Salgado R, Gevaert T. 2021. Quantity of Immune Cells Predict Response to Immunotherapy in
1240 Cancer. *eClinicalMedicine* **41**:101170. doi:10.1016/j.eclinm.2021.101170

1241 Sansoni P, Vescovini R, Fagnoni F, Biasini C, Zanni F, Zanlari L, Telera A, Lucchini G, Passeri
1242 G, Monti D, Franceschi C, Passeri M. 2008. The immune system in extreme longevity. *Exp*
1243 *Gerontol* **43**:61–65. doi:10.1016/J.EXGER.2007.06.008

1244 SD J, M C, TH T, AA MZ, KC A, ES C. 2020. Evaluating the Polarization of Tumor-Associated
1245 Macrophages Into M1 and M2 Phenotypes in Human Cancer Tissue: Technicalities and
1246 Challenges in Routine Clinical Practice. *Front Oncol* **9**. doi:10.3389/FONC.2019.01512

1247 Shalu Sharma A, Kishore Mukherjee A, Shekhar Roy S, Nesse G, Prakash Pandey D, Sharma
1248 S, Bagri S, Lier S, Verma M, Sengupta A, Kumar M, Chowdhury S, Mukherjee AK, Roy SS,
1249 Bagri S, Lier S, Verma M, Sengupta A, Kumar M, Nesse G, Pandey DP, Chowdhury S.
1250 2021. Human telomerase is directly regulated by non-telomeric TRF2-G-quadruplex
1251 interaction. *CellReports* **35**:109154. doi:10.1016/j.celrep.2021.109154

1252 Shay JW. 2016. Role of Telomeres and Telomerase in Aging and Cancer. *Cancer Discov*
1253 **6**:584–593. doi:10.1158/2159-8290.CD-16-0062

1254 Shay JW, Wright WE. 2000. Hayflick, his limit, and cellular ageing. *Nat Rev Mol Cell Biol* **1**:72–
1255 76.

1256 Shen J, Terry MB, Gurvich I, Liao Y, Senie RT, Santella RM. 2007. Short Telomere Length and
1257 Breast Cancer Risk: A Study in Sister Sets. *Cancer Res* **67**:5538–5544. doi:10.1158/0008-
1258 5472.CAN-06-3490

1259 Shun CT, Tsai M-F, Chen C-H. 2005. Tumor-Associated Macrophages: The Double-Edged
1260 Sword in Cancer Progression. *Artic J Clin Oncol*. doi:10.1200/JCO.2005.12.172

1261 Simonet T, Zaragosi L-E, Philippe C, Lebrigand K, Schouteden C, Augereau A, Bauwens S, Ye
1262 J, Santagostino M, Giulotto E, Magdinier F, Horard B, Barbry P, Waldmann R, Gilson E.
1263 2011. The human TTAGGG repeat factors 1 and 2 bind to a subset of interstitial telomeric
1264 sequences and satellite repeats. *Cell Res* **21**:1028–1038. doi:10.1038/cr.2011.40

1265 Teo H, Ghosh S, Luesch H, Ghosh A, Wong ET, Malik N, Orth A, de Jesus P, Perry AS, Oliver
1266 JD, Tran NL, Speiser LJ, Wong M, Saez E, Schultz P, Chanda SK, Verma IM, Tergaonkar
1267 V. 2010. Telomere-independent Rap1 is an IKK adaptor and regulates NF-kappaB-
1268 dependent gene expression. *Nat Cell Biol* **12**:758–767. doi:10.1038/ncb2080

1269 TL R, I H. 2011. Tumour macrophages as potential targets of bisphosphonates. *J Transl Med* **9**.
1270 doi:10.1186/1479-5876-9-177

1271 Unver N. 2019. Macrophage chemoattractants secreted by cancer cells: Sculptors of the tumor
1272 microenvironment and another crucial piece of the cancer secretome as a therapeutic
1273 target. *Cytokine Growth Factor Rev* **50**:13–18. doi:10.1016/J.CYTOGFR.2019.05.010

1274 Vinayagamurthy S, Bagri S, Mergny JL, Chowdhury S. 2023. Telomeres expand sphere of
1275 influence: emerging molecular impact of telomeres in non-telomeric functions. *Trends*
1276 *Genet* **39**:59–73. doi:10.1016/J.TIG.2022.10.002

1277 Vinayagamurthy S, Ganguly A, Chowdhury S. 2020. Extra-telomeric impact of telomeres:
1278 Emerging molecular connections in pluripotency or stemness. *J Biol Chem* **295**:10245–
1279 10254. doi:10.1074/JBC.REV119.009710

1280 Wang C, Lin Y, Zhu H, Zhou Y, Mao F, Huang X, Sun Q, Li C. 2022. The Prognostic and
1281 Clinical Value of Tumor-Associated Macrophages in Patients With Breast Cancer: A
1282 Systematic Review and Meta-Analysis. *Front Oncol* **12**:905846.

1283 doi:10.3389/FONC.2022.905846/BIBTEX

1284 Wang M, Zhao J, Zhang L, Wei F, Lian Y, Wu Y, Gong Z, Zhang S, Zhou J, Cao K, Li X, Xiong
1285 W, Li G, Zeng Z, Guo C. 2017. Role of tumor microenvironment in tumorigenesis. *J Cancer*
1286 **8**:761–773. doi:10.7150/jca.17648

1287 Weng N ping. 2012. Telomeres and immune competency. *Curr Opin Immunol* **24**:470–475.
1288 doi:10.1016/J.COI.2012.05.001

1289 Went PT, Lugli A, Meier S, Bundi M, Mirlacher M, Sauter G, Dirnhofer S. 2004. Frequent
1290 EpCam protein expression in human carcinomas. *Hum Pathol* **35**:122–128.
1291 doi:10.1016/J.HUMPATH.2003.08.026

1292 Wentzensen IM, Mirabello L, Pfeiffer RM, Savage SA. 2011. The Association of Telomere
1293 Length and Cancer: a Meta-analysis. *Cancer Epidemiol Prev Biomarkers* **20**:1238–1250.
1294 doi:10.1158/1055-9965.EPI-11-0005

1295 Willeit P, Willeit J, Mayr A, Weger S, Oberhollenzer F. 2010. Telomere length and risk of
1296 incident cancer and cancer mortality. *JAMA* **304**.

1297 Wright WE, Brasiskyte D, Piatyszek M a, Shay JW. 1996. Experimental elongation of telomeres
1298 extends the lifespan of immortal x normal cell hybrids. *EMBO J* **15**:1734–1741.

1299 Yang D, Xiong Y, Kim H, He Q, Li Y, Chen R, Songyang Z. 2011. Human telomeric proteins
1300 occupy selective interstitial sites. *Cell Res* **21**:1013–1027. doi:10.1038/cr.2011.39

1301 Ye J, Renault VM, Jamet K, Gilson E. 2014. Transcriptional outcome of telomere signalling. *Nat*
1302 *Rev Genet 2014 157* **15**:491–503. doi:10.1038/nrg3743

1303 YR H, IK C. 2013. p300-mediated acetylation of TRF2 is required for maintaining functional
1304 telomeres. *Nucleic Acids Res* **41**:2267–2283. doi:10.1093/NAR/GKS1354

1305 Yuan Z-Y, Luo R-Z, Peng R-J, Wang S-S, Xue C. 2014. High infiltration of tumor-associated
1306 macrophages in triple-negative breast cancer is associated with a higher risk of distant
1307 metastasis. *Onco Targets Ther* **7**:1475. doi:10.2147/OTT.S61838

1308 Yuan ZY, Luo RZ, Peng RJ, Wang S Sen, Xue C. 2014. High infiltration of tumor-associated
1309 macrophages in triple-negative breast cancer is associated with a higher risk of distant
1310 metastasis. *Onco Targets Ther* **7**:1475–1480. doi:10.2147/OTT.S61838

1311 Zhang P, Gu Y, Fang H, Cao Y, Wang J, Liu H, Zhang H, Li H, He H, Li R, Lin C, Xu J. 2022.
1312 Intratumoral IL-1R1 expression delineates a distinctive molecular subset with therapeutic
1313 resistance in patients with gastric cancer. *J Immunother Cancer* **10**:e004047.
1314 doi:10.1136/JITC-2021-004047

1315

1316

Additional supplementary figure 1

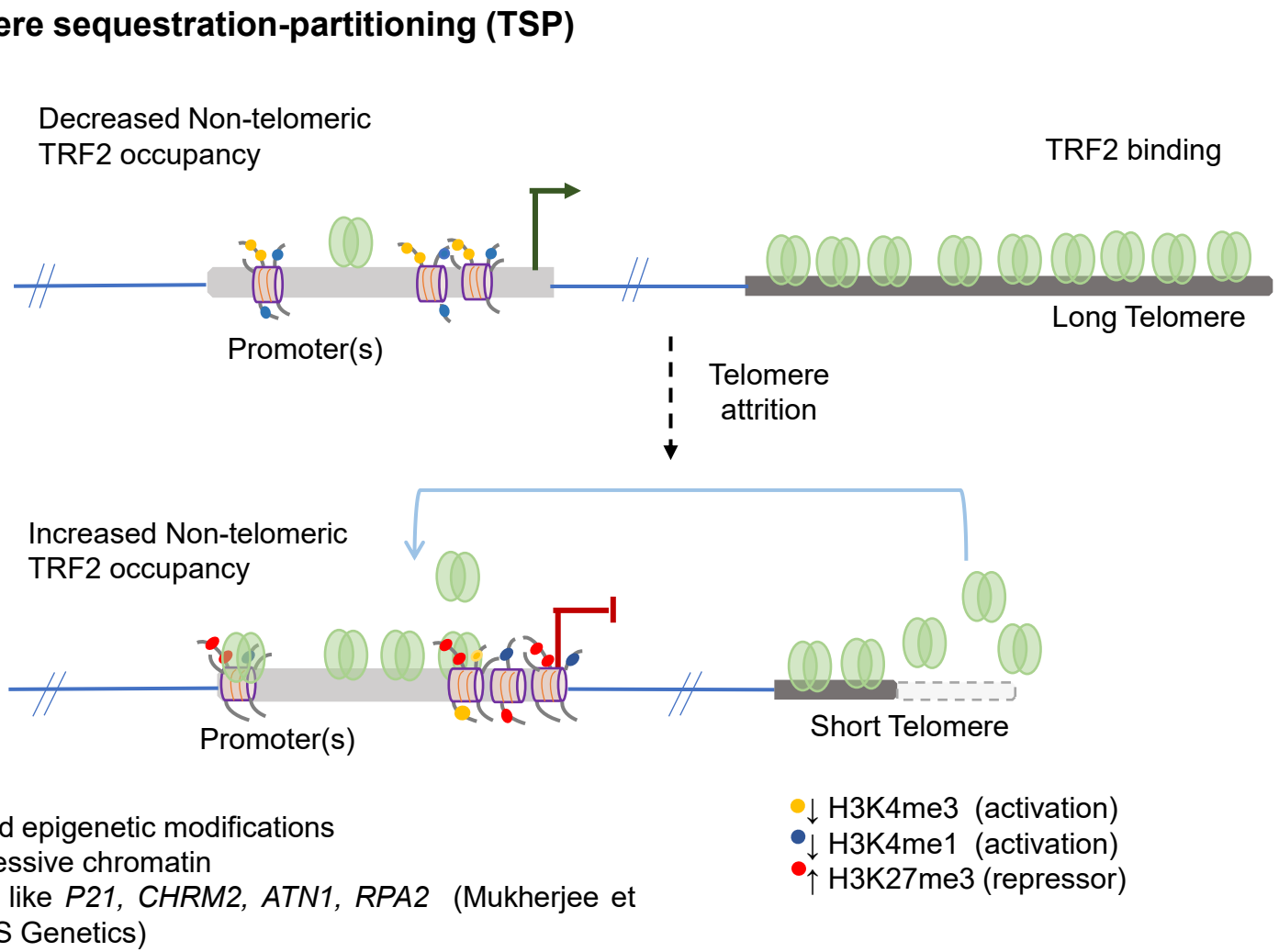

Graphical representation of the Telomere Sequestration Partitioning (TSP) model. The binding of TRF2 outside of telomeric regions (non-telomeric) is dependent on telomere length. When telomeres shorten, the presence of TRF2 at telomeres diminishes, resulting in increased TRF2 binding at non-telomeric sites. This shift in TRF2 distribution triggers epigenetic modifications at promoters showing telomere-dependent gene regulation. Described in Mukherjee et al. *PLoS Genetics,* 2018.

Figure 1

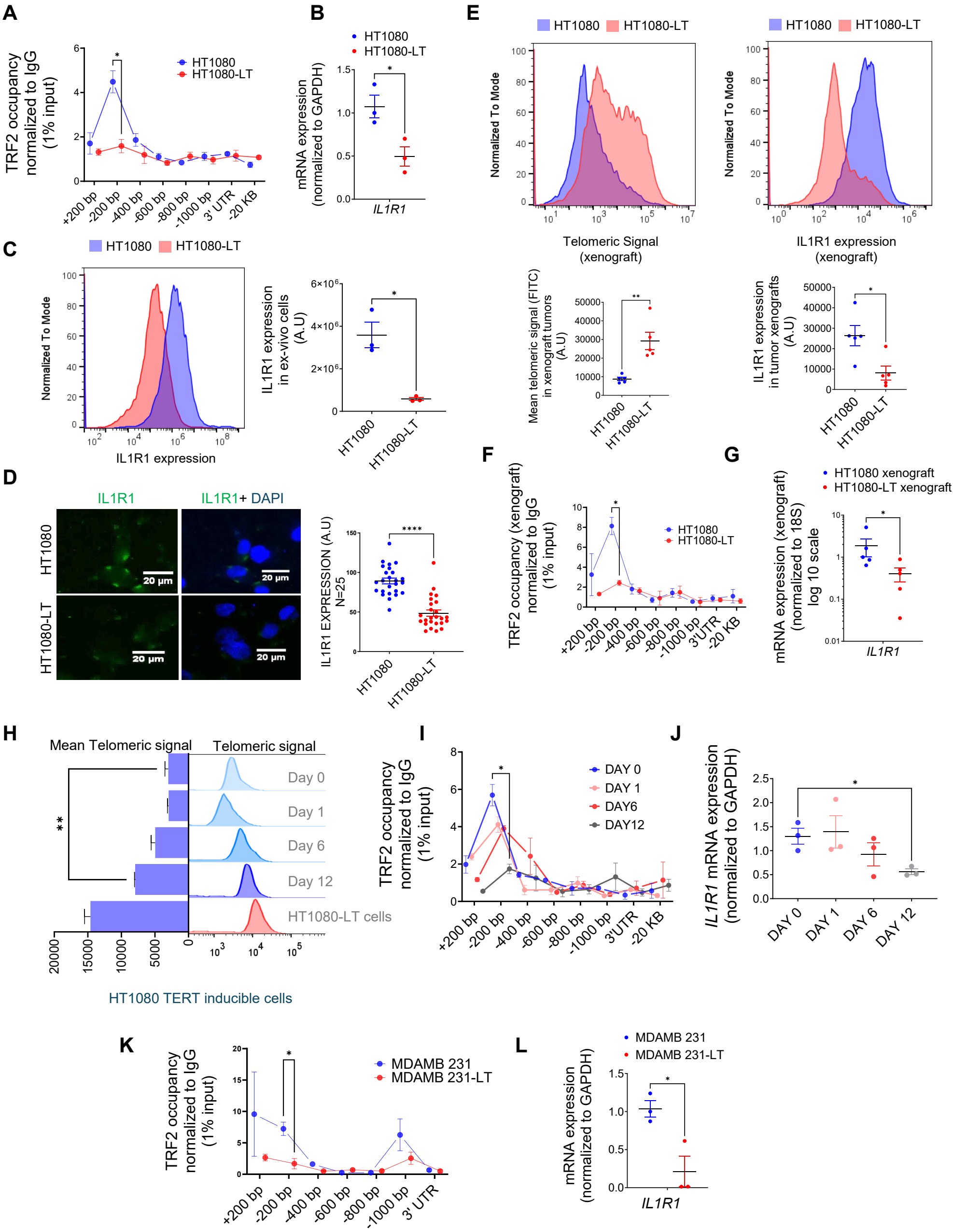
A
TRF2 occupancy normalized to IgG (1% input)
HT1080
HT1080-LT
+200 bp
-200 bp
-400 bp
-600 bp
-800 bp
-1000 bp
3' UTR
-20 KB
B
mRNA expression (normalized to GAPDH)
IL1R1
C
Normalized To Mode
IL1R1 expression
IL1R1 expression in ex-vivo cells (A.U)
D
IL1R1
IL1R1+ DAPI
20 µm
IL1R1 EXPRESSION (A.U) N=25
E
Telomeric Signal (xenograft)
IL1R1 expression (xenograft)
Mean telomeric signal (FITC) in xenograft tumors (A.U)
IL1R1 expression in tumor xenografts (A.U)
F
TRF2 occupancy (xenograft) normalized to IgG (1% input)
G
HT1080 xenograft
HT1080-LT xenograft
mRNA expression (xenograft) (normalized to 18S) log 10 scale
H
Mean Telomeric signal
Telomeric signal
Day 0
Day 1
Day 6
Day 12
HT1080-LT cells
HT1080 TERT inducible cells
I
DAY 0
DAY 1
DAY6
DAY12
J
IL1R1 mRNA expression (normalized to GAPDH)
K
MDAMB 231
MDAMB 231-LT
L

Figure 1: Expression of IL1R1 is regulated by telomere length-dependent enrichment of non-telomeric TRF2 on the gene promoter

A. Occupancy of TRF2 was checked by ChIP-qPCR on the *IL1R1* promoter spanning +200 to -1000 bp of TSS was reduced *ex-vivo* HT1080 cells with long telomeres (HL1080-LT) relative to ones with short telomeres (HT1080) cells (N=3 in each case) ;IL1R1-3'UTR or a region 20 kb upstream were used as negative controls for TRF2 binding. Statistical significance was calculated using unpaired T test with Welch's correction (p values: * ≤ 0.05, ** ≤ 0.01, *** ≤ 0.001, **** ≤ 0.0001).

B. mRNA expression of *IL1R1* in *ex-vivo* HT1080 or HT1080-LT cells; *GAPDH* was used for normalization [N=3]. Statistical significance was calculated using unpaired T test with Welch's correction (p values: * ≤ 0.05, ** ≤ 0.01, *** ≤ 0.001, **** ≤ 0.0001).

C. IL1R1 protein expression was checked by immuno-flow cytometry in HT1080 or HT1080-LT cells in three independent replicates; Mean IL1R1 expression has been plotted along the X-axis in log scale (right panel) [N=3]. Statistical significance was calculated using unpaired T test with Welch's correction (p values: * ≤ 0.05, ** ≤ 0.01, *** ≤ 0.001, **** ≤ 0.0001).

D. IL1R1 levels by immunofluorescence microscopy in HT1080 or HT1080-LT cells; cells were stained with DAPI for marking the cell nucleus; IL1R1 levels from 25 individual cells shown in graph (right panel). [N=25] Statistical significance was calculated using Mann-Whitney's non-parametric test (p values: * ≤ 0.05, ** ≤ 0.01, *** ≤ 0.001, **** ≤ 0.0001).

E. Telomere length of the xenograft tumors made in NOD SCID mice using HT1080 cells with long telomeres (HL1080-LT) and short telomeres (HT1080) was checked by flow-cytometry and was higher in HT1080-LT xenograft tumors. Following this, IL1R1 expression was checked by flow cytometry for these samples. Mean Telomeric signal and Mean IL1R1 expression has been plotted respectively (panels below) [N=5] Statistical significance was calculated using Mann-Whitney's non-parametric test (p values: * ≤ 0.05, ** ≤ 0.01, *** ≤ 0.001, **** ≤ 0.0001).

F. Occupancy of TRF2 by ChIP-qPCR at the *IL1R1* promoter spanning +200 to -1000 bp of TSS was reduced in xenograft tumors made from HT1080 cells with long telomeres (HL1080-LT) relative to ones with short telomeres (HT1080) cells (N=3 in each case; IL1R1-3'UTR or a region 20 kb upstream were used as negative controls for TRF2 binding). [N=3] Statistical significance was calculated using unpaired T test with Welch's correction (p values: * ≤ 0.05, ** ≤ 0.01, *** ≤ 0.001, **** ≤ 0.0001).

G. mRNA expression of *IL1R1* in xenograft tumors (HT1080 or HT1080-LT cells); *18S* was used for normalization. [N=5] Statistical significance was calculated using Mann-Whitney's non-parametric test (p values: * ≤ 0.05, ** ≤ 0.01, *** ≤ 0.001, **** ≤ 0.0001).

H. Telomere length by flow-cytometry of telomeric signal in HT1080 cells (hTERT-inducible stable line) following 0, 1, 6, 12 or 20 days of hTERT induction; HT1080-LT shown as positive control for enhanced telomere length; mean telomeric signal (FITC) plotted bar graph (left). [N=3] Statistical significance was calculated using unpaired T test with Welch's correction (p values: * ≤ 0.05, ** ≤ 0.01, *** ≤ 0.001, **** ≤ 0.0001).

I. TRF2 occupancy ChIP-qPCR on the *IL1R1* promoter spanning +200 to -1000 bp of TSS in HT1080 cells following 0, 1, 6 or 12 days of hTERT induction in ex-vivo culture; primers and normalization as in Figure 2A; IL1R1-3'UTR or a region 20 kb upstream used as negative controls. [N=3] Statistical significance was calculated using unpaired T test with Welch's correction (p values: * ≤ 0.05, ** ≤ 0.01, *** ≤ 0.001, **** ≤ 0.0001).

J. *IL1R1* mRNA expression (normalized to *GAPDH*) in HT1080 cells following 0, 1, 6 or 12 days of hTERT induction in ex-vivo culture. [N=3] Statistical significance was calculated using unpaired T test with Welch's correction (p values: * ≤ 0.05, ** ≤ 0.01, *** ≤ 0.001, **** ≤ 0.0001).

K. TRF2 occupancy by ChIP-qPCR on the *IL1R1* promoter in MDAMB23 or MDAMD231-LT cells using primers and normalization described earlier. [N=3] Statistical significance was calculated using unpaired T test with Welch's correction (p values: * ≤ 0.05, ** ≤ 0.01, *** ≤ 0.001, **** ≤ 0.0001).

L. Expression for *IL1R1* in MDAMB231 cells or MDAMD231-LT cells; *GAPDH* was used for normalization. [N=3] Statistical significance was calculated using unpaired T test with Welch's correction (p values: * ≤ 0.05, ** ≤ 0.01, *** ≤ 0.001, **** ≤ 0.0001).

Error bars correspond to standard error of mean from independent experiments.

Supplementary Figure 1

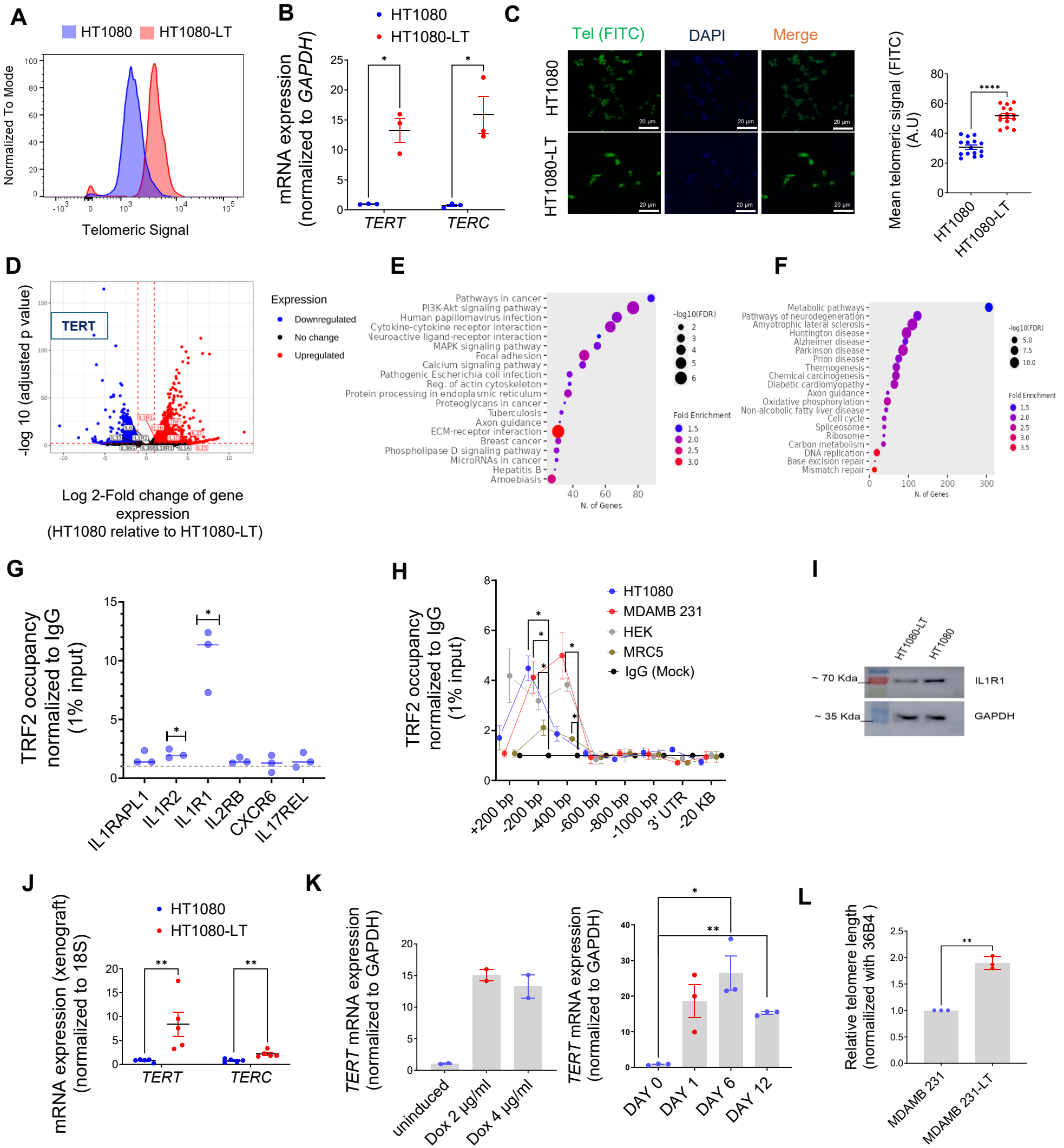

Supplementary Figure 1:

A. Telomer length (TL) by flow-cytometry analysis of telomeric signal (FITC labeled PNA probe) showing increase in TL in HT1080-LT cells relative to HT1080 cells; plotted along x-axis in log scale .

B. *hTERT* and *TERC* expression as expected was enhanced in HT1080-LT relative to HT1080 cells (normalized to GAPDH). [N=3] Statistical significance was calculated using unpaired T test with Welch's correction (p values: * ≤ 0.05, ** ≤ 0.01, *** ≤ 0.001, **** ≤ 0.0001).

C. Immuno-histochemical (IHC) staining of previously reported and well-characterized cells with short/long telomeres (fibrosarcoma HT1080 or the long-telomere version HT1080-LT cells in cell-isogenic background) hybridized with telomere-specific FITC-labelled PNA probe, counterstained with DAPI (left panel); telomeric signal was enhanced in HT1080-LT cells (quantified in right panel). [N=15] Statistical significance was calculated using Mann-Whitney's non-parametric test (p values: * ≤ 0.05, ** ≤ 0.01, *** ≤ 0.001, **** ≤ 0.0001).

D. Volcano plot of expressed genes in RNA-seq in HT1080 or HT1080-LT cells; x-axis has log-2 fold change for genes and the y-axis represents adjusted p values in log-10 scale. Key inflammation-related genes that have been marked in figure – most differentially expressed genes like *IL1R1*,*IL1B* and *IL10* were found to have higher expression in HT1080 cells compared to HT1080-LT cells. TERT which (as expected) is significantly lower in HT1080 cells compared to HT1080-LT cells have been also marked. Upregulated and downregulated genes listed in supplementary file 1.

E. Gene Ontology (KEGG) for upregulated genes in HT1080 cells over HT1080-LT cells.

F. Gene Ontology (KEGG) for down-regulated genes in HT1080 cells over HT1080-LT cells.

G. Occupancy of TRF2 by ChIP-qPCR checked in HT1080 cells for cytokine-related genes. Enrichment was plotted relative to mock IgG (post normalization to 1% input) [N=3] Statistical significance was calculated using unpaired T test with Welch's correction (p values: * ≤ 0.05, ** ≤ 0.01, *** ≤ 0.001, **** ≤ 0.0001).

H. TRF2 occupancy on the *IL1R1* promoter in HT1080, MDAMB231, HEK293T or MRC5 cells by chromatin-immunoprecipitation (ChIP) followed by qPCR. Primers spanning +200 to -1000 bp of TSS used for TRF2 enrichment on the gene promoter; 3'UTR and -20 Kb upstream of TSS used as negative control for TRF2 binding; fold-change of occupancy was calculated over mock IgG after normalizing signal to 1% input. [N=3] Statistical significance was calculated using unpaired T test with Welch's correction (p values: * ≤ 0.05, ** ≤ 0.01, *** ≤ 0.001, **** ≤ 0.0001).

I. IL1R1 protein levels in HT1080 and HT1080-LT cells by western blot ; GAPDH was used as loading control.

J. mRNA expression of *hTERT* and *TERC* (normalized to 18S) in xenograft tumors in NOD-SCID mice injected with HT1080 or HT1080-LT cells. *18S* has been used as a normalizing control. [N=5] Statistical significance was calculated using Mann-Whitney's non-parametric test (p values: * ≤ 0.05, ** ≤ 0.01, *** ≤ 0.001, **** ≤ 0.0001).

K. *hTERT* mRNA expression in hTERT-inducible HT1080 cells on treatment with different concentrations of doxycycline [N=2] (left panel) and at different days following induction [N=3] (right panel). *GAPDH* was used for normalization. Statistical significance was calculated using unpaired T test with Welch's correction (p values: * ≤ 0.05, ** ≤ 0.01, *** ≤ 0.001, **** ≤ 0.0001).

L. Relative telomere length by qRT-PCR in MDAMB231 or MDAMD231-LT (long telomere) cells in three independent experiments. [N=3] Statistical significance was calculated using unpaired T test with Welch's correction (p values: * ≤ 0.05, ** ≤ 0.01, *** ≤ 0.001, **** ≤ 0.0001).

Error bars correspond to standard error of mean from independent experiments.

Figure 2

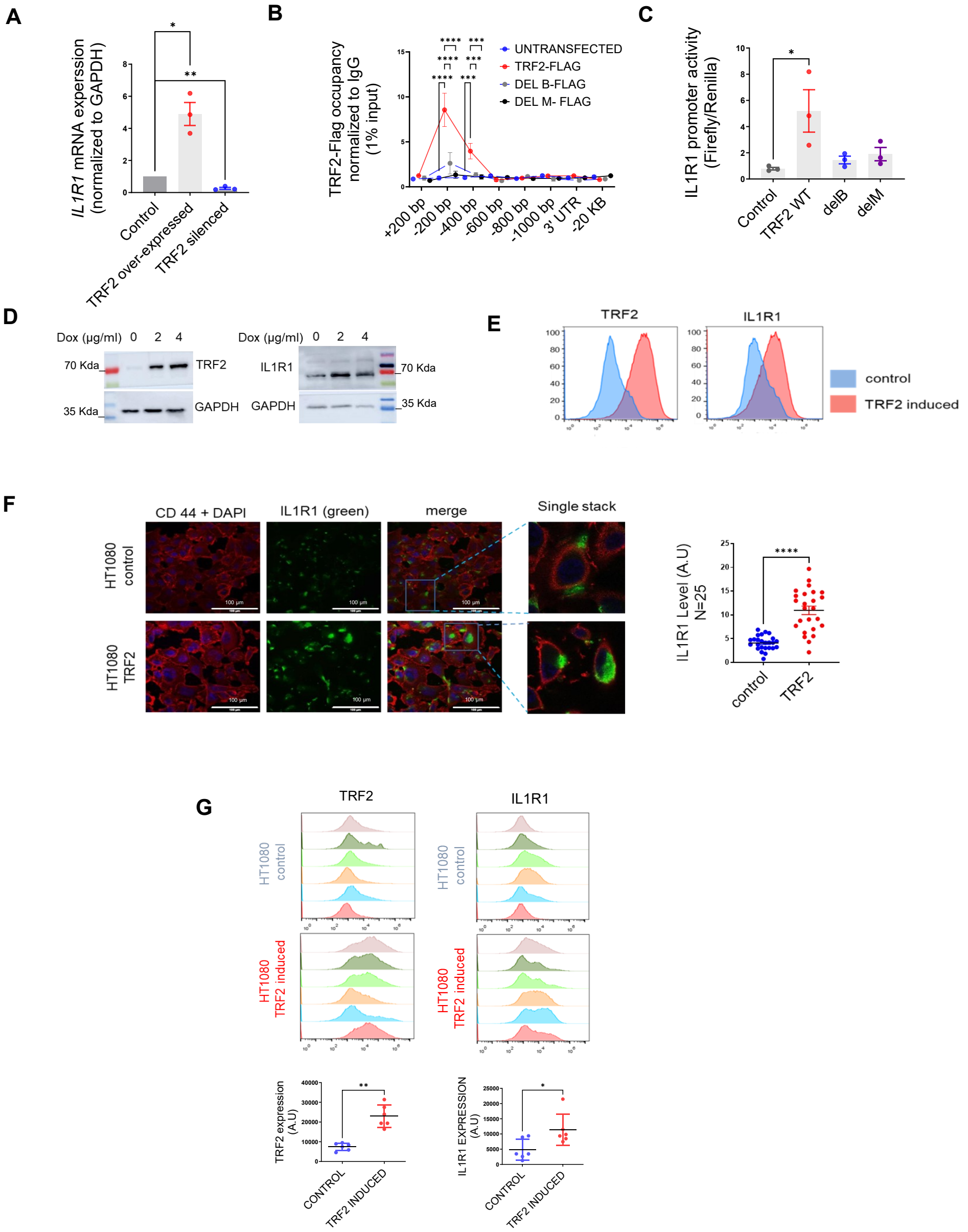
A
IL1R1 mRNA experssion (normalized to GAPDH)
Control
TRF2 over-expressed
TRF2 silenced
B
TRF2-Flag occupancy normalized to IgG (1% input)
UNTRANSFECTED
TRF2-FLAG
DEL B-FLAG
DEL M- FLAG
+200 bp
-200 bp
-400 bp
-600 bp
-800 bp
-1000 bp
3' UTR
-20 KB
C
IL1R1 promoter activity (Firefly/Renilla)
Control
TRF2 WT
delB
delM
D
Dox (µg/ml) 0 2 4
70 Kda
TRF2
35 Kda
GAPDH
IL1R1
E
TRF2
IL1R1
control
TRF2 induced
F
CD 44 + DAPI
IL1R1 (green)
merge
Single stack
HT1080 control
HT1080 TRF2
IL1R1 Level (A.U) N=25
control
TRF2
G
TRF2
IL1R1
HT1080 control
HT1080 TRF2 induced
TRF2 expression (A.U)
IL1R1 EXPRESSION (A.U)
CONTROL
TRF2 INDUCED

Figure 2: TRF2 is a transcriptional activator of IL1R1

A. *IL1R1* expression by qRT PCR following expression of TRF2-flag or TRF2 silencing (48 hrs. of transient transfection) ; *GAPDH* was used for normalization. [N=3] Statistical significance was calculated using unpaired T test with Welch's correction (p values: * ≤ 0.05, ** ≤ 0.01, *** ≤ 0.001, **** ≤ 0.0001).

B-C. TRF2 ChIP-qPCR spanning +200 to -1000 bp of *IL1R1* TSS for TRF2 occupancy (B) and promoter activity (luciferase reporter including -1500 bp TSS; C) following expression of flag-tag TRF2 full-length, or the mutants TRF2-delB or TRF2-delM; anti-flag antibody used for ChIP; IL1R1-3'UTR or a region 20 kb upstream were used as negative controls. [N=3] Statistical significance was calculated using Tukey's multiple comparisons test (p values: * ≤ 0.05, ** ≤ 0.01, *** ≤ 0.001, **** ≤ 0.0001).

D. TRF2 and IL1R1 levels by western blots following TRF2 induction with 2 or 4 µg/ml doxycycline (Dox) in HT1080 cells (stably transformed for Dox-inducible TRF2); GAPDH as loading.

E. TRF2 and IL1R1 expression in control or TRF2-induced HT1080 cells by flow-cytometry; TRF2/IL1R1 in x-axis in log scale for 20 thousand cells.

F. IL1R1 levels in control or TRF2-induced HT1080 cells. CD44 used for cell-surface marker and nuclei were stained with DAPI; 25 cells in each condition were scored and plotted in the summary graph. [N=25] Statistical significance was calculated using Mann-Whitney's non-parametric test (p values: * ≤ 0.05, ** ≤ 0.01, *** ≤ 0.001, **** ≤ 0.0001).

G. TRF2 (left panel), IL1R1 (right panel) levels from xenograft tumors in NOD-SCID mice (control or doxycycline-induced TRF2 in HT1080 cells; N=6 mice in each group) by immuno-flow cytometry; mean fluorescence signal from individual tumors in control or TRF2-induced tumors plotted in adjacent graphs. [N=6] Statistical significance was calculated using Mann-Whitney's non-parametric test (p values: * ≤ 0.05, ** ≤ 0.01, *** ≤ 0.001, **** ≤ 0.0001).

Error bars correspond to standard error of mean from independent experiments.

Supplementary Figure 2

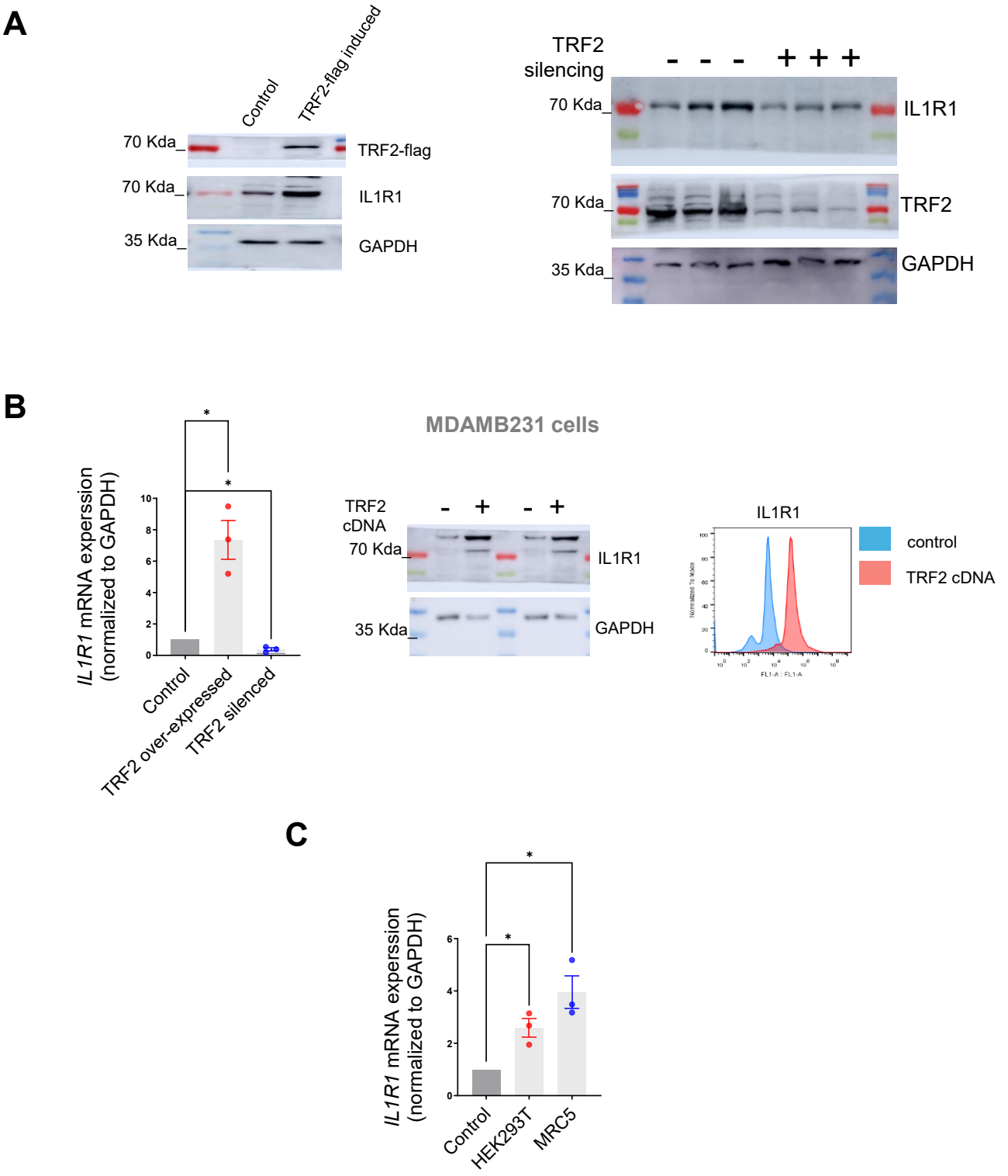

Supplementary Figure 2:

A.IL1R1 protein levels on TRF2-flag induction (left) or TRF2 silencing (right) in HT1080 cells following 48 hrs. of transfection.

B.IL1R1 mRNA expression in MDAMB231 cells following expression of TRF2 cDNA or TRF2 silencing for 48 hrs; GAPDH used as normalizing control (left). [N=3] Statistical significance was calculated using unpaired T test with Welch's correction (p values: * ≤ 0.05, ** ≤ 0.01, *** ≤ 0.001, **** ≤ 0.0001). IL1R1 protein levels in MDAMB231 cells following TRF2 induction for 48 hrs by western blot (centre) and immuno-flow cytometry (right).

C.IL1R1 mRNA expression in HEK293T and MRC5 cells following transfection of TRF2-cDNA for 48 hrs; *GAPDH* was used as normalizing control. [N=3] Statistical significance was calculated using unpaired T test with Welch's correction (p values: * ≤ 0.05, ** ≤ 0.01, *** ≤ 0.001, **** ≤ 0.0001).

Error bars correspond to standard error of mean from independent experiments.

Figure 3

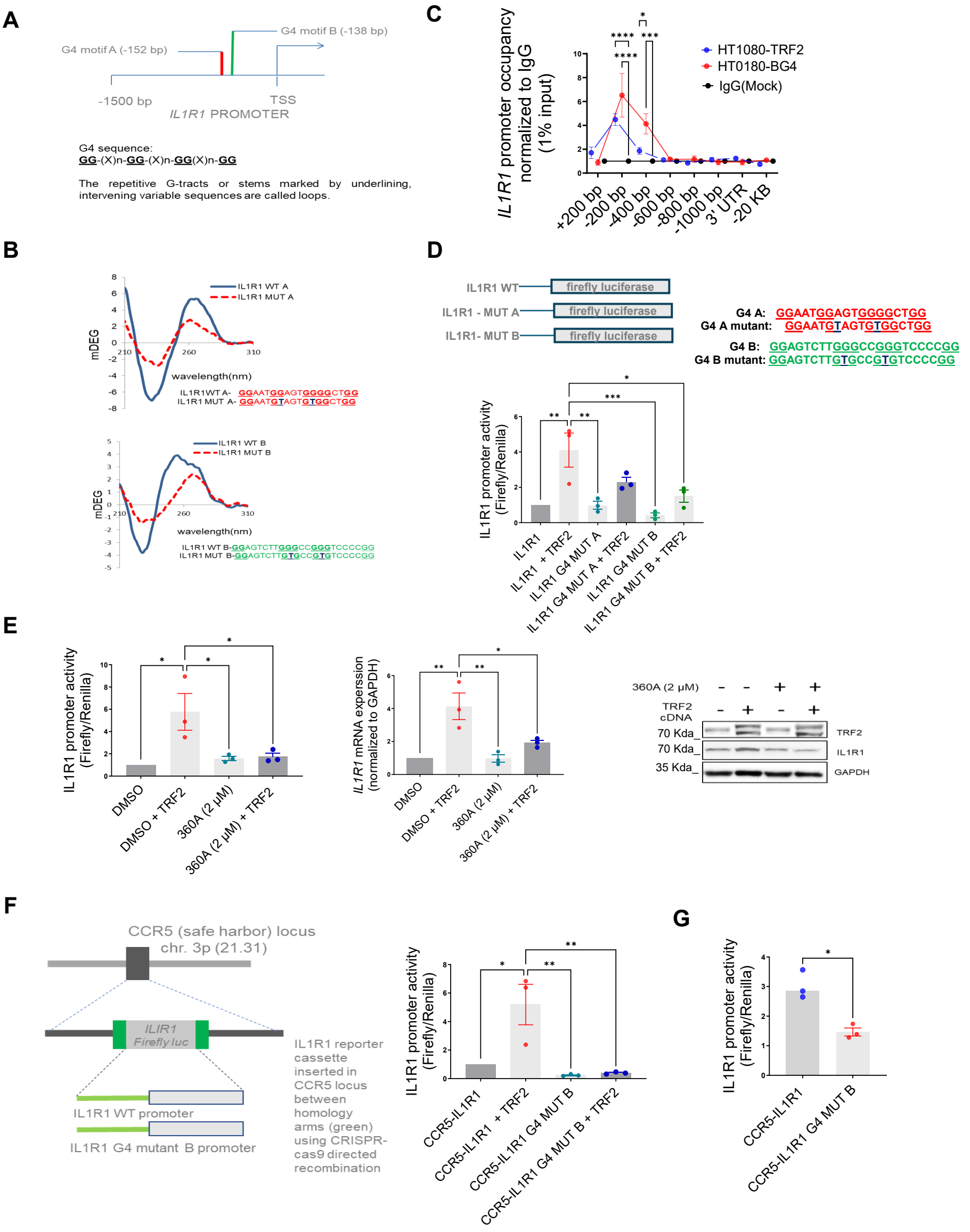
A
G4 motif B (-138 bp)
G4 motif A (-152 bp)
-1500 bp
TSS
IL1R1 PROMOTER
G4 sequence:
GG-(X)n-GG-(X)n-GG(X)n-GG
The repetitive G-tracts or stems marked by underlining, intervening variable sequences are called loops.
B
IL1R1 WT A
IL1R1 MUT A
mDEG
wavelength(nm)
IL1R1WT A- GGAATGGAGTGGGGCTGG
IL1R1 MUT A- GGAATGTAGTGTGGCTGG
IL1R1 WT B
IL1R1 MUT B
IL1R1 WT B-GGAGTCTTGGGCCGGGTCCCCGG
IL1R1 MUT B-GGAGTCTTGTGCCGTGTCCCCGG
C
IL1R1 promoter occupancy normalized to IgG (1% input)
HT1080-TRF2
HT0180-BG4
IgG(Mock)
+200 bp
-200 bp
-400 bp
-600 bp
-800 bp
-1000 bp
3' UTR
-20 KB
D
IL1R1 WT
IL1R1 - MUT A
IL1R1- MUT B
firefly luciferase
G4 A: GGAATGGAGTGGGGCTGG
G4 A mutant: GGAATGTAGTGTGGCTGG
G4 B: GGAGTCTTGGGCCGGGTCCCCGG
G4 B mutant: GGAGTCTTGTGCCGTGTCCCCGG
IL1R1 promoter activity (Firefly/Renilla)
IL1R1
IL1R1 + TRF2
IL1R1 G4 MUT A
IL1R1 G4 MUT A + TRF2
IL1R1 G4 MUT B
IL1R1 G4 MUT B + TRF2
E
IL1R1 promoter activity (Firefly/Renilla)
DMSO
DMSO + TRF2
360A (2 μM)
360A (2 μM) + TRF2
IL1R1 mRNA experssion (normalized to GAPDH)
360A (2 μM)
TRF2 cDNA
70 Kda
35 Kda
TRF2
IL1R1
GAPDH
F
CCR5 (safe harbor) locus
chr. 3p (21.31)
ILIR1
Firefly luc
IL1R1 WT promoter
IL1R1 G4 mutant B promoter
IL1R1 reporter cassette inserted in CCR5 locus between homology arms (green) using CRISPR-cas9 directed recombination
CCR5-IL1R1
CCR5-IL1R1 + TRF2
CCR5-IL1R1 G4 MUT B
CCR5-IL1R1 G4 MUT B + TRF2
G

Figure 3: DNA secondary structure G-quadruplexes are important for TRF2 binding to IL1R1 promoter

A. Schematic depicting G4 motifs (A and B) and their respective positions on the *IL1R1* promoter; sequence scheme depicting generic G4 motifs;

B. Circular dichroism profile (220-310 nm wavelength) of oligonucleotides (5 μM) with sequence of the G4 motifs A or B (or respective mutants with base substitutions) in solution.

C. ChIP-qPCR following BG4 ChIP at the IL1R1 promoter (fold enrichment over mock) overlaid with TRF2 occupancy (fold enrichment over IgG) in HT1080 cells. [N=3] Statistical significance was calculated using Šídák's multiple comparisons test (p values: * ≤ 0.05, ** ≤ 0.01, *** ≤ 0.001, **** ≤ 0.0001).

D. IL1R1 promoter activity in HT1080 cells from luciferase-reporter without or with G4-deforming substitutions against G4 motif A (IL1R1G4-MUT-A) or G4 motif B (IL1R1-G4 MUT-B) in presence or absence of TRF2 induction; G4 motifs A and B as shown in schematic; specific base substitutions have been indicated in blue font. [N=3] Statistical significance was calculated using Tukey's multiple comparisons test (p values: * ≤ 0.05, ** ≤ 0.01, *** ≤ 0.001, **** ≤ 0.0001).

E. IL1R1 promoter activity, mRNA and protein levels in presence/absence of the G4 binding ligand 360A with or without TRF2 induction. For Left and centre panels- [N=3] Statistical significance was calculated using Tukey's multiple comparisons test (p values: * ≤ 0.05, ** ≤ 0.01, *** ≤ 0.001, **** ≤ 0.0001).

F. IL1R1 promoter-firefly luciferase reporter cassette, with or without substitutions deforming the G4 motif B, was artificially inserted at the CCR5 locus using CRISPR-cas9 gene editing in HEK293T cells (scheme in left panel). Promoter activity from (right panel). [N=3] Statistical significance was calculated using Tukey's multiple comparisons test (p values: * ≤ 0.05, ** ≤ 0.01, *** ≤ 0.001, **** ≤ 0.0001).

G. TRF2 occupancy by ChIP-qPCR (right panel) at the artificially inserted IL1R1 promoter without or with G4-deforming substitutions (IL1R1G4 MUT-B);ChIP-qPCR primers designed specific to the inserted promoter using the homology arms(see methods). [N=3] Statistical significance was calculated using unpaired T test with Welch's correction (p values: * ≤ 0.05, ** ≤ 0.01, *** ≤ 0.001, **** ≤ 0.0001).

Error bars correspond to standard error of mean from independent experiments.

Supplementary Figure 3

A

TRF2 ChIP-seq peak sequence (+39 to -632 bp of TSS) shown below.
G4 motif A in red font (on + strand)
G4 motif B in green font (on - strand)

5'-
CCTCCTTAAGTGAAAAATCTGTGAGGAGTTTTCTATCTT
TCTAAGTCTTTGTGGCACACTTATCACATGCATAGTACT
ATTTCTCAAGTTACCCAGGCACACACAGATGTATGGCTT
TCAGGAAGCCATACATCTGTGTAGCTCTGAGGCCCAGC
CTTGTTCAACACTTCACTCAGAAGAATTGCTGGCCTGAT
GACCAACAATAATTGTCAACAACTTAAAACTTCATTGAC
GGCTCCTAAAAAAAATCAGTGTGCATGTGTGTGTGTATG
TGTGTGTGCGTGTGTGTGTGTGTGTGTGTGTATGAGTGTG
TGTATAACATTCATTACTGCAAACT**GG**AAT**GG**AGT**GGGG**
CT**GG**AAGGCAGCCCAGAAGCAAGGCTCAGAGCCTGGA
GCTGCTGACCTCTTGGGGACACTGCAGCCCTGGCCTG
GCCTACTTTTCTCTTCTCCCATATCTGGAAAATGAAAGT
AGCCTGACGTAT**CC**GGGGA**CCC**GG**CCC**AAGACT**CC**AC
CCATTGGCAGCTCTTCACTTGTATCTTTTCATATCAAAA
– 3'

B

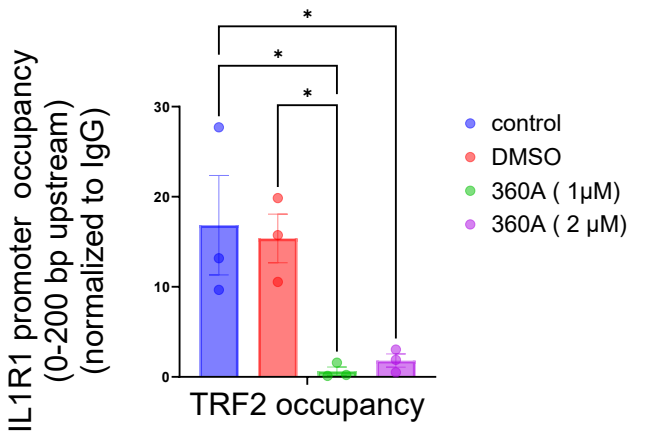

C

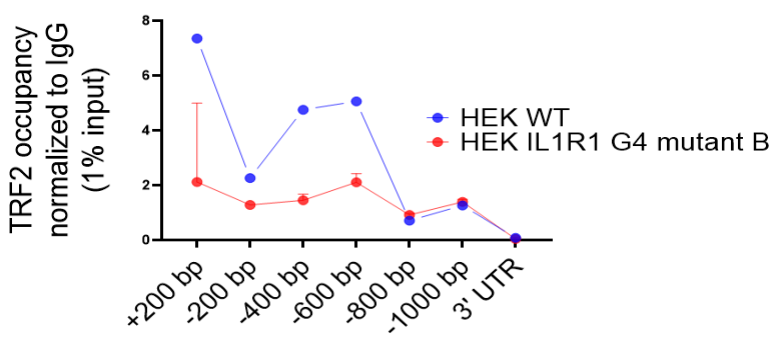

D

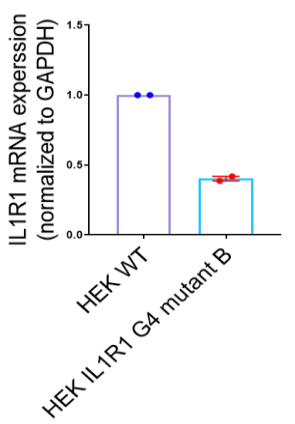

Supplementary Figure 3:

A.TRF2 ChIP-seq peak with sequence of the G4 motifs (A and B) and their respective positions on the *IL1R1* promoter

B.Occupancy of TRF2 by ChIP-qPCR at the *IL1R1* promoter at the region of 0-200 bp of TSS in presence of ligand 360A in three independent experiments in HT1080 cells. The dosage of 360A used has been previous standardized (Mukherjee et al, 2019) [N=3] Statistical significance was calculated using Tukey's multiple comparisons test (p values: * ≤ 0.05, ** ≤ 0.01, *** ≤ 0.001, **** ≤ 0.0001).

C-D. Base substitutions for the G4 motif B in the IL1R1 promoter (as shown in Figure 3D) were introduced using CRSIPR in HEK293T cells. TRF2 ChIP-qPCR spanning the IL1R1 promoter (left) and *IL1R1* mRNA expression (right) in HEK293T cells with or without the G4-disrupting substitution in two replicates. [N=2]

Error bars correspond to standard error of mean from independent experiments.

Figure 4

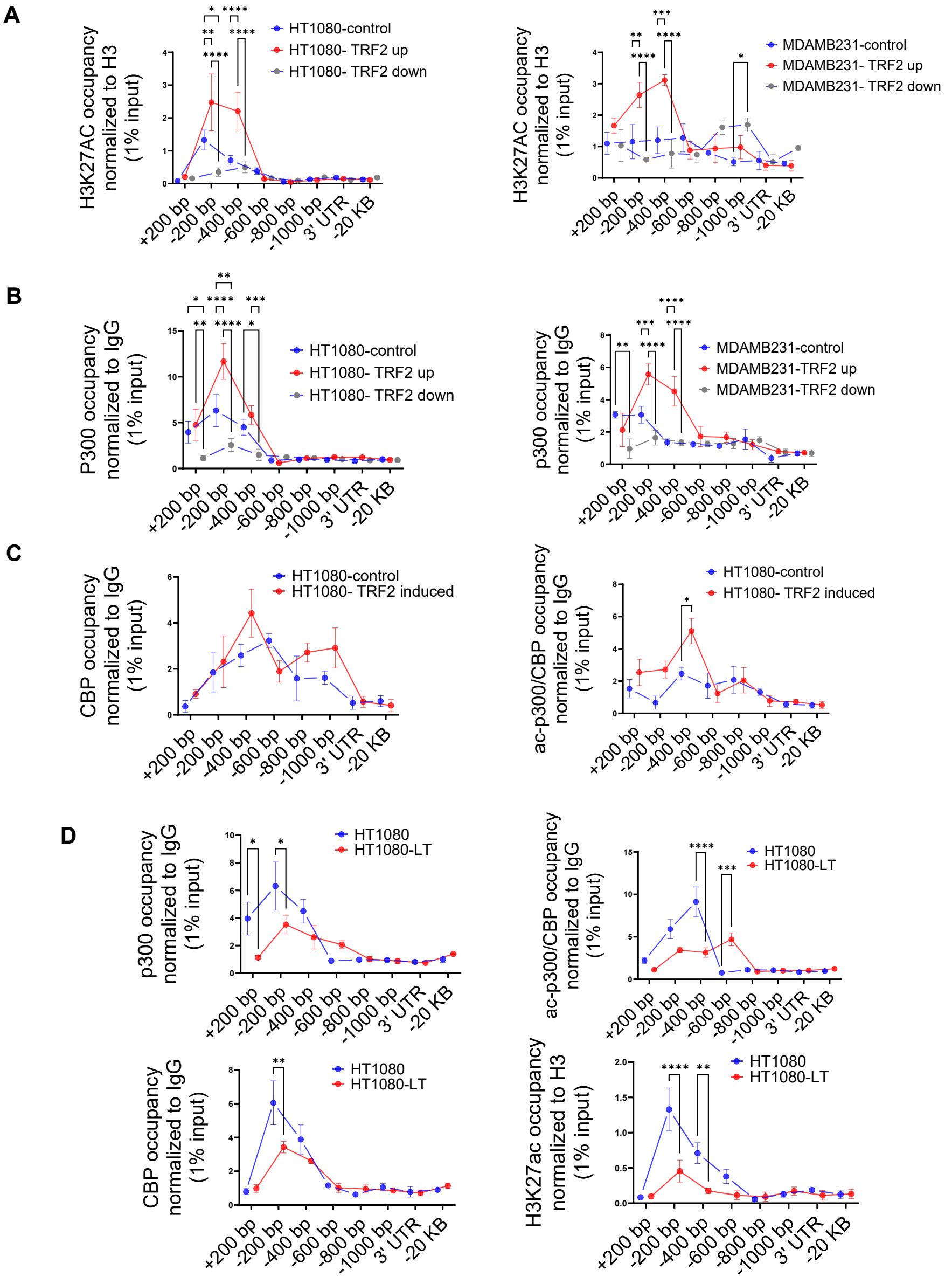
A
H3K27AC occupancy normalized to H3 (1% input)
HT1080-control
HT1080- TRF2 up
HT1080- TRF2 down
MDAMB231-control
MDAMB231- TRF2 up
MDAMB231- TRF2 down
B
P300 occupancy normalized to IgG (1% input)
p300 occupancy normalized to IgG (1% input)
MDAMB231-TRF2 up
MDAMB231-TRF2 down
C
CBP occupancy normalized to IgG (1% input)
HT1080- TRF2 induced
ac-p300/CBP occupancy normalized to IgG (1% input)
D
HT1080
HT1080-LT
H3K27ac occupancy normalized to H3 (1% input)
+200 bp
-200 bp
-400 bp
-600 bp
-800 bp
-1000 bp
3' UTR
-20 KB

Figure 4: TRF2 recruits the histone acetyl transferase p300 to the *IL1R1* promoter

A. H3K27ac occupancy at the *IL1R1* promoter spanning +200 to -1000 bp of TSS by ChIP-qPCR in HT1080 (left panel) and MDAMB231 cells (right panel) in control (uninduced), TRF2-induced (up) or TRF2-down conditions; IL1R1-3'UTR or a region 20 kb upstream were used as negative controls. [N=3] Statistical significance was calculated using Tukey's multiple comparisons test (p values: * ≤ 0.05, ** ≤ 0.01, *** ≤ 0.001, **** ≤ 0.0001).

B. p300 occupancy on the *IL1R1* promoter in HT1080 (left panel) and MDAMB231 cells (right panel) in control (uninduced), TRF2-induced or TRF2-down conditions; IL1R1-3'UTR or a region 20 kb upstream were used as negative controls. [N=3] Statistical significance was calculated using Tukey's multiple comparisons test (p values: * ≤ 0.05, ** ≤ 0.01, *** ≤ 0.001, **** ≤ 0.0001).

C. CBP (left panel) and ac-p300/CBP (right panel) occupancy on the *IL1R1* promoter in HT1080 cells in control (uninduced) or TRF2-induced conditions; IL1R1-3'UTR or a region 20 kb upstream were used as negative controls. [N=3] Statistical significance was calculated using Šídák's multiple comparisons test (p values: * ≤ 0.05, ** ≤ 0.01, *** ≤ 0.001, **** ≤ 0.0001).

D. p300, CBP, acp300/CBP and H3K27Ac occupancy on the *IL1R1* promoter in HT1080 and HT1080-LT cells; IL1R1-3'UTR or a region 20 kb upstream were used as negative controls. [N=3] Statistical significance was calculated using Šídák's multiple comparisons test (p values: * ≤ 0.05, ** ≤ 0.01, *** ≤ 0.001, **** ≤ 0.0001).

All protein ChIP, other than histones, were normalized to 1% input and fold-change have been calculated over respective IgG. Histone ChIP were normalized to 1% Input and fold change over total H3 have been calculated for individual samples (Further details in the methods section)

Error bars correspond to standard error of mean from independent experiments.

Supplementary Figure 4

A

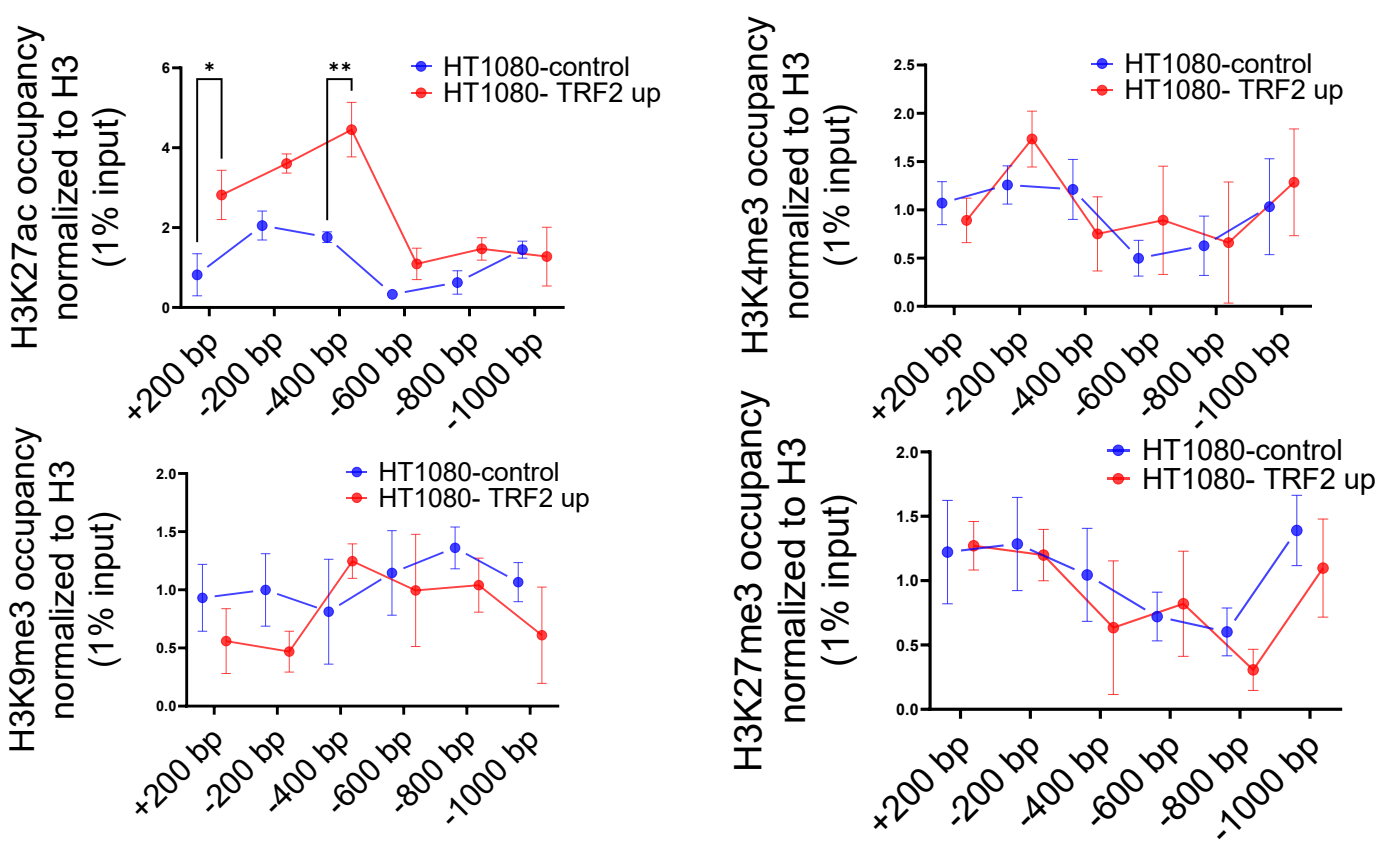

B

IL1R1 PROMOTER

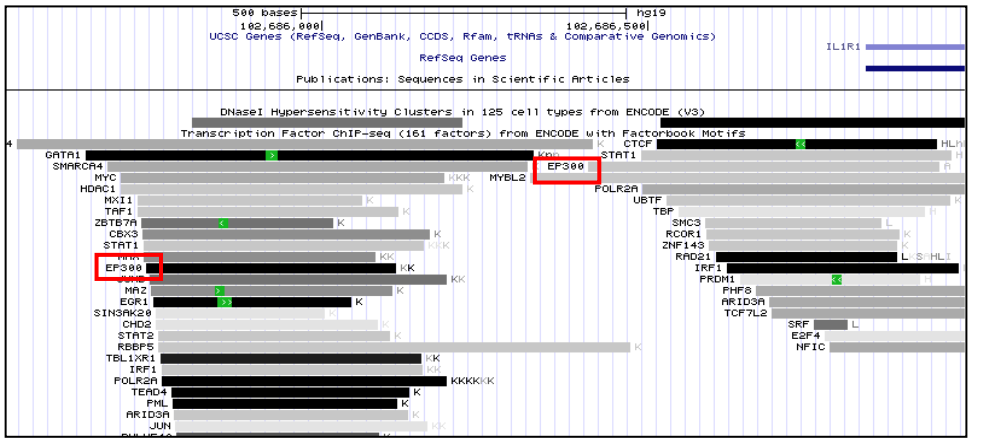

P300 marked in red box

C

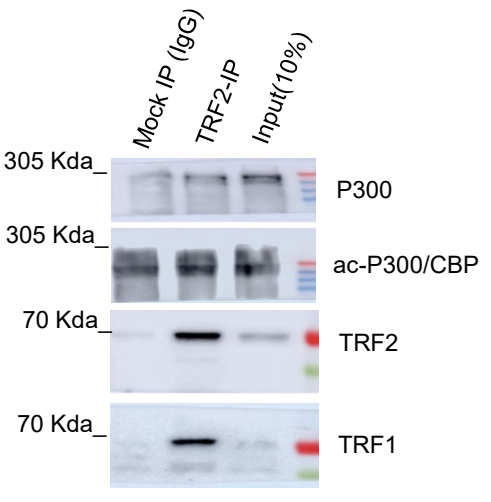

D

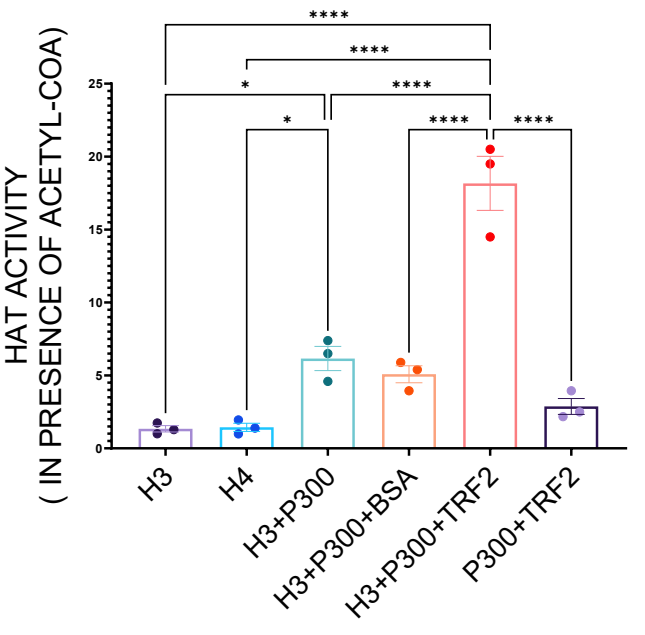

Supplementary Figure 4:

A. Enrichment of histone marks H3K27ac, H3K4me3, H3K27me3, H3K9me3 (normalized to total H3) by ChIP-qPCR on the *IL1R1* promoter in HT1080 cells in TRF2-up (induced) condition or un-induced corresponding control cells. [N=3] Statistical significance was calculated using Šídák's multiple comparisons test (p values: * ≤ 0.05, ** ≤ 0.01, *** ≤ 0.001, **** ≤ 0.0001).
B. Transcription factors/histone remodelers on the IL1R1 proximal promoter (-750 bp) across seven cell lines curated from ENCODE was plotted using UCSC genome browser hg19 human genome assembly. P300 enrichment marked in red box.

C. Immunoprecipitation using TRF2 antibody probed for p300, acp300/CBP, TRF2 or TRF1 (positive control) in input, TRF2 IP fraction or mock IP fraction in HT1080 cells.

D. Histone acetyl transferase (HAT) assay using purified histone H3/H4 and full-length p300 as substrate in presence/absence of recombinant TRF2; BSA (bovine serum albumin) was used as a non-specific mock protein. [N=3] Statistical significance was calculated using Tukey's multiple comparisons test (p values: * ≤ 0.05, ** ≤ 0.01, *** ≤ 0.001, **** ≤ 0.0001).

Error bars correspond to standard error of mean from independent experiments.

Figure 5

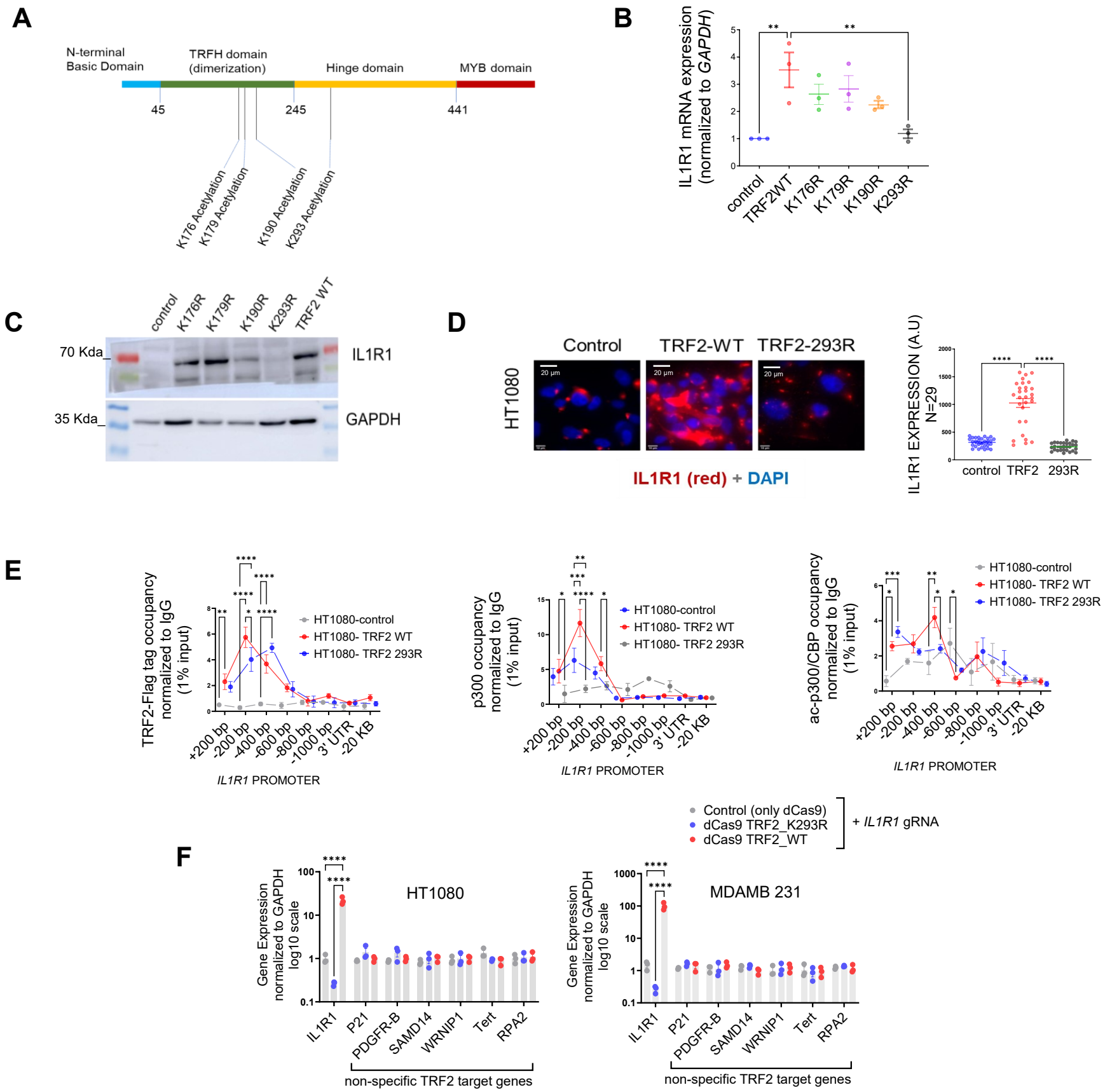
A
N-terminal Basic Domain
TRFH domain (dimerization)
Hinge domain
MYB domain
45
245
441
K176 Acetylation
K179 Acetylation
K190 Acetylation
K293 Acetylation
B
IL1R1 mRNA expression (normalized to GAPDH)
control
TRF2WT
K176R
K179R
K190R
K293R
C
control
K176R
K179R
K190R
K293R
TRF2 WT
70 Kda
35 Kda
IL1R1
GAPDH
D
Control
TRF2-WT
TRF2-293R
HT1080
20 µm
IL1R1 (red) + DAPI
IL1R1 EXPRESSION (A.U)
N=29
control
TRF2
293R
E
TRF2-Flag tag occupancy normalized to IgG (1% input)
HT1080-control
HT1080- TRF2 WT
HT1080- TRF2 293R
+200 bp
-200 bp
-400 bp
-600 bp
-800 bp
-1000 bp
3' UTR
-20 KB
IL1R1 PROMOTER
p300 occupancy normalized to IgG (1% input)
ac-p300/CBP occupancy normalized to IgG (1% input)
F
Control (only dCas9)
dCas9 TRF2_K293R
dCas9 TRF2_WT
+ IL1R1 gRNA
Gene Expression normalized to GAPDH log10 scale
HT1080
MDAMB 231
IL1R1
P21
PDGFR-B
SAMD14
WRNIP1
Tert
RPA2
non-specific TRF2 target genes

Figure 5: Acetylation of TRF2 at Lysine residue 293 is necessary for p300 recruitment on the *IL1R1* promoter

A. Schematic showing positions (amino acid residues) where acetylation and deacetylation of TRF2 have been reported.

B. IL1R1 mRNA expression post 48 hrs. of transient over-expression of various TRF2 acetylation mutants. *GAPDH* was used for normalization. [N=3] Statistical significance was calculated using Dunnett's multiple comparisons test (p values: * ≤ 0.05, ** ≤ 0.01, *** ≤ 0.001, **** ≤ 0.0001).

C. IL1R1 protein level following post 48 hrs. of transient over-expression of various TRF2 acetylation mutants; GAPDH used as loading control.

D. Immunofluorescence for IL1R1 in HT1080 cells without (control) or with induction of flag-tag TRF2 WT or mutant TRF2-293R; quantification from 29 cells in each case shown in graph. [N=29] Statistical significance was calculated using Mann-Whitney's non-parametric test (p values: * ≤ 0.05, ** ≤ 0.01, *** ≤ 0.001, **** ≤ 0.0001).

E. Occupancy of flag-tag TRF2-WT or TRF2-293R on the IL1R1 promoter by ChIP-qPCR in HT1080 cells (left panel); IL1R1-3'UTR or a region 20 kb upstream were used as negative controls. Occupancy by ChIP-qPCR of p300 (middle panel) and acp300/CBP (right panel) without (control) or with induction of TRF2-WT and TRF2-293R. [N=3] Statistical significance was calculated using Tukey's multiple comparisons test (p values: * ≤ 0.05, ** ≤ 0.01, *** ≤ 0.001, **** ≤ 0.0001).

F. TRF2-wild type (WT) and TRF2-2293R mutant proteins fused with dCAS9 expressed and targeted to the IL1R1 promoter using *IL1R1*-specific gRNA in HT1080 and MDAMB231 cells . Following this, expression of *IL1R1* or other TRF2 target genes (non-specific with respect to the IL1R1-gRNA) in HT1080 (left) or MDMB231 cells (right). [N=3] Statistical significance was calculated using Tukey's multiple comparisons test (p values: * ≤ 0.05, ** ≤ 0.01, *** ≤ 0.001, **** ≤ 0.0001).

Error bars correspond to standard error of mean from independent experiments.

Supplementary Figure 5

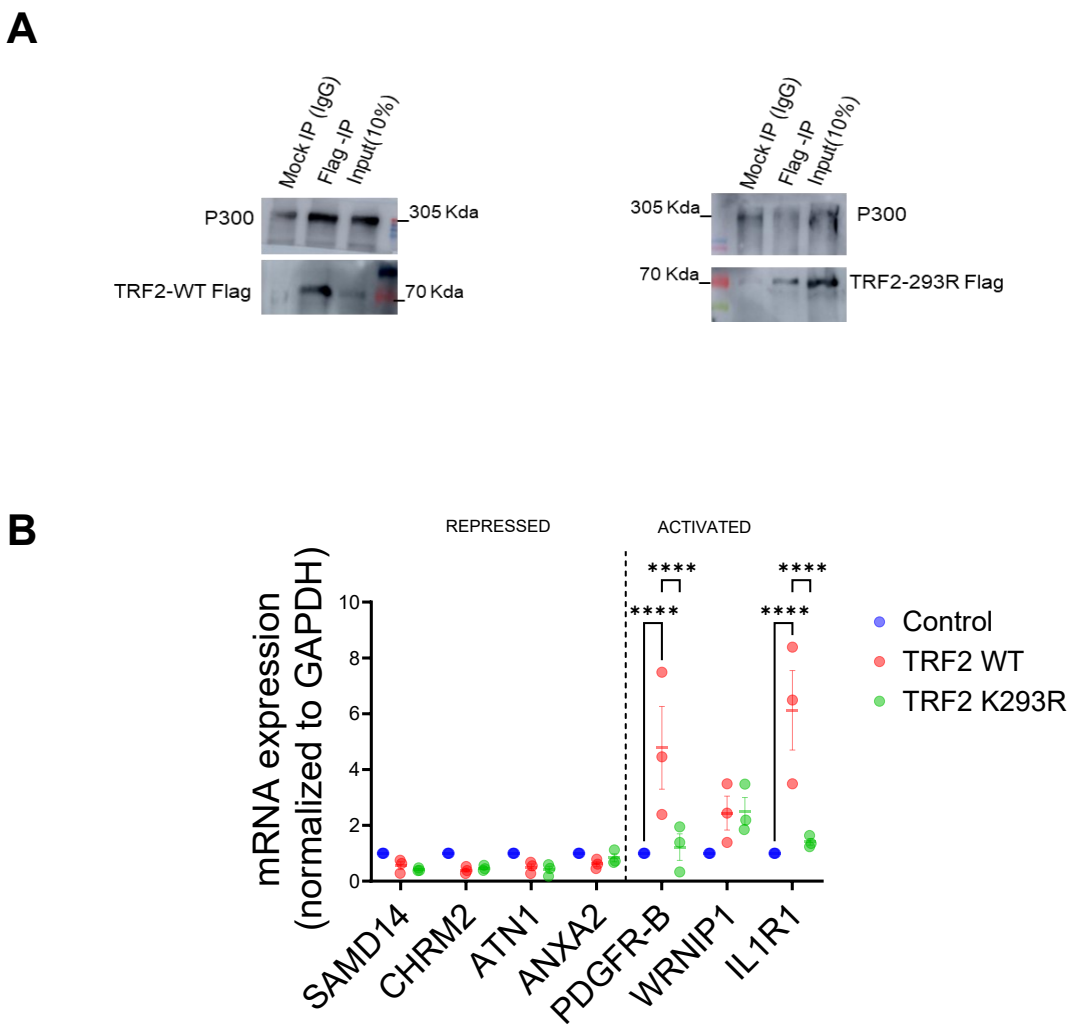

Supplementary Figure 5:

A. TRF2-WT Flag or TRF2 K293R-Flag was stably over expressed in HT1080 cells and immunoprecipitation was performed using Anti-Flag antibody or Mock IgG. Enrichment for p300 in IP faction was tested for TRF2-WT (left) and TRF2 K293R(right)

B. Previously reported TRF2 target genes (Mukherjee et al, 2018) were checked following transient over-expression of TRF2 WT and TRF2 K293R in HT1080 cells. While K293R did not affect TRF2 mediated repression , it affected TRF2 activated genes PDGFR-B and IL1R1 but not WRNIP1. [N=3] Statistical significance was calculated using Tukey's multiple comparisons test (p values: * ≤ 0.05, ** ≤ 0.01, *** ≤ 0.001, **** ≤ 0.0001).

Error bars correspond to standard error of mean from independent experiments.

Figure 6

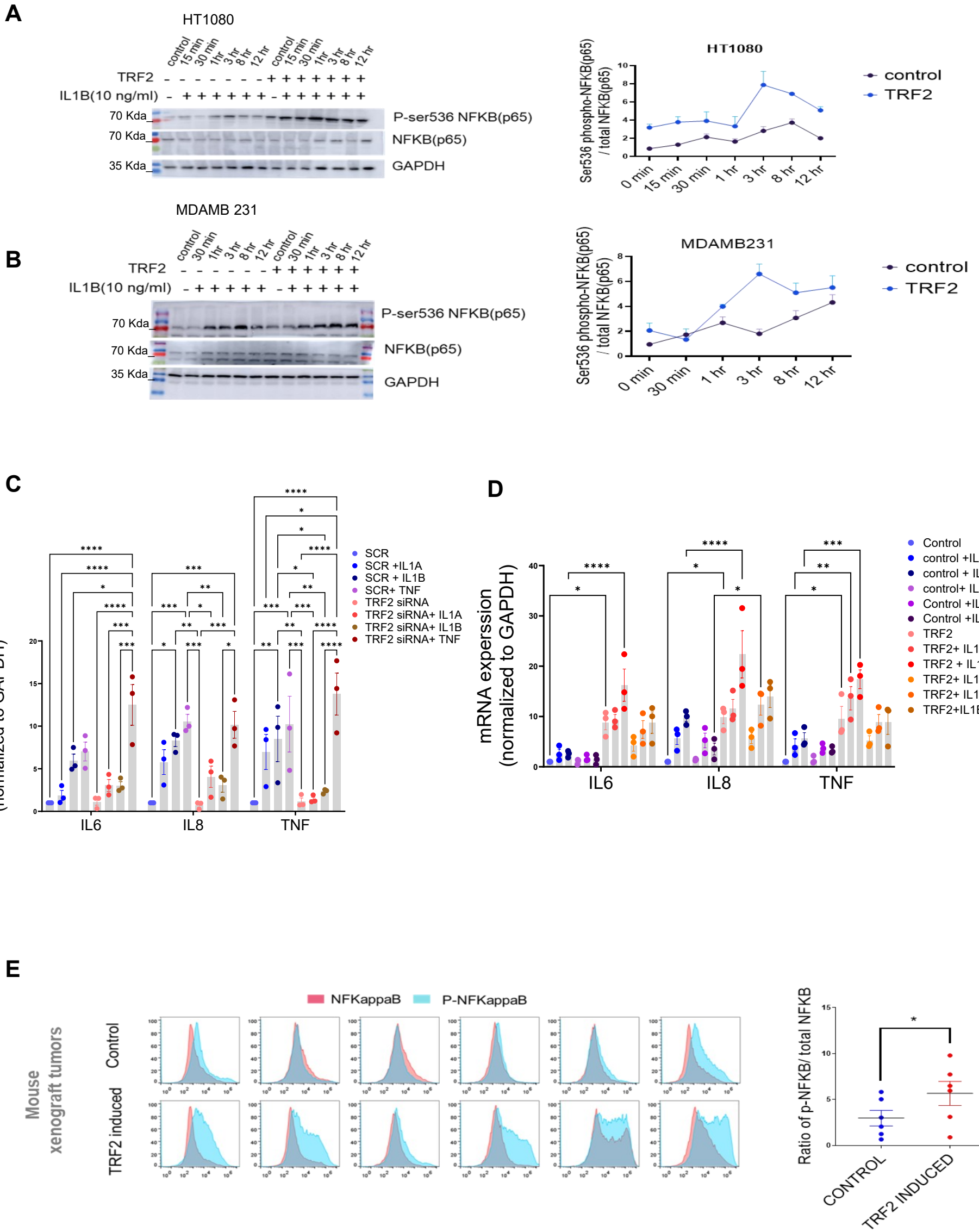
A
HT1080
control
15 min
30 min
1hr
3 hr
8 hr
12 hr
TRF2
IL1B(10 ng/ml)
70 Kda
35 Kda
P-ser536 NFKB(p65)
NFKB(p65)
GAPDH
Ser536 phospho-NFKB(p65) / total NFKB(p65)
0 min
1 hr
control
TRF2
B
MDAMB 231
30 min
MDAMB231
C
mRNA experssion (normalized to GAPDH)
IL6
IL8
TNF
SCR
SCR +IL1A
SCR + IL1B
SCR+ TNF
TRF2 siRNA
TRF2 siRNA+ IL1A
TRF2 siRNA+ IL1B
TRF2 siRNA+ TNF
D
mRNA experssion (normalized to GAPDH)
Control
control +IL1A
control + IL1B
control+ IL1RA
Control +IL1A +IL1RA
Control +IL1B+IL1RA
TRF2
TRF2+ IL1A
TRF2 + IL1B
TRF2+ IL1RA
TRF2+ IL1A+ IL1RA
TRF2+IL1B+IL1RA
E
Mouse xenograft tumors
Control
TRF2 induced
NFKappaB
P-NFKappaB
Ratio of p-NFKB/ total NFKB
CONTROL
TRF2 INDUCED

Figure 6: TRF2-dependent IL1 pathway activates NFkappa B (p65) in cancer cells

A-B. NFKappaB activation in presence of IL1B (10 ng/ml) in HT1080 (A) or MDAMB231 (B) cells with or without TRF2 induction; activation signaling was confirmed through NFKappaB-Ser536 phosphorylation (normalized to total NFKappaB); ratio of Ser566-p/total NFKappaB plotted for respective blots from three independent replicates (right panels). [N=2]

C. Expression of NFKappaB targets *IL6, IL8* or *TNF* in presence/absence IL1A, IL1B or TNF-α (10 ng/ml) for 24 hr in control (scrambled siRNA) or TRF2-low (TRF2 siRNA) conditions in HT1080 cells. [N=3] Statistical significance was calculated using Tukey's multiple comparisons test (p values: * ≤ 0.05, ** ≤ 0.01, *** ≤ 0.001, **** ≤ 0.0001).

D. Expression of *IL6, IL8* or *TNF* in control or TRF2-induced conditions on treatment with either IL1A or IL1B (10 ng/ml) for 24 hr in absence (left panel) or presence (right panel) of the IL1-receptor-antagonist IL1RA (20 ng/ml) in HT1080 cells. [N=3] Statistical significance was calculated using Tukey's multiple comparisons test (p values: * ≤ 0.05, ** ≤ 0.01, *** ≤ 0.001, **** ≤ 0.0001).

E. NFkappaB/phosphor-Ser536-NFKappaB levels in xenograft tumors developed in NOD-SCID mice (control or doxycycline-induced TRF2 in HT1080 cells; N=6 mice in each group) by immuno-flow cytometry; mean fluorescence signal from individual tumors in control or TRF2-induced tumors plotted in adjacent graph; activation shown as ratio of pSer536-p-NFkappaB over total NFkappaB; significance was calculated using Wilcoxon's non-parametric test. [N=6] Statistical significance was calculated using Mann-Whitney's non-parametric test (p values: * ≤ 0.05, ** ≤ 0.01, *** ≤ 0.001, **** ≤ 0.0001).

Error bars correspond to standard error of mean from independent experiments.

Supplementary Figure 6

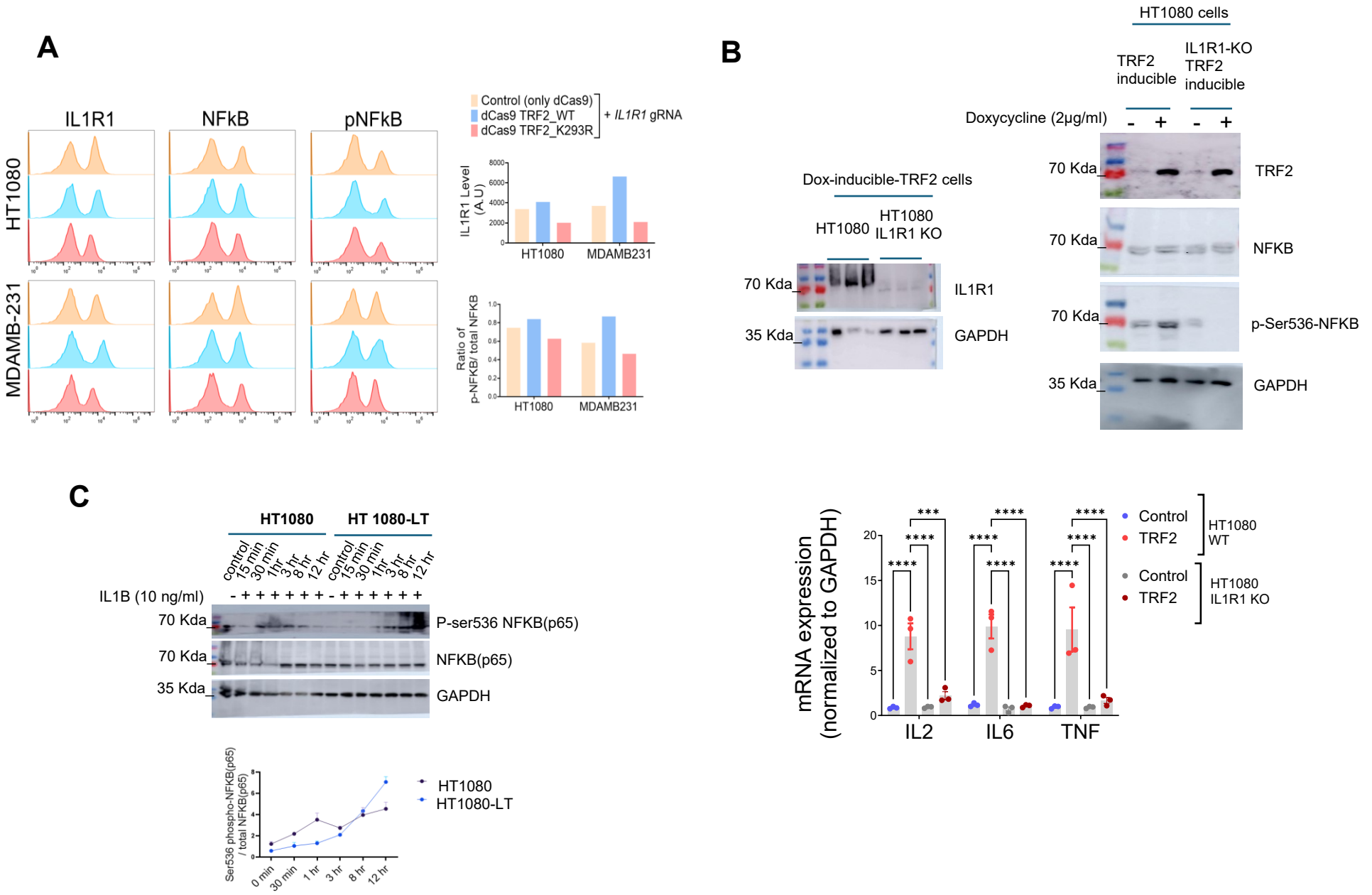

Supplementary Figure 6:

A. TRF2-wild type (WT) and TRF2-2293R mutant proteins fused with dCAS9 expressed and targeted to the IL1R1 promoter using IL1R1-specific gRNA in HT1080 (left) or MDAMB231 cells (right). Following this, NFKB and p-NFKB (Ser536-phosphorylation) levels were assessed by flow-cytometry in ten thousand HT1080 or MDAM231 cells ; mean fluorescence signal for IL1R1 and ratio of p-NFKB/total NFKB plotted in graphs on right panels. [N=1]

B. IL1R1 knockout (KO) HT1080 cells using CRISPR were made and were transduced (lentiviral) to a doxycycline-inducible-TRF2 stable line (top left). TRF2, NFKappa-B and Ser536p-NFKappa-B in IL1R1 knockout or control HT1080 cells with or without TRF2 induction by doxycycline; GAPDH used as loading control (top right). Induction of TRF2 in HT1080 WT and IL1R1 KO cells to check for NFkappaB downstream target gene expression(bottom). Activation of NFKB target genes (~ 2-5 fold) post-TRF2 over-expression was lower in IL1R1KO cells compared to WT cells (~ 10 fold) [N=3] Statistical significance was calculated using Tukey's multiple comparisons test (p values: * ≤ 0.05, ** ≤ 0.01, *** ≤ 0.001, **** ≤ 0.0001).

C. Phospho-NF-Kappa-B-(Ser-536p) and NFkappaB in HT1080 or HT1080-LT cells with or without IL1B stimulation (top panel); ratio of p-NFKB to total NFKB from above western blots plotted from two independent experiments (bottom panel). The NFkappa B (p65/RELA) is detected just below the 70 Kda molecular weight marker.

Error bars correspond to standard error of mean from independent experiments.

Figure 7

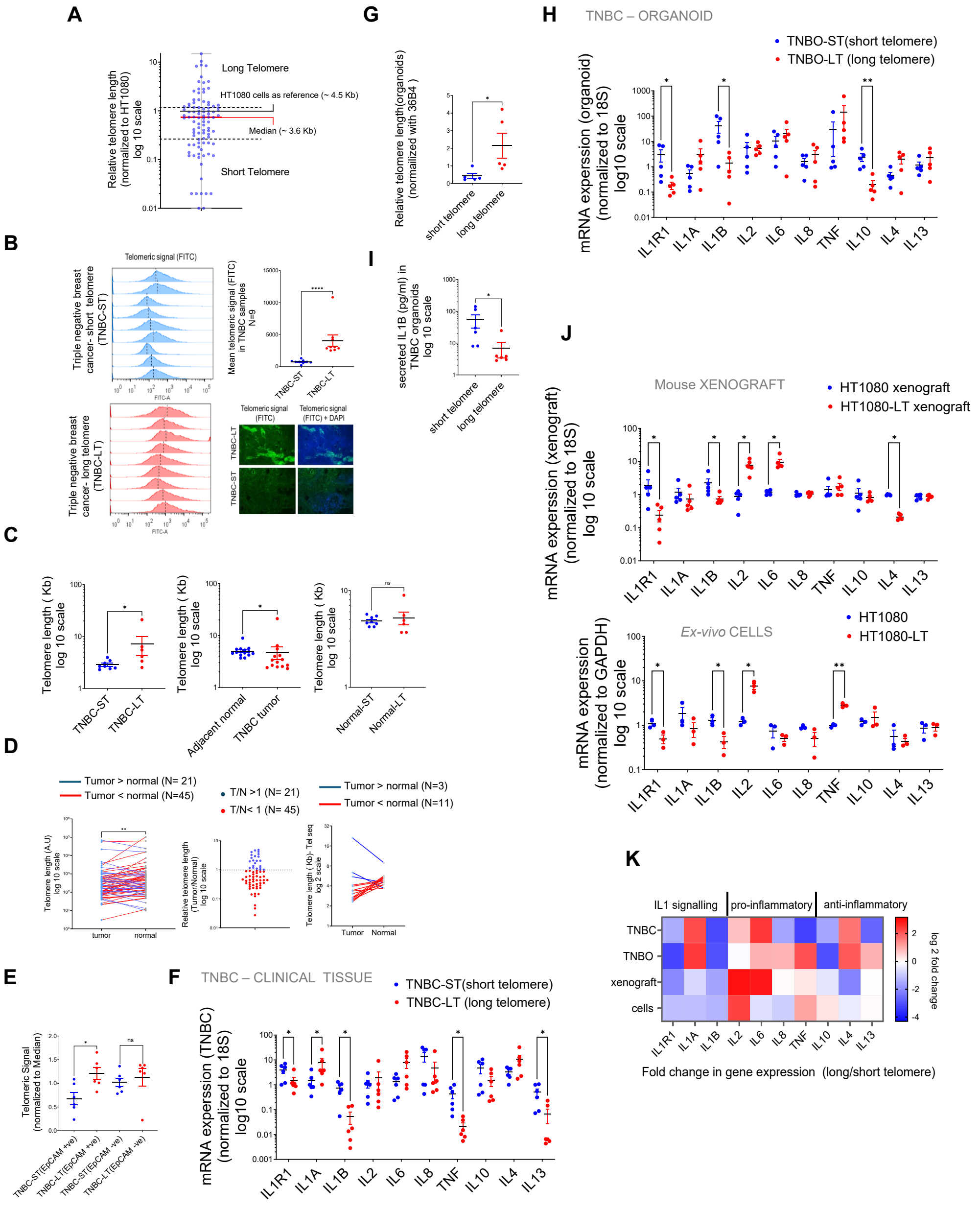
A
Relative telomere length (normalized to HT1080) log 10 scale
Long Telomere
HT1080 cells as reference (~ 4.5 Kb)
Median (~ 3.6 Kb)
Short Telomere
B
Telomeric signal (FITC)
Triple negative breast cancer- short telomere (TNBC-ST)
Triple negative breast cancer- long telomere (TNBC-LT)
Mean telomeric signal (FITC) in TNBC samples N=9
TNBC-ST
TNBC-LT
Telomeric signal (FITC)
Telomeric signal (FITC) + DAPI
C
Telomere length (Kb) log 10 scale
TNBC-ST
TNBC-LT
Adjacent normal
TNBC tumor
Normal-ST
Normal-LT
D
Tumor > normal (N= 21)
Tumor < normal (N=45)
T/N >1 (N= 21)
T/N< 1 (N= 45)
Tumor > normal (N=3)
Tumor < normal (N=11)
Telomere length (A.U) log 10 scale
tumor
normal
Relative telomere length (Tumor/Normal) log 10 scale
Telomere length (Kb)- Tel seq log 2 scale
Tumor
Normal
E
Telomeric Signal (normalized to Median)
TNBC-ST(EpCAM +ve)
TNBC-LT(EpCAM +ve)
TNBC-ST(EpCAM -ve)
TNBC-LT(EpCAM -ve)
F
TNBC – CLINICAL TISSUE
TNBC-ST(short telomere)
TNBC-LT (long telomere)
mRNA expression (TNBC) (normalized to 18S) log10 scale
IL1R1
IL1A
IL1B
IL2
IL6
IL8
TNF
IL10
IL4
IL13
G
Relative telomere length(organoids) (normalized with 36B4)
short telomere
long telomere
H
TNBC – ORGANOID
TNBO-ST(short telomere)
TNBO-LT (long telomere)
mRNA expression (organoid) (normalized to 18S) log10 scale
I
secreted IL1B (pg/ml) in TNBC organoids log 10 scale
J
Mouse XENOGRAFT
HT1080 xenograft
HT1080-LT xenograft
mRNA expression (xenograft) (normalized to 18S) log 10 scale
Ex-vivo CELLS
HT1080
HT1080-LT
mRNA expression (normalized to GAPDH) log 10 scale
K
IL1 signalling
pro-inflammatory
anti-inflammatory
TNBC
TNBO
xenograft
cells
log 2 fold change
Fold change in gene expression (long/short telomere)

Figure 7: IL1R1 expression in Triple Negative Breast cancer (TNBC) samples is sensitive to inter-tumoral variation in telomere length

A. Relative telomere length of Triple Negative Breast Cancer (TNBC) samples (94 patients) by Telo-qPCR as reported earlier; signal from telomere-specific primers was normalized to single copy number gene 36B4 for individual samples. All samples were run with HT1080 DNA as control and telomeric signal from HT1080 cells (telomere length ~4.5 Kb) was used as reference for relative measurement; median telomere length (3.6 Kb) shown by red bar; samples >50% or <50% of median (dotted lines) were designated as long or short telomere samples respectively. [N=94]

B. Flow cytometry analysis of telomere length of TNBC tissues from telomeric signal using telomere–specific FITC-labeled PNA probe; quantification of mean telomeric signal for nine TNBC-ST (short telomere, top left panel) and nine TNBC-LT (long telomere bottom left panel) shown in top right panel. Median telomere length has been indicated by dotted lines (top right). TNBC tissue slides hybridized with telomere-specific PNA probes and counter stained with DAPI. Representative images for long/short telomere TNBC tissue shown (bottom right) [N=9] Statistical significance was calculated using Mann-Whitney's non-parametric test (p values: * ≤ 0.05, ** ≤ 0.01, *** ≤ 0.001, **** ≤ 0.0001).

C. Telomere length was determined using the previously published algorithm Tel-Seq from sequenced genomes of TNBC samples (N=8 for TNBC-ST (short telomere) and N=6 for TNBC-LT (long telomere); and adjacent normal tissue from same patient). Samples identified as long-telomere (TNBC-LT) or short-telomere (TNBC-ST) using telo-qPCR were significantly different in TL, and consistent with telo-qPCR annotation (left); TL of tumor samples was lower that adjacent normal tissue [N=15] (center); and TL from adjacent normal tissues in LT or ST samples did not vary significantly [N= 8; N=6](right) Statistical significance was calculated using Mann-Whitney's non-parametric test (p values: * ≤ 0.05, ** ≤ 0.01, *** ≤ 0.001, **** ≤ 0.0001).

D. Paired telomere length assessment in tumor and adjacent normal tissue for 66 patients. Telomere signal was normalized to 36B4 (single copy gene) by qRT PCR and compared between tumor and adjacent normal samples. The data was plotted pairwise (left) with lines connecting the individual tumor sample to the respective adjacent normal. All samples where tumor telomere length was lower than normal were connected by red lines and the samples where tumor telomeres where higher were connected by blue lines. Relative telomere length(Tumor/Normal) was plotted (middle) with samples with T/N<1 in red and T/N >1 in blue. Out of the 66 samples, 45 samples had T/N < 1 , suggesting that about 2/3 rd of the samples tested had shorter telomeres in the tumors. Analysis of whole genome sequences of 14 pairs of samples using tel-seq pipeline revealed that 11 cases showed lower tumor telomere length compared to their adjacent normal counterparts (right). Left panel-Statistical significance was computed by Wilcoxon matched-pairs signed rank test (p values: * ≤ 0.05, ** ≤ 0.01, *** ≤ 0.001, **** ≤ 0.0001).

E. TNBC tissue (N=6 each for long or short telomere samples) stained with EpCAM (far red) and hybridized with telomere-specific PNA probe (FITC). Mean telomeric signal was plotted in total $EpCAM^{+ve}$ or $EpCAM^{-ve}$ cells. [N=6] Statistical significance was calculated using Mann-Whitney's non-parametric test (p values: * ≤ 0.05, ** ≤ 0.01, *** ≤ 0.001, **** ≤ 0.0001).

F. mRNA expression of *IL1R1* and other key cytokines: *IL1A, IL1B, IL2, IL6, IL8*, *TNF, IL10, IL4* and *IL13* in long or short telomere TNBC tissue,; the *18S* gene was used for normalization . [N=6] Statistical significance was calculated using Mann-Whitney's non-parametric test (p values: * ≤ 0.05, ** ≤ 0.01, *** ≤ 0.001, **** ≤ 0.0001).

G. Relative telomere length of triple negative breast tumor organoids (TNBO) derived from TNBC samples: five TNBO-ST (short telomere) and five TNBO-LT (long telomere) was estimated by telo-qRTPCR . [N=5] Statistical significance was calculated using Mann-Whitney's non-parametric test (p values: * ≤ 0.05, ** ≤ 0.01, *** ≤ 0.001, **** ≤ 0.0001).

H. mRNA expression of *IL1R1* and other key cytokines in triple negative breast tumor organoids (TNBO) derived from TNBC samples-TNBO-ST and TNBO-LT; the *18S* gene was used for normalization . [N=5] Statistical significance was calculated using Mann-Whitney's non-parametric test (p values: * ≤ 0.05, ** ≤ 0.01, *** ≤ 0.001, **** ≤ 0.0001).

I. Secreted IL1B (pg/ml) from organoids TNBO-ST or TNBO-LT by ELISA using media supernatant form organoid culture (see methods).[N=6] Statistical significance was calculated using Mann-Whitney's non-parametric test (p values: * ≤ 0.05, ** ≤ 0.01, *** ≤ 0.001, **** ≤ 0.0001).

J. mRNA expression of *IL1R1* and other key cytokines using xenograft tumors (made from either short (HT1080) or long telomere (HT1080-LT) fibrosarcoma cells, and *ex-vivo* HT1080 or HT1080-LT cells. The *18S* gene was used for normalization for the tumors ;for ex-vivo cells *GAPDH* was used for normalization. Top panel- [N=5] Statistical significance was calculated using Mann-Whitney's non-parametric test (p values: * ≤ 0.05, ** ≤ 0.01, *** ≤ 0.001, **** ≤ 0.0001). ; bottom panel- [N=3] Statistical significance was calculated using unpaired T test with Welch's correction (p values: * ≤ 0.05, ** ≤ 0.01, *** ≤ 0.001, **** ≤ 0.0001).

K. Heat map summarizing the mRNA expression of key cytokines across the models shown above: TNBC tissue, TNBC derived organoids (TNBO), xenograft tumors or ex-vivo cells in long or short telomere cases. Fold change of gene expression (long with respect to short telomeres) color coded as per the reference legend along y-axis.

Error bars correspond to standard error of mean from independent experiments.

Supplementary Figure 7

A

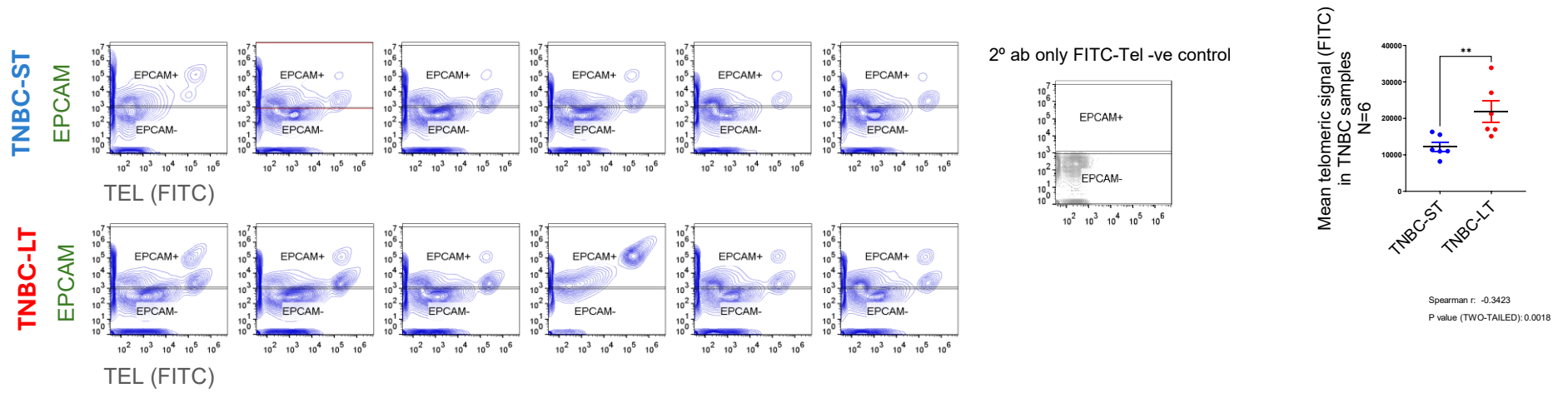

B

Patient ID	Total_reads_Normal	TL-Normal from Tel-Seq (Kb)	Total_reads_Tumor	TL-Tumor from Tel-Seq (Kb)	Annotation by telo-qPCR
15HIV	793841640	5.52	684690974	2.54	Long
17FII	821874738	3.69	798212363	6.37	Long
17FIV	1018357170	3.69	2217147041	3.36	Long
21BIII	857074906	4.50	1939381027	5.52	Long
22BX	937589074	8.92	2039824553	21.11	Long
8CIII	1205476805	4.89	3048252295	4.12	Long
10HVI	1964615991	5.68	2499660737	2.69	Short
11KX	1618874093	5.24	2060088701	2.41	Short
11MIV	1578986029	5.44	1624283175	2.31	Short
12GVII	1142304223	4.21	1399187739	3.06	Short
21CVIII	1253875224	4.74	1460333173	3.96	Short
23AIV	1352144501	4.21	2733959635	2.48	Short
23AVI	1632115660	4.54	2734342597	3.44	Short
4HI	873273625	4.61	1692643267	2.67	Short

C

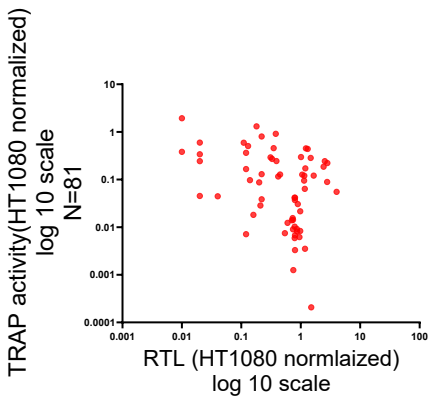

r	-0.3423
95% confidence interval	-0.5264 to -0.1275
P value	
P (two-tailed)	0.0018

D

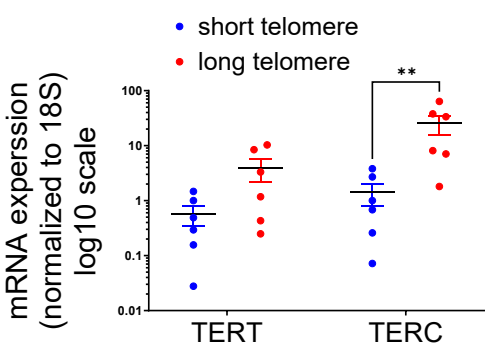

F

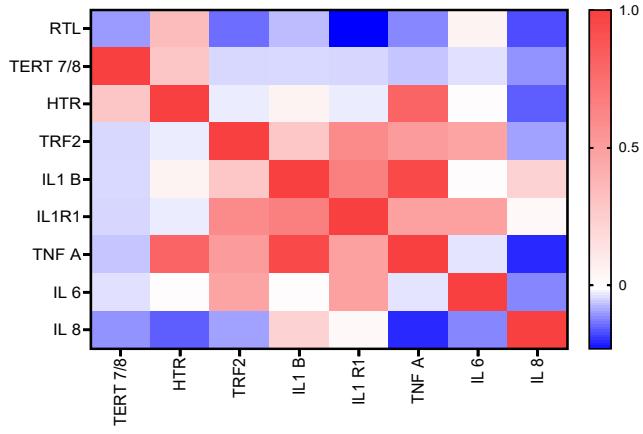

E

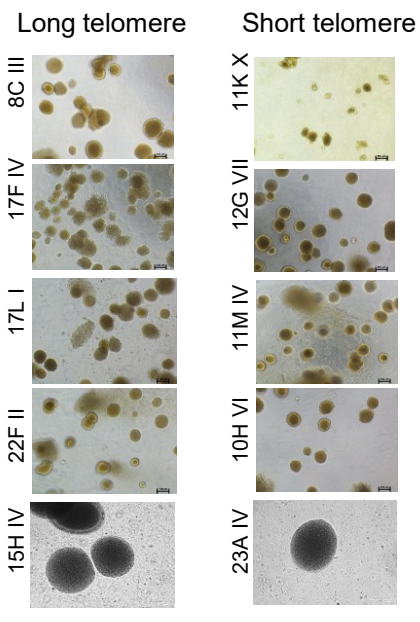

G

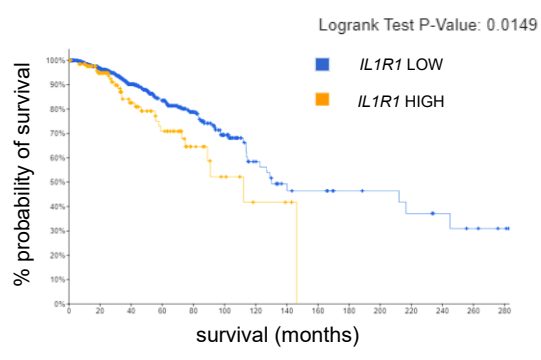

H

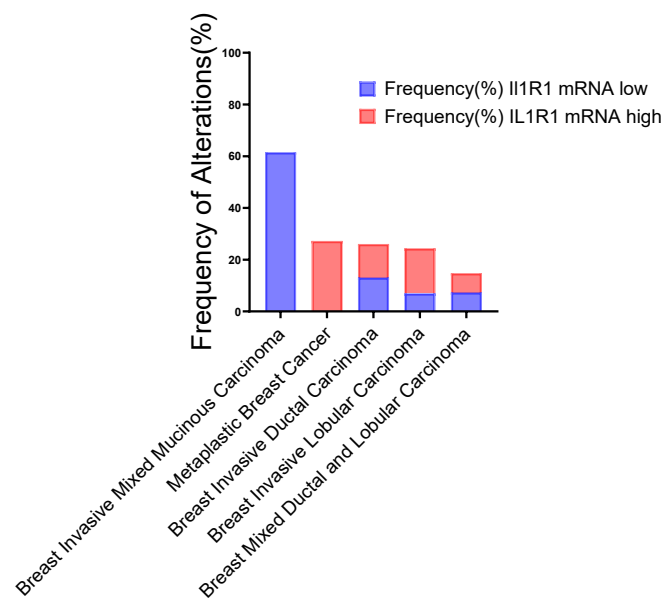

Supplementary Figure 7:

A. TNBC samples (N= 6 each for long or short telomere samples) stained with EpCAM (far red) and then hybridized with telomere specific PNA probe (FITC). Mean telomeric signal was plotted in total cells. [N=6] Statistical significance was calculated using Mann-Whitney's non-parametric test (p values: * ≤ 0.05, ** ≤ 0.01, *** ≤ 0.001, **** ≤ 0.0001).

B. Telomere length was determined using the previously published algorithm Tel-Seq from sequenced genomes of TNBC samples (N=8 for TNBC-ST (short telomere) and N=6 for TNBC-LT (long telomere); and adjacent normal tissue from same patient). Table with sequencing related details of the normal/tumor samples has been provided.

C. Telomerase activity was measured from protein lysates across 64 TNBC samples (long or short telomeres) normalized to the telomerase activity of HT1080 cells for the same amount of protein; spearman correlation was calculated between RTL (relative telomere length) and telomerase activity.

D. mRNA expression of *hTERT* and *TERC* in six TNBC samples (long or short telomeres) normalized to the *18S* gene in respective samples. [N=6] Statistical significance was calculated using Mann-Whitney's non-parametric test (p values: * ≤ 0.05, ** ≤ 0.01, *** ≤ 0.001, **** ≤ 0.0001).

E. TNBC organoids (TNBO) formed from TNBO-ST (short telomere) and TNBO-LT (long telomere) samples .

F. Spearman correlation of ,*TERT*, *TERC, IL1R1* and cytokine related gene expression and RTL (Relative telomere length*)* in 34 TNBC tissue samples with each other and RTL represented as heat map; gene expression was normalized to the18S gene; for telomere length the 36B4 single-copy gene was used for normalization (as in Figure 1D); fold change of TL was calculated with respect to TL in HT1080 cells.

G. Overall Survival for breast cancer patients (BRCA) with high IL1R1 mRNA expression [N=254] or low IL1R1 mRNA expression [N=709] from TCGA datasets (see Supplementary file 4 for details) – graph tabulated using cBIOPORTAL with custom queries. Logrank p-value was found to be 0.0149.

H. Frequency of occurrence of samples with high / low IL1R1 mRNA expression in various annotated sub-types of breast cancer from TCGA (see Supplementary file 4 for details)

Error bars correspond to standard error of mean from independent experiments.

Figure 8

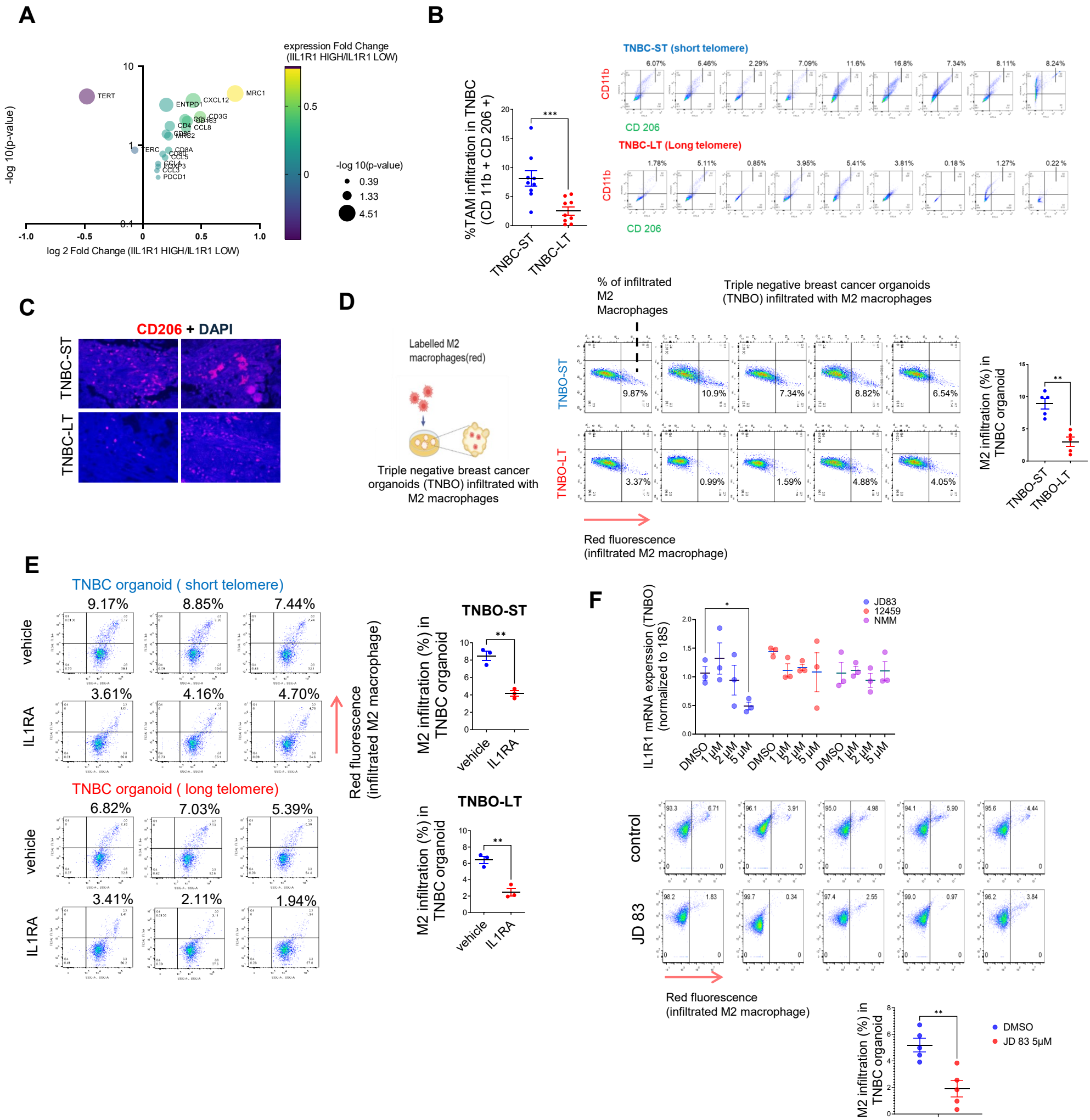
A
expression Fold Change (IIL1R1 HIGH/IL1R1 LOW)
-log 10(p-value)
log 2 Fold Change (IIL1R1 HIGH/IL1R1 LOW)
TERT
MRC1
CXCL12
ENTPD1
CD3G
CD4
CCL8
TERC
CD8A
CCL5
FOXP3
CCL3
PDCD1
-log 10(p-value)
0.39
1.33
4.51
B
TNBC-ST (short telomere)
TNBC-LT (Long telomere)
CD11b
CD 206
%TAM infiltration in TNBC (CD 11b + CD 206 +)
TNBC-ST
TNBC-LT
C
CD206 + DAPI
TNBC-ST
TNBC-LT
D
Labelled M2 macrophages(red)
Triple negative breast cancer organoids (TNBO) infiltrated with M2 macrophages
% of infiltrated M2 Macrophages
Triple negative breast cancer organoids (TNBO) infiltrated with M2 macrophages
TNBO-ST
TNBO-LT
M2 infiltration (%) in TNBC organoid
Red fluorescence (infiltrated M2 macrophage)
E
TNBC organoid (short telomere)
vehicle
IL1RA
TNBC organoid (long telomere)
Red fluorescence (infiltrated M2 macrophage)
TNBO-ST
TNBO-LT
M2 infiltration (%) in TNBC organoid
F
IL1R1 mRNA experssion (TNBO) (normalized to 18S)
JD83
12459
NMM
DMSO
1 μM
2 μM
5 μM
control
JD 83
Red fluorescence (infiltrated M2 macrophage)
M2 infiltration (%) in TNBC organoid
DMSO
JD 83 5μM

Figure 8: Telomere length sensitive IL1R1 expression modulates Tumor associated macrophage (TAM) infiltration in TNBC

A. Key Immune marker expression (TAM markers, TAM related chemokines, T cell markers), *TERT* and *TERC* were plotted for fold change of transcript level expression (IL1R1 high / IL1R1 low) and adjusted p-values in breast cancer (BRCA) samples categorized as IL1R1 high or low from TCGA (See supplementary file 4).

B. Percentage tumor-associated-macrophage (TAM) infiltration in TNBC tissue with short (TNBC-ST) or long (TNBC-LT) telomeres using markers CD11b and CD206 ($CD11b^{+}CD206^{+}$ cells shown in top right quadrant); quantification of TAM infiltration from individual TNBC-ST or TNBC-LT samples have been plotted . [N=9] Statistical significance was calculated using Mann-Whitney's non-parametric test (p values: * ≤ 0.05, ** ≤ 0.01, *** ≤ 0.001, **** ≤ 0.0001).

C. TNBC tissue slides stained with TAM-specific marker CD206 for macrophage infiltration within tissue (counterstained with DAPI); representative images for two independent long or short telomere TNBC tissues shown.

D. Labelled (red) M2 macrophages derived from THP1 cells incubated with triple negative breast tissue-derived organoids (TNBO) for 12 hours (scheme in left panel). Infiltration of M2 macrophages in organoids shown as percentage of labelled (red) M2 macrophages in individual flow-cytometry plots (florescence signal (FL3) in x-axis in log scale); percentage infiltration from five TNBO-ST or five TNBO-LT samples shown in right panel. [N=5] Statistical significance was calculated using Mann-Whitney's non-parametric test (p values: * ≤ 0.05, ** ≤ 0.01, *** ≤ 0.001, **** ≤ 0.0001).

E. Labelled (red) M2 macrophage infiltration in presence/absence of receptor antagonist IL1RA (20 ng/ml) for tumor organoids with short (TNBO-ST) or long telomeres (TNBO-LT) in three replicates; percentage values for M2 infiltration plotted in right panel. Red florescence (FL3; y-axis in log scale) and respective percentage M2 infiltration values marked on top of individual flow cytometry plots. [N=3] Statistical significance was calculated using unpaired T test with Welch's correction (p values: * ≤ 0.05, ** ≤ 0.01, *** ≤ 0.001, **** ≤ 0.0001).

F. mRNA expression of *IL1R1* was checked in presence of varying concentrations of G-quadruplex binding ligands (48 hr treatment) using TNBO. *18S* gene was used for normalization. Following this, the ligand JD83 was used to check M2 infiltration in TNBO as in (C-D). The M2 infiltration has been plotted for control and JD 83 treated samples. Top panel- [N=3] Statistical significance was calculated using unpaired T test with Welch's correction (p values: * ≤ 0.05, ** ≤ 0.01, *** ≤ 0.001, **** ≤ 0.0001).; bottom panel- [N=5] Statistical significance was calculated using Mann-Whitney's non-parametric test (p values: * ≤ 0.05, ** ≤ 0.01, *** ≤ 0.001, **** ≤ 0.0001).

Error bars correspond to standard error of mean from independent experiments.

Supplementary Figure 8

A

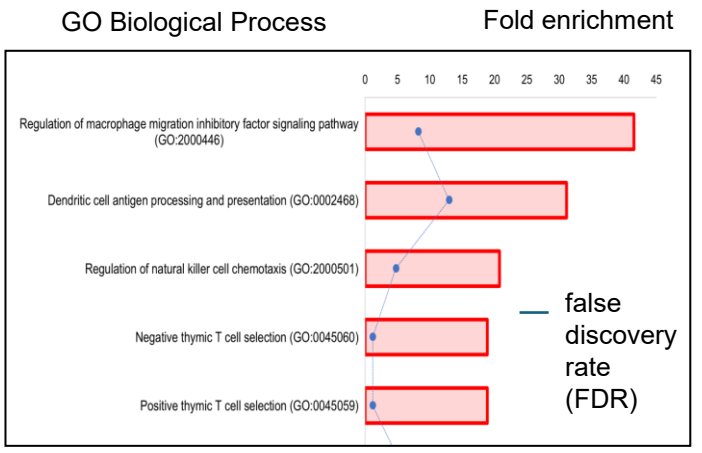

B

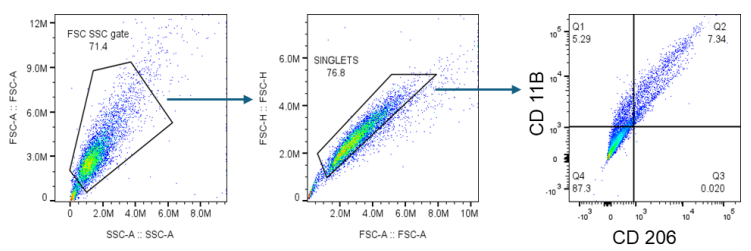

C

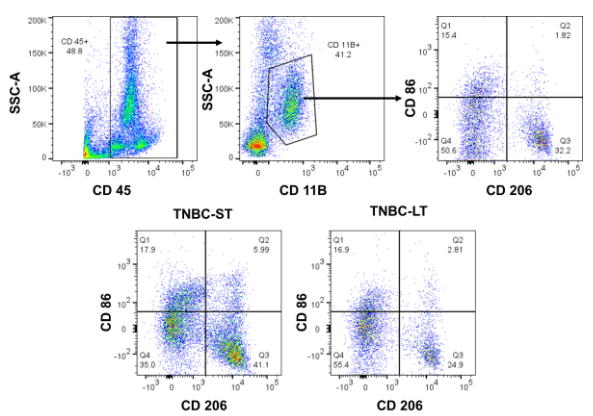

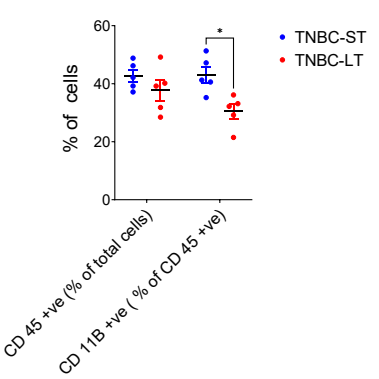

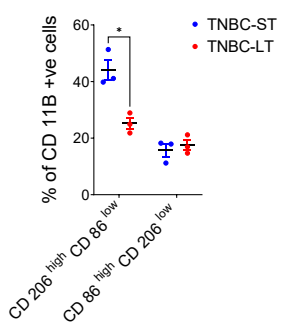

E

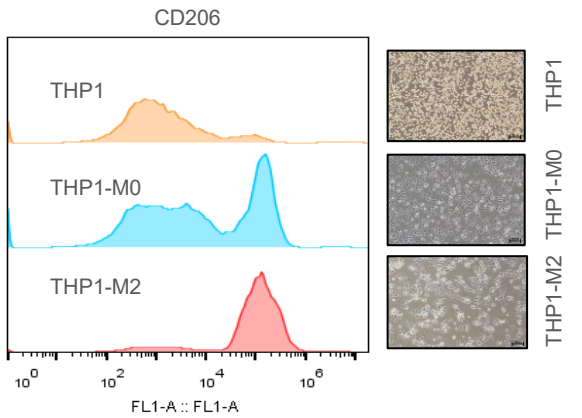

F

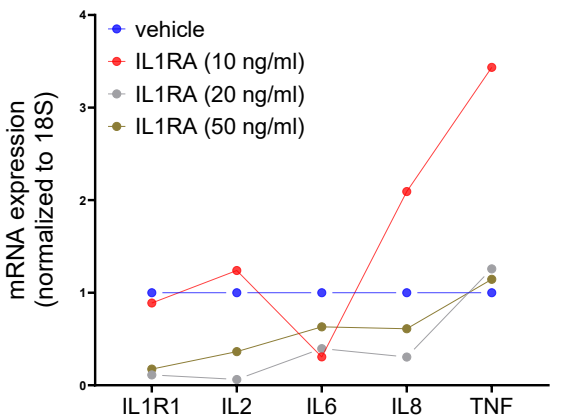

D

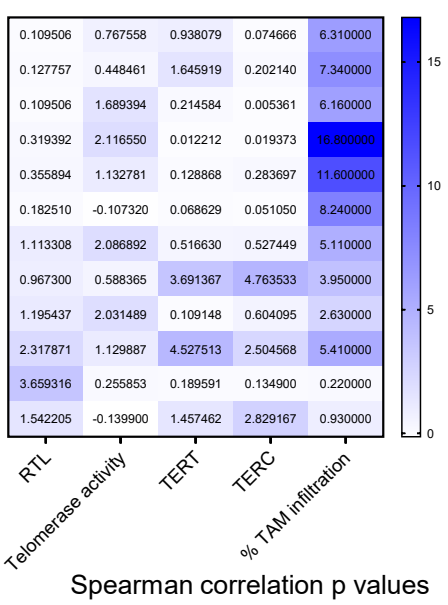

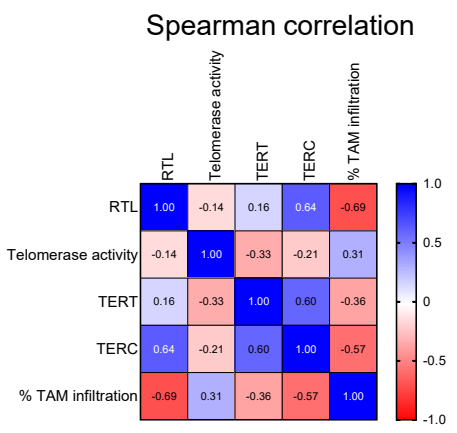

Spearman correlation p values

	RTL	Telomerase activity	TERT	TERC	% TAM infiltration
RTL		0.65460168	0.614324771	0.028166586	0.015831563
Telomerase activity	0.65460168		0.297333479	0.51371329	0.331040614
TERT	0.614324771	0.297333479		0.042800479	0.246411152
TERC	0.028166586	0.51371329	0.042800479		0.059052513
% TAM infiltration	0.015831563	0.331040614	0.246411152	0.059052513	

G

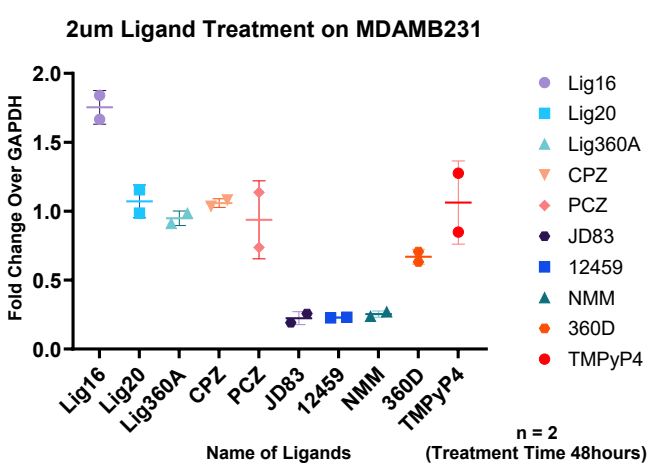

Supplementary Figure 8:

A. Gene Ontology (GO) analysis of top 500 genes correlated with telomere elongation across 31 cancer types(as reported in Barthel et al., 2017) Top 5 hits for 'biological processes' represented in descending order of enrichment; respective fold enrichments shown by individual bars (x-axis – top); the false discovery rate (FDR) shown by blue line.
B. Gating strategy for Figure 8B.
C. Gating strategy for CD 45 +ve c gated ells and CD 11B +ve gated cells in TNBC. Percentage of CD 45 +ve and CD11B +ve (in CD 45 +ve population) was checked for TNBC-ST and TNBC-LT samples. [N=5] Statistical significance was calculated using Mann-Whitney's non-parametric test (p values: * ≤ 0.05, ** ≤ 0.01, *** ≤ 0.001, **** ≤ 0.0001).. In the CD11B +ve (in CD 45 +ve population) , CD 206 (M2 macrophage marker) and CD 86 (M1 macrophage marker) +ve cells were quantified. Percentage of CD 206 high CD 86 low (M2 macrophages) and CD86 high Cd206 low (M1 macrophages) in the myeloid cell population (CD 45 +ve CD 11B +ve) was plotted for three TNBC-ST and TNBC-LT samples each. [N=3] Statistical significance was calculated using unpaired T test with Welch's correction (p values: * ≤ 0.05, ** ≤ 0.01, *** ≤ 0.001, **** ≤ 0.0001).
D. TNBC tissue (N=6 each for long or short telomere samples) were tested for TERT and TERC expression (The Telomerase activity for these samples was estimated with HT1080 cell lysate as a reference . The normalized values (to the group average) were plotted in a heat map (left) for telomerase activity ,TERT and TERC gene expression in the TNBC samples used in Supplementary Figure 7D along with corresponding % TAM values (top left). The Spearman correlation matrix (top right) and p values (bottom).have been provided.
E. CD206 levels by immuno-flow cytometry in THP1 cells and macrophages differentiated from THP1 cells into M0 or M2 types (described in Methods) and plotted along X-axis in log scale (top panel). Bright-field images at 10X magnification for each cell stage shown in top right panel.
F. Different dosages of IL1RA was checked based on previously published reports and the minimal concentration where change in IL1R1 expression was seen (20 ng/ml) was used in other functional assays. [N=1]
G. mRNA expression of IL1R1 was tested in MDAMB-231 cells after a 48-hr. treatment with various reported G4- binding ligands. *GAPDH* was used as a normalizing control. [N=2]

Error bars correspond to standard error of mean from independent experiments.

Figure 9

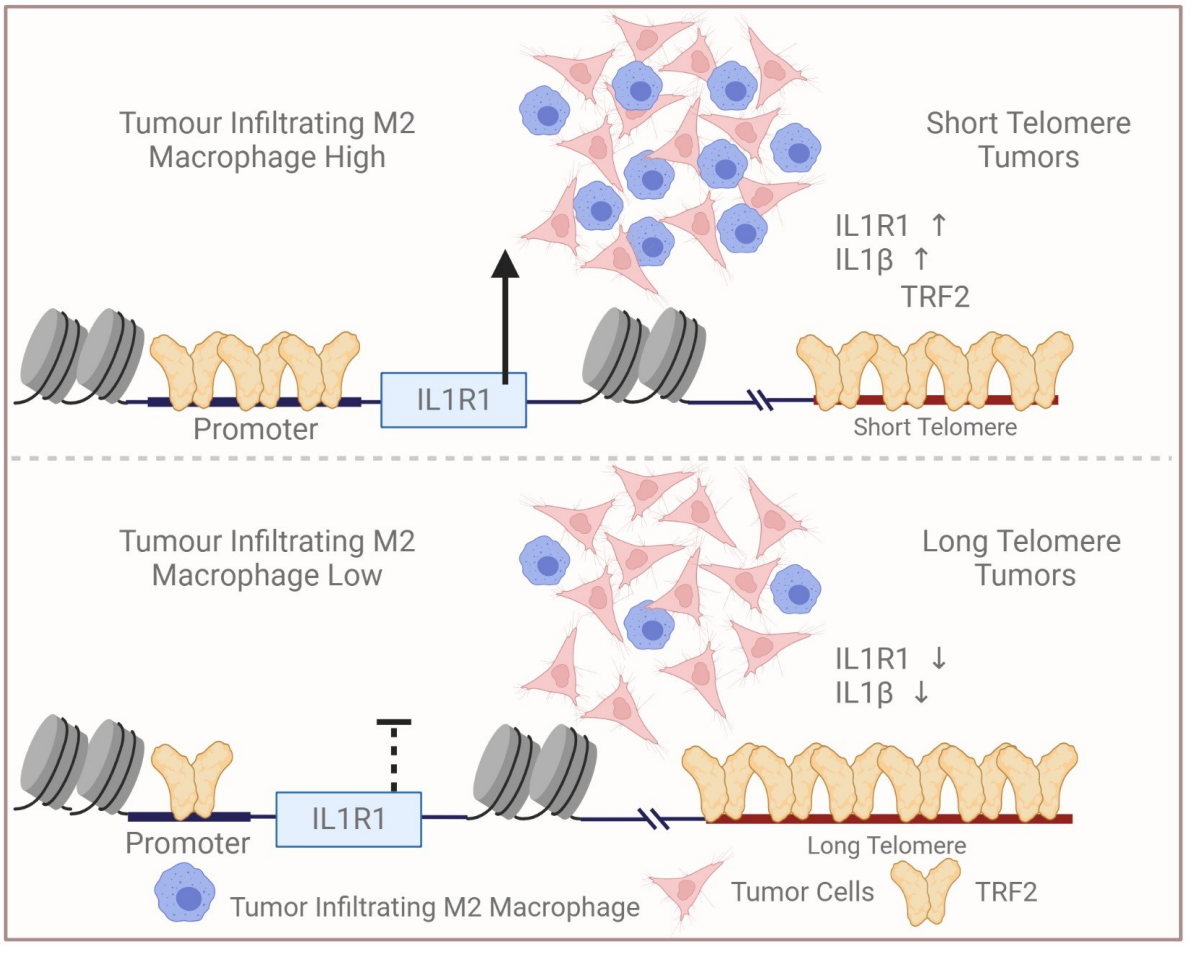

Scheme depicting relatively low infiltration of TAM in tumors with relatively long telomeres vis-à-vis tumors with short telomeres. Reduced non-telomeric TRF2 binding at the IL1R1 promoter in tumors with long telomeres, and consequent low IL1R1 activation, attenuated p65-mediated IL1-beta and macrophage infiltration. Figure created with BioRender.com.